Universidade Nova de Lisboa

Instituto de Tecnologia Química e Biológica

Metabolism of Primary Astrocytes Studied by NMR

Metabolic Trafficking and Neuroprotection

This dissertation was presented to obtain a Ph.D. degree in Biochemistry at the Instituto de Tecnologia Química e Biológica, Universidade Nova de Lisboa.

By Luís Maria de Figueiredo Mascarenhas Lopes da Fonseca

Supervised by Prof. Dr. Helena Santos

Oeiras, September, 2006

From left to right: Dr. Manuel Carrondo, Dr. António Ferreira, Dr. Carlos Duarte, Dr. Arne Schousboe, Luís Lopes da Fonseca, Dr. Helena Santos, Dr. Paula Alves, Dr Carlos Geraldes and Dr. Miguel Teixeira. Oeiras, September 11, 2006.

Supervisor: Dr. Helena Santos.

Examiners: Dr. Arne Schousboe, Dr. Carlos Duarte, Dr. António Ferreira, Dr Carlos Geraldes, Dr. Paula Alves and Dr. Manuel Carrondo.

Dissertation presented to obtain a Ph. D. degree in Biochemistry by Universidade Nova de Lisboa, Instituto de Tecnologia Química e Biológica.

ACKNOWLEDGEMENTS

I would like to start by thanking everyone that somehow helped me or contributed to this thesis. A lot of people supported, encouraged and helped me with the work presented in this thesis. So many that it is impossible to name them all. To all of those my most sincere thanks.

I would also like to thank:

My supervisor, Prof. Dr. Helena Santos, for accepting me in her group, for the continuing support and patience, and for never giving up on me. Especially, I would like to thank her for her honesty, integrity, fairness and scientific rigor, and above all for inspiring her best qualities on her students.

Prof. Dr. Manuel J. T. Carrondo, for giving me access to his internationally recognized laboratory, for the excellent working conditions and for all valuable discussions.

Prof. Dr. Ruy Pinto as director of the Instituto de Investigação Científica Bento da Rocha Cabral, Prof. Dr. Cristina Santos and Sr. João for the support and kindness shown by supplying most of the animals required for this work. I would also like to thank Prof Dr. Ruy Pinto for all the motivation and fruitful discussions. But, most of all, to express the honor that it was for me to have as a biochemistry teacher, a pupil of Sir Hans Krebs himself.

Dr. Sebastián Cerdán, for opening his laboratory to me, for inviting me to collaborate in his projects and for all the friendly discussions and sympathy shown. I also would like to thank all Cerdán's lab members: Alejandra Sierra, Marina Benito, Tiago Rodrigues, Susana Garrido, Patricia Sánchez and Pilar López for making my stay so enjoyable. Especially, Sandra for all the help in the experiments, Susy for teaching me her techniques concerning the NMR samples and Tiago for all encouragement and support.

Dr. Paula M. Alves, for introducing me to the daily life in the lab and teaching me many of the techniques that I know today, and also for all the encouragement, friendship, guidance, suggestions and endless support shown.

Eng. José Luis Moreira, for all his teachings, discussions and examples of good leadership, they shell not be forgotten.

Dr. António Maretzek, for all the help and knowledge supplied in all aspects of NMR and computing.

Dr. António Ferreira for introducing me to the world of flux analysis and teaching me the basics of the determination of metabolic fluxes by solving the sets of ODE's.

Miguel Monteiro for putting up with my crazy experimental schedules, for all the help in the experimental work, and friendship. I have no words to thank you, apart from saying that I couldn't have done all this work and remained sane without your help!

The ITQB staff that made my life easier, Miguel Loureiro, Isabel Baia, Luís Gonçalves, Fátima Madeira and especially Cristina Barreiros who always made her best to facilitate the lab ware that I required.

All my colleagues of the Animal Cell Technology group Angela Almeida, Dr Lídia Gonçalves, Dr. Pedro Cruz, Dr. Helder Cruz, Dr. Verónica Carvalhal, Eng. Cristina Peixoto, Rosário Clemente, Eng. Sandra Marques, Dr. Ana Coroadinha, Isabel Marcelino, Délia Gonçalves, Dr. Luis Maranga, Marcos Sousa, Tiago Ferreira, Marlene Carmo, Teresa Rodrigues, Carina Silva, Sónia Sá Santos, Sofia Leite, Hélio Crespo, Célia Verissimo, Claudia Istrate (Multumesc) and Marta Mendes, for creating a good working atmosphere and valuable incentive for my work.

All my colleagues of the 4th floor (and associates), from the Glycobiology group, Prof. Dr. Júlia Costa, Dr. Victor Costa, Dr. Vanessa Morais, Angelina Palma, Teresa Costa, Cidália Vila Verde, Catarina Brito, Nuno barata and Rui Almeida, from the Biosensors laboratory Prof. Dr. Abel Oliva, Dr. Joana Miranda, Marta Silva, Elisabete Nascimento and Óscar Silvestre, from the Mass spectrometry group Gonçalo Costa and Elisabete Pires, from the ECBio Luís Apolónia and Vera Basto, from the Biotecnol Telmo Graça, José Forte and Dr. Nuno Fontes, from the Plant cell biotechnology laboratory, Dr. Alexandre Campos and from the IBET team Sandra Monteiro, Filipe Pinto and Rui Gomes (Domo arigato). Thanks for the friendship, companionship, suggestions, discussions and the most excellent times.

All my colleagues in the Cell Physiology & NMR group, Dr Pedro Lamosa, Dr Tiago Faria, Dr. Claudia Sánchez, Dr. Clélia Neves, Dr. Helena Pereira, Dr. Mané Sampaio, Dr. Margarida Santos, Dr. Nuno Borges, Dr Rute Neves, Dr Paula Fareleira, Rui Neves, Anabela Bernardo, Ana Isabel Mingote, Ana Lúcia, Carla Jorge, Carla Patrícia Almeida, Filipa Cardoso, João Cavalheiro, Luís Gafeira, Marta Rodrigues, Melinda Noronha, Paula Gaspar, Rute Castro and Susana Gonçalves for all the help, support and for the good working atmosphere. But especially to Dr Pedro Lamosa for all his patience and teachings regarding theoretical and experimental NMR.

My good friend Dr. Ilídio Correia, for his continuing encouragement and friendship.

My parents and my sister for their continuing support and patience.

Sónia Cardoso for her love, understanding, patience and incentive.

And finally, Fundação para a Ciência e a Tecnologia – PRAXIS XXI, for the financial support that made this doctoral work possible (PRAXIS XXI/BD/21532/99).

ABSTRACT

The human brain is the product of 600 million years of evolution and it is by far the most complex structure in the known universe. The vertebrates' brain is composed of several different cell types, which perform the different functions required. The two most abundant cell types are neurons, which are the brain function unit, and glial cells, which are responsible for a myriad of housekeeping, homeostatic and structural functions. Glial metabolism is so far interconnected with the neuronal metabolism, that it is difficult to state where one finishes and the other starts. Trafficking between the two compartments include metabolites of almost all metabolic pathways (glycolysis, TCA, amino acids, ketone bodies, etc) and also ions.

Nuclear magnetic resonance was used as the primary technique to investigate the effect of ethanol (40, 80, and 160 mM) on the levels of high-energy phosphates, glycolytic flux, anaplerotic and oxidative fluxes to the tricarboxylic acid (TCA) cycle, the contribution of the pentose phosphate pathway (PPP), and the uptake and release of amino acids on primary cultures of rat astrocytes. On line ^{31}P-NMR spectroscopy showed that long-term exposure to ethanol caused a drop in the levels of ATP and phosphocreatine. The ratio between the fluxes through the pyruvate dehydrogenase and pyruvate carboxylase reactions also decreased, whereas the glycolytic flux and the ratio between formation of lactate and glucose consumption increased when cells were exposed to acute doses of ethanol. Flux through the pentose phosphate pathway was not affected. The uptake of cysteine and the release of glutamine were stimulated by ethanol, whereas the release of methionine was inhibited. Moreover, the fractional enrichment in serine was enhanced. The changes in the amino acid metabolism are interpreted as a response to oxidative stress induced by ethanol.

Glutamate metabolism in astrocytes was studied using an experimental set-up that simulates the role of neurons (glutamate producers and glutamine consumers) by the addition of glutaminase to the culture medium. Thereby, a steady supply of glutamate was imposed at the expense of glutamine, and the stress intensity was

manipulated by changing the glutaminase concentration. Glutamate supply rates in the range 8 to 23 nmol/min/mg protein were examined. When the glutamate supply rate exceeded the uptake rate of this amino acid, a transient increase in the extracellular concentration of glutamate was observed. In response to this stress, the fluxes through the glutamate transporter and glutamine synthetase were considerably increased and the extracellular concentration of glutamate was eventually restored to a low level. The increased levels of glutamine synthetase were demonstrated by immunoblotting analysis. The effect on glutamate metabolism of the transaminase inhibitor, AOAA, and of NH_4Cl was also investigated. The accumulation of glutamate caused a concomitant reduction in the levels of phosphocreatine, phosphoethanolamine and phosphocholine without affecting the ATP pool. It was shown that glutamine synthetase is a key element in the control of glutamate metabolism in astrocytic cultures. The metabolic fate of glutamate depended greatly on the time of endurance to the challenge: in naive cells, glutamate was primarily metabolised through the transaminase pathway, while in well-adapted cells glutamate was converted almost exclusively through glutamine synthetase.

We investigated the recycling of lactate between extracellular space and the cytosolic pool of pyruvate through the monocarboxylate transporters of the plasma membrane and the lactate dehydrogenase. For this purpose, primary cultures of astrocytes and neurons were incubated in Krebs Ringer bicarbonate buffer containing 50% ^2H_2O and [3-^{13}C]lactate (1 to 20 mM). Samples of incubation medium were collected at different time points and analyzed by ^{13}C-NMR to determine the deuteration kinetics of [3-^{13}C]lactate. A mathematical model was developed to analyze the time courses of lactate deuteration, which accounted for: (i) the bidirectional lactate transport in and out of the cells, (ii) the intracellular interconversion between lactate and pyruvate catalyzed by lactate dehydrogenase, and (iii) the pyruvate consumption. Results demonstrate that lactate recycling occurs in both cell types and increases with the extracellular concentrations of lactate. In the same conditions astrocytes showed to have a higher lactate recycling activity than neurons, which was due to the differences in the reaction rates of the lactate dehydrogenase isozymes. Lacate dehydrogenase was the rate

limiting step of lactate recycling process and favoured the neuronal pyruvate consumption and the glial lactate production. The use of ^{13}C-NMR spectroscopy to detect deuteration in the geminal and vicinal positions of a carbon-13 labelled precursor proved to be a powerful technique to study hydrogen turnover, providing complementary information to the conventional ^{13}C NMR method used to elucidate carbon turnover.

We report the first approach for growth and maintenance of primary astrocytes in a fully controlled environment. For this purpose, cells were immobilized in Cytodex microcarriers and grown in a stirred tank bioreactor. Crucial bioreaction parameters such as agitation rate, microcarrier type, and concentration, as well as cell inoculum concentration were optimized. Cytodex 3 proved the best microcarrier for astrocyte growth, with the highest cell densities obtained for 6 g/L of Cytodex 3 using an inoculum of approx. 0.15×10^6 cells/mL in vessels operated at 60 rpm, using a re-feed operational mode consisting of complete medium replacement every 5 days. Using such optimized conditions, cells were maintained in steady-state for approximately 24 days, allowing online monitoring and control of environmental variables such as temperature, pH, and O_2. To further test the advantages of this fully controlled system, astrocytes were subjected to a 5 hours hypoxic stress. The cell numbers were not affected by hypoxia but the glycolytic flux was enhanced during this period. To check whether this experimental set-up was suitable for metabolic flux analysis, the metabolism of [U-^{13}C]glucose pulse was followed by ^{13}C-NMR for a period of 24-hour. The culture system described is a novel tool to study brain cell metabolism, allowing sampling over time and the monitoring of cellular behaviour in response to stressful conditions as well as during recovery.

Carbon-13 labelling experiments coupled to ^{13}C-NMR techniques are a valuable tool in metabolic flux analysis. In contrast to other techniques, ^{13}C-NMR allows the collection of quantitative as well as positional information of the ^{13}C label within molecules. These important features allow the characterization of metabolic networks that cannot be approached by any other means. This is accomplished by taking advantage of the ^{13}C homo- and heteronuclear scalar coupling. These multiple couplings result in the splitting of the original ^{13}C resonance into a large number of peaks, which makes the analysis of the ^{13}C-NMR spectra difficult and

requires the use of computer assistance. ^{13}C multiplets are described as the sum of fine-structures (doublets, triplets, quartets, etc). Furthermore, each fine-structure is represented by a sum of positional constrained Pearson type VII functions. This approach provides a means to identify the fine-structures within the multiplets. The use of these simulating routines combined with a least-square fitting procedure enabled the quantification of the areas of these fine-structures in a semi-automatic fashion. This type of program may one day become fully automated, which would greatly increase the informational output of the ^{13}C-NMR techniques.

RESUMO

O cérebro humano é o resultado de 600 milhões de anos de evolução e é de longe a mais complexa estrutura no universo. O cérebro dos vertebrados é composto por vários tipos de células, que executam as diferentes funções (necessárias). Os dois tipos de células mais abundantes são os neurónios, que são as unidades funcionais do cérebro, e as células da glia, que são responsáveis por todo um leque de funções de manutenção, homeoestáticas e estruturais. O metabolismo das células da glia está de tal maneira intercruzado com o metabolismo neuronal, que se torna difícil dizer onde um acaba e o outro começa. O tráfego metabólico entre os dois compartimentos incluiu não só metabolítos de quase todas as vias metabólicas (glicólise, ciclo dos ácidos tricarboxílicos, amino ácidos, corpos cetónicos, etc.), mas também iões.

A ressonância magnética nuclear foi usada como técnica principal para investigar o efeito do etanol (40, 80, 160 mM) nos níveis dos fosfatos energéticos, no fluxo glicolítico, nos fluxos anapleroticos e oxidativos de entrada no ciclo dos ácidos tricarboxílicos, na contribuição relativa da via dos fosfatos de pentose e no transporte e libertação de amino ácidos em culturas primárias de astrócitos de rato. Espectroscopia de RMN de ^{31}P em tempo real mostrou que exposições longas ao etanol causam uma descida nos níveis de ATP e fosfocreatina. A razão entre os fluxos através das reacções de desidrogenase e de carboxilase do piruvato também apresentaram uma diminuição, enquanto que o fluxo glicolítico e a razão entre a formação de lactato e o consumo de glucose aumentaram quando as células foram expostas a doses agudas de etanol. No entanto, o fluxo através da via dos fosfatos de pentose não foi alterado. O transporte de cisteína e a libertação de glutamina foram estimulados pelo etanol, enquanto que a libertação de metionina foi inibida. Além de mais, o enriquecimento fraccional na serina foi aumentado. As variações sofridas ao nível do metabolismo dos amino ácidos foram interpretadas como uma resposta ao stress oxidativo induzido pelo etanol.

O metabolismo do glutamato em astrócitos foi estudado usando um sistema experimental que simula a presença dos neurónios (como produtores de

glutamaina e consumidores de glutamato) por adição de glutaminase ao meio de cultura. Deste modo impôs-se um fluxo estável de glutamato à custa de glutamina e a intensidade do stress foi manipulada por alteração da concentração de glutaminase. Foram estudadas taxas de produção de glutamato entre 8 e 23 nmol/min/mg de proteína. Quando a taxa de produção de glutamato era superior à taxa de transporte deste amino ácido, observou-se um aumento transiente da concentração extracelular de glutamato. Em resposta a este stress, os fluxos através do transportador de glutamato e da sintetase de glutamina foram consideravelmente aumentados, o que levou, eventualmente, a que a concentração extracelular de glutamato voltasse para valores baixos. Foi possível observar por análise imunológica um aumento dos níveis de sintetase de glutamina. Foram também estudados os efeitos do ácido amino-oxoacético e do cloreto de amónio no metabolismo de glutamato. A acumulação de glutamato causou uma redução concomitante nos níveis de fosfocreatina, fosfoetanolamina e fosfocolina, sem no entanto afectar os níveis de ATP. Demonstrou-se que a sintetase de glutamina é um elemento fundamental no controlo do metabolismo de glutamato em astrócitos. O destino metabólico do glutamato depende grandemente do tempo a que as células estiveram sujeitas ao stress: em células que nunca foram expostas a glutamato, este foi primordialmente metabolizado pela via da transaminase, enquanto que em células adaptadas à presença de glutamato, este é quase exclusivamente metabolizado pela sintetase de glutamina.

Investigamos a reciclagem de lactato entre o espaço extracelular e o piruvato intracelular, através dos transportadores de monocarboxilatos da membrana plasmática e do desidrogenase de lactato. Para isto, culturas primárias de astrócitos e de neurónios foram incubadas em tampão de bicarbonato Krebs Ringer contendo 50% de $^{2}H_{2}O$ e [3-^{13}C]lactato (1 to 20 mM). Amostras do meio de incubação foram recolhidas a diferentes tempos e analisadas por RMN de ^{13}C para determinar a cinética de deuteração do [3-^{13}C]lactato. Um modelo matemático foi desenvolvido para analisar o curso da deuteração do lactato, que teve em conta (i) o transporte bidireccional de lactato para dentro e fora das células, (ii) a interconversão entre lactato intracelular e piruvato catalizada pelo desidrogenase

de lactato, e (iii) o consumo do piruvato. Os resultados demonstram que a reciclagem de lactato ocorre em ambos os tipos da células, aumentando com a concentração extracelular de lactato. Nas mesmas circunstâncias os astrócitos mostraram ter uma actividade de reciclagem de lactato mais elevada do que os neurónios, devido às diferenças nas taxas de reacção dos isoenzimas de desidrogenase de lactato. Os resultados apontam para que o desidrogenase de lactato seja o passo limitante do processo de reciclagem do lactato, favorecendo o consumo neuronal de piruvato e a produção glial de lactato. O uso da espectroscopia de RMN de ^{13}C para a detecção da deuteração em posições geminais e vicinais a um carbono 13, mostrou ser uma técnica poderosa para o estudo da substituição do hidrogénio, fornecendo informações complementares ao método RMN de ^{13}C convencionalmente usado para elucidar substituições em carbonos.

Relatamos aqui, a primeira tentativa para efectuar o crescimento e manutenção de culturas primárias de astrócitos num ambiente inteiramente controlado. Para este fim, as células foram imobilizadas em micro-suportes Cytodex e cultivadas num bio-reactor agitado. Os parâmetros mais importantes da bio-reacção tais como a taxa de agitação, o tipo e concentração de micro-suportes, assim como a concentração do inóculo de células foram avaliados. O Cytodex 3 provou ser o melhor suporte para o crescimento dos astrócitos. As densidades celulares mais elevadas foram obtidas com 6 g/L de Cytodex 3, usando um inóculo de aproximadamente 0.15×10^6 celulas/mL, em bio-reactor operado a 60 RPM, com trocas completas de meio todos os 5 dias. Nestas condições, as células foram mantidas em estado estacionário, aproximadamente 24 dias, o que permitiu monitorizar e controlar, em tempo real, parâmetros ambientais, tais como a temperatura, o pH, e o oxigénio. Para testar as vantagens deste sistema inteiramente controlado, submeteram-se astrócitos a um período de 5 horas de hipóxia; o número de células não foi afectado pela hipóxia mas o fluxo glicolítico foi superior durante o "stress" imposto. Verificou-se ainda se este sistema experimental era apropriada para a análise de fluxos metabólicos. Para isso, seguiu-se o metabolismo de [U-^{13}C]glucose por RMN de ^{13}C durante 24 horas. O sistema da cultura aqui descrito constitui uma nova ferramenta para o estudo do

metabolismo de células de cérebro, permitindo a amostragem ao longo do tempo e a monitorização do comportamento celular em resposta a condições de "stress", assim como durante os correspondentes períodos de recuperação.

As experiências com carbono marcado com ^{13}C acopladas a técnicas de RMN de ^{13}C constituem ferramentas valiosas na análise dos fluxos metabólicos. Em contraste com outras técnicas, RMN de ^{13}C permite a obtenção de dados quantitativos assim como de informação posicional dos carbonos marcados com ^{13}C dentro das moléculas. Estas características importantes permitem a caracterização das redes metabólicas que não poderiam ser determinadas por outros meios. Para isto, faz-se uso dos acoplamentos escalares homo e heteronucleares do ^{13}C. Estes acoplamentos múltiplos resultam na divisão das ressonâncias originais do ^{13}C em um grande número picos, o que torna a análise dos espectros de RMN de ^{13}C difícil, requerendo o auxílio de computadores. Os multipletos de ^{13}C foram descritos, matematicamente, como a soma de estruturas finas (dupletos, tripletos, quadrupletos, etc.). Além disso, cada estrutura fina pode ser representada por uma soma de funções de Pearson tipo VII. Esta aproximação fornece os meios para identificar as estruturas finas dentro dos multipletos. O uso destas rotinas de simulação combinadas com um procedimento apropriado de ajuste de parâmetros pelo método da minimização da soma dos quadrados das diferenças permitiu a quantificação das áreas destas estruturas finas de uma forma semi-automática. Este tipo de programa pode um dia tornar-se completamente automatizado, o que aumentaria em muito o volume de informação obtida através das técnicas de RMN de ^{13}C.

CONTENT

THESIS OUTLINE

Astrocytes are a very important part of the metabolic puzzle we call brain. Given that until the year 2000 there hadn't been any work done towards the full determination of the metabolic fluxes in cultures of primary astrocytes, we selected this goal as our final target.

In chapter 1, an introduction to the metabolism of astrocytes is made. Since this thesis is the second one coming from the same lab and almost on the same subject, an attempt was made to produce a different introduction to the metabolism of brain cells. Therefore, this introduction targeted the astrocytes, which are the "stars" of this work, and focused on the metabolic interactions between these cells and neurons.

The measurement of the metabolic fluxes *per se*, although not yet accomplished, was thought to be more meaningful if coupled to a stressful condition. In this way we would known not only the distribution of the fluxes in control conditions but also how cells react, metabolically, to a given stress. From the search of an interesting, easily applied stress, emerged chapter 2. In this chapter the metabolism of ethanol was investigated. The astrocytic metabolism showed to be quite resistant to the effects of this substance, and in order to get some measurable differences between control and ethanol exposed cells, ethanol concentrations had to be increased up to 180 mM (8.3 g/L). Given that the maximum permitted by Portuguese law for the blood alcohol concentration is 0.5 g/L, that above 1.2 g/L it is considered a felony resulting in the imprisonment and that for the average unaccustomed person 4.8 g/L of alcohol results in coma, ethanol was, in the end, considered a bad candidate for a possible stressful agent in the metabolic flux determination. Practical reasons also determined ethanol to be excluded, as this is a volatile substance which evaporated from the culture medium and required either a special apparatus to get constant concentrations, or in open systems, its concentration had to be monitored and corrected as the experiment developed. Nevertheless, the effects of different concentrations of ethanol on the levels of high-energy phosphates, glycolytic flux, anaplerotic and oxidative fluxes to the tricarboxylic acid cycle, the contribution of the pentose phosphate pathway, and the uptake and release of amino acids on

primary cultures of rat astrocytes are presented and discussed in this chapter. The work reported in this chapter also showed the need for a procedure that would allow for the deconvolution of ^{13}C-NMR multiplets, as this would be a task required for the determination of fluxes. This program was developed and described in appendix 1.

In chapter 3, glutamate was evaluated as a stressful agent for astrocytes. However the astrocytic capacity to take up this amino acid did not favour its use for metabolic flux analysis, since glutamate metabolism is fast and glutamate concentrations decrease rapidly. Also, there is physiological limit to the concentrations one can subject cells to. To solve these problems a process capable of delivering a constant supply of glutamate was devised. In order to supply astrocytes with a constant flux, glutaminase was introduced in the incubation medium, thus ensuring the conversion of glutamine, present in the medium, into glutamate and ammonia. This method has the advantage of, artificially, closing the glutamate-glutamine cycle, which is an incomplete cycle in astrocyte cultures due to the lack of neurons. The usage of this method allowed us to study the glutamate-glutamine cycle in a more realistic manner. In this chapter this process was characterized and the effects of glutaminase on cultures of astrocytes analysed and discussed.

Previous observations revealed that astrocytes were able to produce lactate from glucose or, in the absence of glucose, consume lactate. This feature required clarification in order to be correctly modelled. Also, this type of bidirectional transport may not be restricted to lactate transport, which increases the importance of this type of studies. Glutamine transport by astrocytes, which plays a central role in brain metabolism, may also show similar properties. However, to study the transport of any given substance in both directions is not an easy task. This difficulty was solved by the system recently developed by Dr. Sebastián Cerdán, capable of studying fast exchange by ^{13}C-NMR. In chapter 4, we apply Dr. Cerdán's method to the recycling of lactate through the plasma membrane up to the level of the lactate dehydrogenase in primary cultures of neurons and astrocytes.

In chapter 5, we study alternative methods of culturing astrocytes, compatible with metabolic flux analysis. Given that mono-layer culturing systems are not usable, as

they do not allow the medium composition to be monitored or controlled, cell growth can not be measured and sampling of medium and cells, simultaneously, is not possible in the same culture. For these reasons a reactor system was developed and its operation mode characterized and optimized.

In chapter 6, the final remarks are made.

In appendix 1, it is shown how a software tool, for the deconvolution of ^{13}C NMR multiplets may be implemented. This software tool allows a faster and more reliable method of integrating NMR peaks. Given the higher amount of information gathered from ^{13}C NMR experiments performed either with multiple (uniformly) labelled ^{13}C enriched substrates or with other nuclei, it is essential to have a process capable of performing the determination of the areas of very closed together peaks. These peaks arise from homo- or heteronuclear scalar coupling, and are almost always semi-superimposed, which makes the standard area-determining processes unreliable. In this chapter multiplets were modelled as sums of fine-structures, which in turn were modelled as sums of positional constrained NMR peaks. NMR peaks do not have a pure Gaussian or Lorentzian distributions, being more accurately described by the Voigthian function. However, this function is difficult to work with and to integrate so another function was proposed to simulate a NMR peak – the Pearson type VII function.

ABBREVIATIONS

2D NMR	Two dimensional nuclear magnetic resonance
AA	Ascorbic acid, vitamin C
AAT	Alanine aminotransferase, EC 2.6.1.2
ADP	Adenosine diphosphate
AGC1	Aspartate/glutamate carrier 1
Ala	Alanine
ANLS	Astrocyte-neuronal lactate shuttle
AOAA	Aminooxyacetic acid
AP	Action potential
ATP	Adenosine triphosphate
BCAT	Branched-chain amino acid aminotransferase, EC 2.6.1.42
BMG	Basement membrane gel
BSA	Bovine serum albumin
c	Center
CA	Carbonic anhydrase
CNS	Central nervous system
COSY	Correlation spectroscopy
Cys	Cysteine
CysGly	Cysteinylglycine
GSSG	Oxidized glutathione
DHA	Dehydroascorbate
DMEM	Dulbecco's modified Eagle's medium
DNA	Deoxyribonucleic acid
EAAT	Excitatory amino acid transporter
ECF	Extracellular fluid
EDTA	Ethylenediaminetetraacetic acid
FAS	Foetal alcohol syndrome
FBS	Foetal bovine serum
$F_{Glycolysis}$	Glycolytic flux

FID	Free induction decay
F_{Lacate}	Lactate release flux
GDH	Glutamate dehydrogenase, EC 1.4.1.2
GFAP	Glial fibrillary acidic protein
GLAST	Glutamate/aspartate transporter
Glc	Glucose
Gln	Glutamine
Glnase	Glutaminase, EC 3.5.1.2
GlnT	Glutamine transporter
GLT	Glutamate transporters
GLT-1	Glutamate transporter 1
Glu	Glutamate
GLUT	Glucose transporter
GluT	Glutamate transporter
GLUT1	Glucose transporter 1
GLUT3	Glucose transporter 3
Gly	Glycine
GS	Glutamine synthetase, EC 6.3.1.2
GSH	Glutathione (reduced)
GUI	Graphical user interface
h	Height
HPLC	High-performance liquid chromatography
HS	Horse serum
IgG	Immunoglobulin G
KIC	α-Ketoisocaproic acid
Lac	Lactate
LDH	Lactate dehydrogenase, EC 1.1.1.27
LDH-1	Lactate dehydrogenase isoform 1
LDH-5	Lactate dehydrogenase isoform 5
Leu	Leucine
MCT	Monocarboxylate transporter
MCT1	Monocarboxylate transporter 1

MCT2	Monocarboxylate transporter 2
MCT4	Monocarboxylate transporter 4
MLI	Multiplet line intensity
Na^+/K^+ ATPase	Na^+/K^+ exchanger, EC 3.6.3.9
NADH	Nicotinamide adenine dinucleotide
NMR	Nuclear magnetic resonance
NTP	Nucleoside triphosphate
O1P	Transmitter frequency offset 1
p	Parameter p of the Pearson type VII function
PAG	Phosphate-activated glutaminase, EC 3.5.1.2
PBS	Phosphate-buffered saline
PC	Pyruvate carboxylase, EC 6.4.1.1
PCr	Phosphocreatine
Pd	Probability of deuteration
PDH	Pyruvate dehydrogenase (lipoamide) complex, EC 1.2.1.51
Pi	Inorganic phosphate
$Pi_{(ext)}$	Extracellular inorganic phosphate
$Pi_{(int)}$	Intracellular inorganic phosphate
PNS	Peripheral nervous system
ppm	Parts per million
PPP	Pentose phosphate pathway
prot	Protein
Pyr	Pyruvate
SAT1	System A transporter 1
SDS-PAGE	Sodium dodecyl sulfate polyacrylamide gel electrophoresis
SI	Size of real spectrum
SN1	System N transporter 1
SVCT2	Sodium-dependent vitamin-C transporter 1
SW	Spectral width
TA	Transaminase
TBS	Tris-buffered saline
TCA	tricarboxylic acid

Tris	2-amino-2-hydroxymethyl-1,3-propanediol
V_e	Extracellular volume
V_i	Intracellular volume
w	Width
WALTZ	Wide-band alternating phase low power technique for zero-residue splitting
αKG	α-ketoglutarate or 2-oxoglutarate
γ-ATP	Refers to the γ-phosphate of an ATP molecule
γGluCys	γ-Glutamylcysteine
γGT	γ-glutamyl transferase, EC 2.3.2.2
γ-NTP	Refers to the γ-phosphate of a NTP molecule

CHAPTER 1

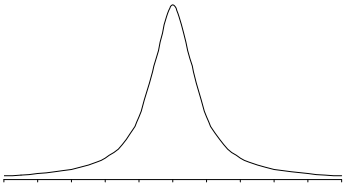

Introduction

Chapter | 1 | Contents

The Brain

Since the appearance of the first animals on this planet that the development of nervous systems was a highly favoured process throughout evolution. Nervous systems allowed animals to react to and interact with the environment with unpreceding speed and complexity, paving the way to the development of more complex animals. The first nervous systems were simple nerve nets, but early in the evolution nature began to concentrate nervous cells in small aggregates, resulting in the appearance of ganglia, as is the case of *Platyhelminthes*, which have a nervous system composed of several interconnected ganglia. In the course of evolution the head ganglion became larger and more complex, and ended up taking over the other ganglia, resulting in a brain. The brain together with the spinal cord form the central nervous system (CNS) which processes and controls all motor and sensor functions and is also responsible for memory and behaviour. (Thompson, 1993)

The brain comprises several types of cells that can be generally divided in neurons and glia. Neurons are the brain's functional unit. They are very specialized cells committed to the transport and processing of the nervous signal. Neurons are classified functionally into three categories: sensory neurons, interneurons and motor neurons. In essence they play the three different roles of an informational system: input, process and output. Sensory neurons transform physical stimuli into electrical signals and deliver these signals to the interneurons. Interneurons are the most abundant type of neurons and are organized in networks responsible for most of the complex computations that produce behaviour. Motor neurons innervate the effector organs (like the muscles or gland cells) and are in charge of sending the output signals to the organ responsible for the resulting action (physical or chemical). Neurons transport the nervous signal electrically throughout their dendrites, cell bodies and axons and transmit nervous signals from one neuron to the next, chemically (with rare exceptions), through the synapses. In resting conditions the neuron has an asymmetric distribution of sodium and potassium ions across its cytosolic membrane, thus maintaining the neuronal membrane polarized. The polarization results from the action of the Na^+/K^+ ATPase, which pumps three Na^+ ions out and two K^+ ions into the cell for each ATP molecule hydrolysed. The

nervous signal consists in a depolarization of the neuronal membrane, which is transmitted along the dendrites and axons in a unidirectional way. The depolarization is possible due to the presence of special proteins of which the voltage-gated Na^+ and K^+ channels are the most important. Thus the passage of a signal is accompanied by short local increases of extracellular K^+ and intracellular Na^+. When the signal (depolarization) reaches the axon terminal, the presynaptic element, special voltage-gated Ca^{2+} channels, allow the entry of Ca^{2+}, which causes the synaptic vesicles to fuse with the presynaptic membrane and release the neurotransmitter into the synaptic cleft. Once released, the neurotransmitter molecules diffuse and bind the ligand-gated ion channels in the post-synaptic membrane, which may lead to the depolarization of the next neuron. The neurotransmitter is either enzymatically inactivated and the products recycled by the presynaptic element, or removed by the neurons involved in the synapse or by a neighbouring cell.

It was Rudolf Virchow who first named glial cells back in the XIX century, as neuroglia. These cells were named after what was thought to be their only function, neuro glue ('Nervenkitt'), i.e. the glue that holds neurons together (Dermietzel and Spray, 1998; Perea and Araque, 2002; Kimelberg, 2004). Nowadays glial cells are recognized as having several other functions besides providing mere physical support to neurons. Studies on glial cells in the last years have been changing our views on the fundamental neuronal liaison, the synapse, and what was once considered to be a purely neuronal affair is now recognized as a '*ménage à trois*', where the glial cells play a very important third-party role in the formation, induction, maturation, maintenance and termination of the relationship between the two partners (Araque *et al.*, 1999; Pfrieger, 2002; Slezak and Pfrieger, 2003). Moreover, from an evolutionary point of view the presence of multifunctional glial cells, may have allowed the neuronal evolution to follow a path of progressive specialization, which resulted in a neuronal cell highly specialized in processing, encoding and transferring information. The phylogenetic analysis is quite clear: in leeches a ganglion with 25 to 30 neurons has only one glial cell; in a human brain there are 1.4 astrocytes per neuron (Nedergaard *et al.*, 2003). As the nervous systems grew in complexity it became necessary to isolate the different circuits to avoid cross talks. (Laming *et al.*, 2000) Glial cells may have evolved to isolate the different

components and avoid events such as neurotransmitter spill over from neighbouring synapses.

Glial cells are divided into macroglia and microglia. The microglia are not true glial cells but originate from the immune system and invade the brain during gestation. Their main function is to provide some immunological defence in the brain. Macroglia encompasses the myelinating glia, the ependymoglia and the astrocytes. Oligodendrocytes and their peripheral nervous system (PNS) counterparts, the myelinating Schwann cells, are responsible for the myelination of the neuronal axons to attain electrical insulation and achieve higher rates of signal transmission. These cells achieve this goal by ensheathing the axons with several layers of extensions of their own cytoplasmatic membrane. During the myelination process the membranes are enriched in special lipids like cholesterol, cerebrosides and ethanolamine phospholipids. Ependymoglia are an important group of cells that line the interior of the cerebral ventricles and other cavities of the brain and spinal cord. Ependymoglia include the tanycytes, which form the ventricular cerebrospinal fluid interface, the ependymal cells in the pia limitans, and the Müller cells in the retina. Astrocytes, as the name reveals, are star-shaped cells with non-excitable membranes, responsible for the majority of the housekeeping functions in the brain. Apart from being responsible for the physical support of the brain during development, the astrocytes assist in the guidance of neurons, axons and dendrites, and intervene in the formation (and destruction) of synapses. In the mature brain, astrocytes are responsible for the formation and maintenance of the blood-brain barrier, for the removal of neurotransmitters (either by uptake or by enzymatic inactivation), for the control of the composition of the extracellular fluid, and for the supply of nutrients and the removal of products of neuronal metabolism. By evolving into cells capable of performing all housekeeping functions needed by neurons, the astrocytes released the neurons from these tasks, allowing them to evolve into very specialized cells in the transmission of the nervous signal. Thus, the more complicated the nervous system got, i.e. the higher an animal is in the phylogenetic tree, the greater was the demand on astrocytes to sustain an increasingly specialized number of neurons.

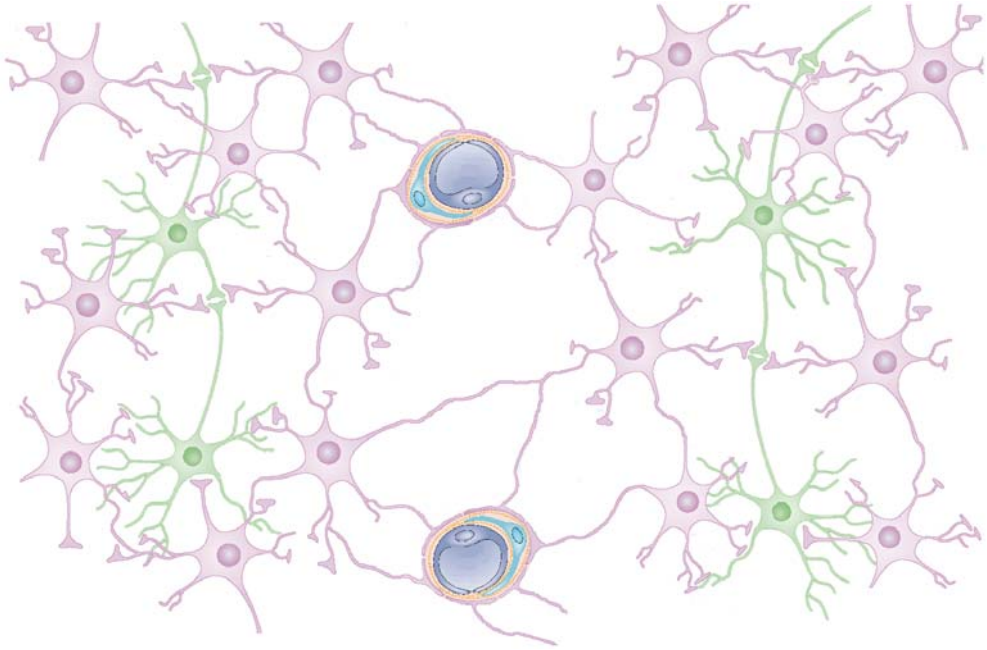

Figure 1.1 – Astrocityc connections to the different brain components. Astrocytes (in purple) establish connections to the neuronal perikarya and the synapses (in green) and to the capillaries (in blue). The blood brain barrier is formed by the tight apposition of the capillary endothelial cell (in dark blue), the basal lamina (in orange) and the astrocytic perivascular endfeet. Also, astrocytes interact with each other through gap junction, forming the astrocytic syncytium. In light blue are represented the pericytes. Adapted from (Abbott *et al.*, 2006).

Neuronal-Glial Metabolism

The neuronal-glial association developed early in the evolution of the CNS and resulted in a "borderless" brain metabolism, where metabolic cross-talk between both cell types occurs at several points throughout the main metabolic pathways. In order to understand metabolism it is important to take into account the spatial distribution of the different cells in the brain. Neurons form wide networks, connecting to each other through synapses, and forming the different functional regions of the brain. Glia surrounds neurons, blood vessels, and other structures, being thus strategically located to enable the trafficking of metabolites and ions to and from neurons (Fig 1.1). Also, the blood brain barrier is a structure formed from the interaction of astrocytic perivascular endfeet and the endothelial cell which lines the walls of the capillaries. This structure imposes severe restrictions on the free diffusion between the blood components and the extracellular brain space.

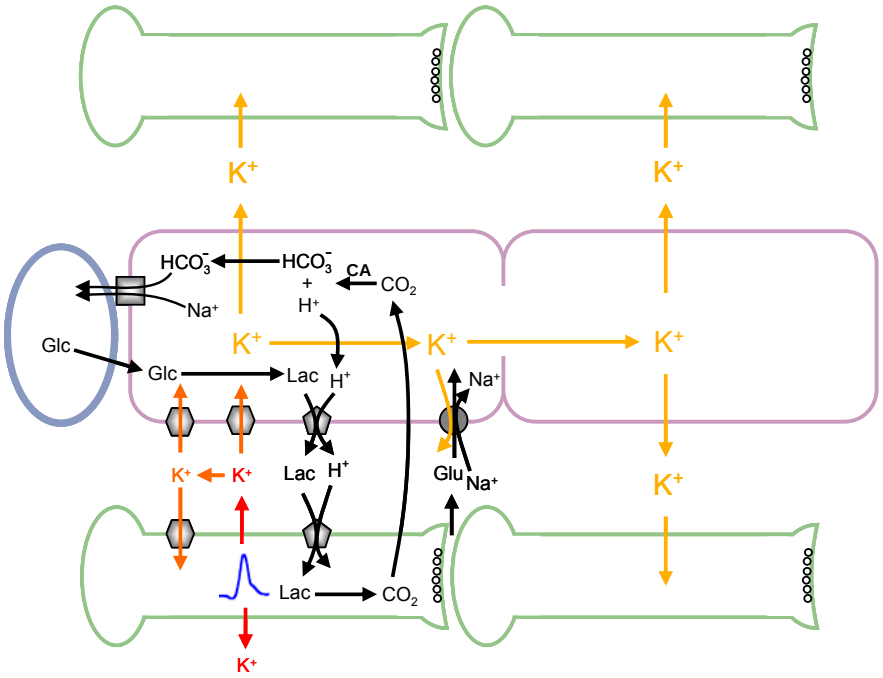

Figure 1.2 – The neuronal-astrocytic ionic interactions. As the action-potential (AP, in blue) travels down the axon (in green), depolarization results in the movement of sodium ions inwards (not shown) and potassium ions outward (in red). After the AP, the neuronal membrane repolarizes by the action of the Na^+/K^+ ATPase (⬡), which is also responsible for the astrocytic uptake of potassium. In astrocytes (in purple), the potassium ions can be spatially buffered (through the syncytium) and used either to prime adjacent neurons for the arrival of an AP, or for the transport of glutamate by the EAAT (●). The K^+ movements are shown with colored arrows. Neuronal repolarization is an ATP requiring process, which must be balanced by respiration. Due to the low neuronal carbonic anhydrase (**CA**) activity, CO_2 diffuses out to the astrocytes where this enzyme turns it into bicarbonate and hydrogen ions. The bicarbonate ions can then be released into the capillaries (grayish blue) by the sodium-bicarbonate cotransporter (▭) or other transporters present in astrocytes. Resulting protons may be used to drive lactate transport (⬠) from astrocytes to neurons to be oxidized to CO_2.

Furthermore, astrocytes are connected to each other through specialized structures called gap junctions, which enable direct intercellular communication between the cytoplasm of neighbouring cells, forming what is denominated a panglial syncytium (Fig 1.1). Given the wide number of interactions between astrocytes and neurons, these will be divided in two kinds: ionic and metabolic.

Ionic Interactions Between Astrocytes and Neurons

The transport of the nervous signal is associated with ions fluxes, especially K^+ and Na^+. Furthermore, cerebral metabolism can also lead to the production ions. In

Figure 1.2 are illustrated some of the ionic interactions between astrocytes and neurons. Upon the action potential-dependent K^+ release, astrocytes, having a relatively high K^+ permeability and a more negative membrane potential than neurons (Walz, 1989; Deitmer, 2001), take up this ion through the K^+/Na^+ ATPase (Ransom *et al.*, 2000). This aids the neurons repolarization and protects them from elevated extracellular K^+ concentrations (Laming *et al.*, 2000). The astrocytic transported K^+ can then be redistributed throughout the syncytium via the gap junctions (spatial buffering) and either used for the uptake of glutamate, in synaptic regions, or may be released in regions where the K^+ equilibrium potential is more negative than the membrane potential (Ransom *et al.*, 2000). Ultimately, the end product of oxidative metabolism is CO_2. However, the carbonic anhydrase (CA), which reversibly catalyses the conversion of carbonic acid to protons and bicarbonate ions, is present mainly in glia and endothelial cells (Giacobini, 1961; Cammer and Tansey, 1988; Cammer and Zhang, 1991; Nogradi *et al.*, 2003), thus making astrocytes the removers of neuronal CO_2. The bicarbonate ions generated in this way are then exchanged with Na^+ ions, with a 2:1 stoichiometry, using the electrogenic transmembrane-gradient. The protons may either be expelled through the H^+/Na^+ exchanger, or used to drive lactate out of the astrocytes through the monocarboxylate transporter (MCT, for review see Laming *et al.*, 2000; Deitmer, 2001).

Metabolic Trafficking

Cerebral energy consumption is very high. Although the human mature brain only weighs 2% of the total body weight, it consumes 25% of the body's energy supply, 20% of total body oxygen, and receives 15% of the cardiac output (Clarke and Sokoloff, 1994; Wiesinger *et al.*, 1997). In resting conditions the oxygen consumption to glucose utilization ratio is 5.5, indicating that more than 90% of the consumed glucose is completely oxidized to CO_2 and H_2O (Clarke and Sokoloff, 1994). Nevertheless, this does not reveal where the glucose is actually oxidized. According with the astrocyte-neuronal lactate shuttle (ANLS) hypothesis (Pellerin and Magistretti, 1994), astrocytes take up the blood-borne glucose, through GLUT1 (Morgello *et al.*, 1995) and metabolise it to pyruvate via glycolysis (Embden-Meyerhof pathway). Pyruvate is then oxidised to lactate by the lactate dehydrogenase isoform 5 (LDH-5) and released through the monocarboxylate

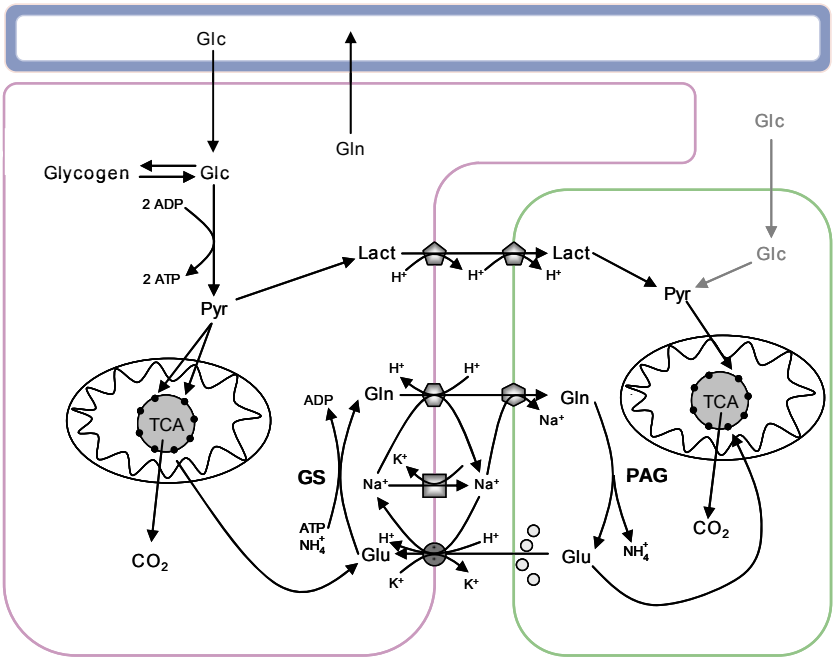

Figure 1.3 – The glutamate-glutamine cycle. The glutamate released from presynaptic terminals (in green) by exocytosis is taken up by astrocytes (in purple), where it is converted to glutamine by glutamine synthetase (**GS**). Glutamine is then released back to the neurons, where glutamate is regenerated via phosphate-activated glutaminase (**PAG**). Glutamate uptake is performed by the glutamate transporters GLT and GLAST (●) with co-transport of 3 Na^+ and 1 H^+ ions in exchange with 1 K^+ ion. Glutamine exits astrocytes through the SN1 transporter (⬡) down its own gradient and is co-transported with a Na^+ ion against its gradient, thus minimizing ATP expenditure by the Na^+/K^+ ATPase (■). This ATPase maintains the Na^+ and K^+ gradients by pumping 3 Na^+ ions out and 1 K^+ ion for each ATP molecule hydrolyzed. Glutamine is taken up by the neurons through the SAT1 transporter (⬡) with co-transport of 1 Na^+ ion. Transported H^+ may facilitate the release of lactate by astrocytes through the MCT (⬠). A blood vessel is represented in blue.

transport 1 (MCT1) and 4 (MCT4) (Hertz and Dienel, 2005). Lactate can be taken up by the neuron (through MCT2), where it is oxidised back to pyruvate (through LDH-1). Pyruvate is oxidised via the tricarboxylic acid (TCA) cycle to fuel the energy-consuming processes.

Glutamate-Glutamine Cycle

In performing their duty glutamaergic neurons continually release glutamate, sinaptically. However, given the high glutamate concentrations in the neuronal cytosol required for their task, it is thermodynamically unfavourable for them to take up glutamate. Moreover, the glutamate transporters are usually located post-

synoptically (Dehnes *et al.*, 1998). Astrocytes, on the other hand, have low intracellular glutamate concentrations, which made them better candidates to perform this function. Astrocytes remove glutamate through glutamate transporters (GLT-1 and GLAST (for review (Anderson and Swanson, 2000; Danbolt, 2001), which co-transport glutamate with 3 Na^+ and one H^+ in exchange with one K^+ ion (Fig 1.3). This is a pricey stoichiometry, which costs about 1 ATP per glutamate transported by astrocytes, but ensures that glutamate can be transported through very steep gradients and, consequently, a low extracellular concentration (ca 1-5 μM) can be maintained. Intracellularly, glutamate is metabolized to glutamine by the action of the enzyme glutamine synthetase (GS), that is localized specifically in glial cells (Martinez-Hernandez *et al.*, 1977). Once formed, glutamine can be exported either to blood (brain nitrogen homeostasis) or to neurons. Astrocytes and neurons possess different but related glutamine transporters (for review (Broer and Brookes, 2001; Chaudhry *et al.*, 2002). Astrocytes export glutamine through a system N transporter (SN1), which co-transports 1 Na^+ in exchange for 1 H^+ by an electroneutral mechanism (Chaudhry *et al.*, 1999). By exchanging one H^+, this transporter reduces the transmebrane gradient of glutamine to about 20 (in/out) under physiological conditions (Kanamori and Ross, 2005). However, it ensures that the transport can be performed in both directions, thus placing astrocytes in the position of controlling the extracellular concentrations of glutamine. On the other hand, the neuronal counterpart is a system A transporter (SAT1 or GlnT, ATA1, SA2), which co-transports glutamine with one Na^+ ion by an electrogenic mechanism. This process couples the uptake of glutamine not only to the sodium gradient but also to the membrane potential, thus allowing the establishment of a glutamine gradient of >100 fold (Chaudhry *et al.*, 2002) and ensuring the directionality of the glutamine transport. In the neuron, glutamine is converted back to glutamate by the phosphate-activated glutaminase (PAG) located in the outer face of the inner mitochondrial membrane (Kvamme *et al.*, 2001). This is known as the glutamate-glutamine cycle and is mainly powered in astrocytes, at the level of the transport of glutamate, which dissipates the sodium-potassium gradient maintained at the expense of ATP by the Na^+/K^+ ATPase (for review Silver and Erecinska, 1997), and at the level of the glutamine synthetase, which uses 1 ATP for each glutamine produced (Fig 1.3). Pellerin and Maggistretti (1994) suggested that the ATP consumption associated with the glutamine synthetase and the Na^+/K^+ ATPase to take up and convert glutamate to

glutamine induces the activation of the astrocytic glycolysis. In this way, activity in the glutamate-glutamine cycle increases the glycolytic flux, which produces the required 2 ATP for this cycle and 2 lactate molecules used to fuel the neuronal metabolism. It has also been shown, by NADH fluorescence imaging, that astrocytes have a substantial cytoplasmatic NADH fraction, indicative of a higher glycolytic capacity, whereas neurons exhibit a granular distribution of NADH compatible with a mitochondrial origin (Kasischke *et al.*, 2004). Moreover, the same authors also provide compelling evidence that neuronal stimulation leads to an increase in the astrocytic glycolysis, compatible with a stimulation-dependent astrocyte to neuron lactate transfer. Although these results confirm the ANLS hypothesis there are still a number of points not fully explained (for review see Gladden, 2004), one of which is the fact that neurons do express a glucose transporter (GLUT3, Vannucci *et al.*, 1997). This suggests that neurons also consume glucose, present in the extracellular space of the cortex in a concentration of 1.66 and 0.82 mM in rats and humans, respectively (Abi-Saab *et al.*, 2002). In order for this to occur, either glucose can pass through the vessels to the extracellular fluid (ECF), avoiding the blood-brain barrier, or the glial syncytium allows the diffusion of glucose. This latter hypothesis seems unlikely due to the presence of hexokinase and the absence of glucose 6-phosphate phosphatase (Gotoh *et al.*, 2000). The balance of metabolites in this cycle is performed by both cells. However, while neurons are only able to remove glutamate by oxidation via the TCA cycle, astrocytes are also able to produce glutamate from glycolytic precursors, by carboxylation of pyruvate to oxaloacetate (Yu *et al.*, 1983; Shank *et al.*, 1985; Cesar and Hamprecht, 1995). This astrocytic enzyme, pyruvate carboxylase, performs the anaplerotic reaction that allows the synthesis of glutamate from the TCA metabolite, α-ketoglutarate. Astrocytes are able to remove the excess of glutamate by either oxidation through the TCA cycle, like neurons, or by releasing glutamine into the blood-stream.

Nitrogen Shuttling

One major consequence of the glutamate-glutamine cycle is the net transport of nitrogen from the astrocytic to the neuronal compartment. In order to maintain a nitrogen homeostasis a method of shuttling the nitrogen back to astrocytes should exist. Due to the toxic nature of the ammonium ion it is unlikely, but not impossible (Marcaggi and Coles, 2001), that these ions are transported back to the astrocytic

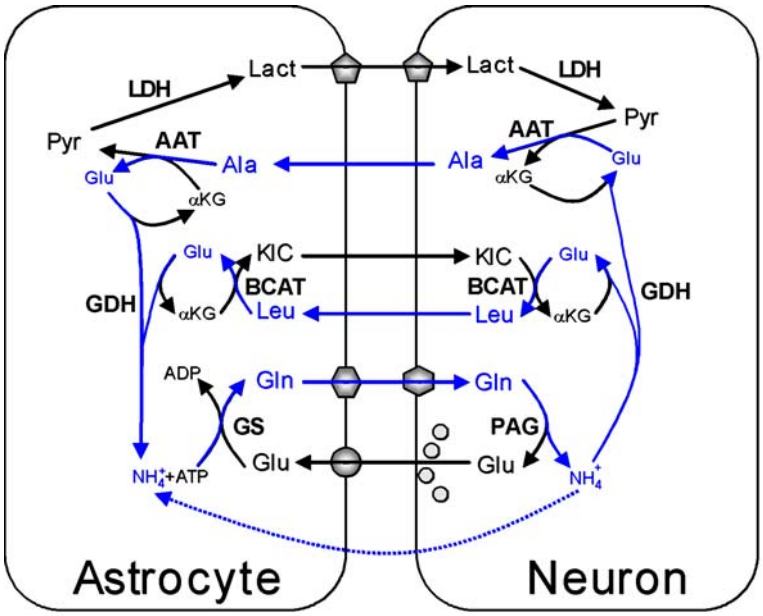

Figure 1.4 – Nitrogen shuttling between astrocytes and neurons. Schematic representation of the glutamate-glutamine cycle, the lactate-alanine shuttle, and branched-chain amino acid nitrogen cycle between glutamatergic neurons and astrocytes. Glutamine is deaminated in the neuronal compartment to glutamate and ammonium ions by the phosphate-activated glutaminase (PAG). The nitrogen shuttle models propose that these ions can be used to aminate α-ketoglutarate to glutamate by the glutamate dehydrogenase (GDH), which then passes the amino group to pyruvate or to α-ketoisocaproate (KIC) by either the alanine or the branched-chain amino acid aminotransferases (AAT or BCAT) to form alanine or leucine, respectively. These amino acids would be then released by neurons and taken up by astrocytes, which would use the same enzymatic activities to generate free ammonium. The ammonium could be re-used in the

compartment in this form (Fig. 1.4.). In 1996, Yudkoff and coworkers (Yudkoff *et al.*, 1996b; Yudkoff *et al.*, 1996a) proposed the existence of a branched-chain amino acid nitrogen cycle where α-ketoisocaproate or α-ketoisovalerate were the potential candidates to transport the ammonium back to astrocytes in the form of their amino conjugates leucine and valine, respectively. Once in the astrocytic compartment, these amino acids could be deaminated to generate ammonium ions and their carbon backbones (branched-chain α-keto acids) recycled back to neurons (Fig. 1.4.). Recently, Sakai and collaborators (Sakai *et al.*, 2004) showed that ^{15}N-enrichment of the amide-N of rat brain glutamine from [^{15}N]leucine, was greater than that of the bulk ammonium pool, suggesting that compartmentalization of the three enzymatic activities required, i.e. branched-chain amino acid aminotransferase, glutamate dehydrogenase, and glutamine synthetase. In 2000

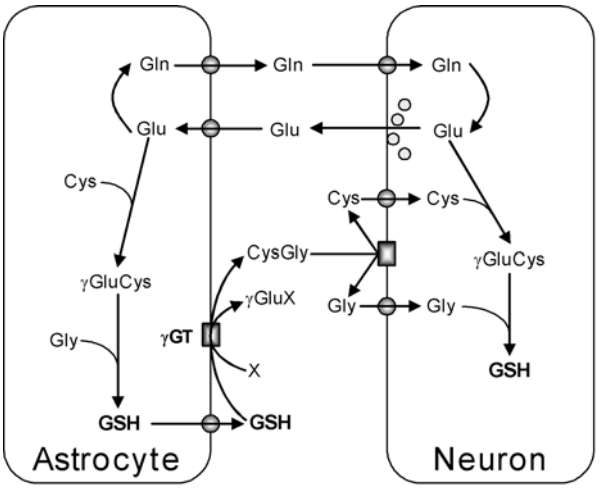

Figure 1.5 – Scheme of the proposed metabolic interaction between astrocytes and neurons in glutathione (GSH) metabolism. The GSH released from astroglial cells is a substrate for the astroglial ectoenzyme γ-glutamyl transferase (γGT). X represents an acceptor of the γ-glutamyl moiety transferred by γGT from GSH. CysGly, generated by the γGT reaction, serves as a precursor for neuronal GSH. Most probably, the hydrolysis of CysGly for neuronal utilization occurs via a neuronal ectopeptidase. In addition, glutamine is released from astrocytes and used by neurons as a precursor for the glutamate necessary as neurotransmitter and for GSH synthesis (adapted from Dringen *et al.,* 2000).

another model, called the lactate-alanine shuttle, was proposed to describe the transfer of nitrogen between neurons and astrocytes (Waagepetersen *et al*., 2000; Zwingmann *et al*., 2000). In this model the proposed carrier is pyruvate, which is aminated to alanine in the neurons and released to be taken up by astrocytes. In the astrocytes alanine could be deaminated back to pyruvate and the pyruvate returned to neurons as lactate (Fig. 1.4.). Although both models use different carriers, both suggest that the ammonium ion is transported as an amino acid. Also, the models are not mutually exclusive and most probably occur simultaneously; given the absence of an urea cycle in the brain it is possible that neurons do not rely only on 2 or 3 amino acids, but that several amino acids may be used to shuttle the ammonium back to astrocytes. Unfortunately, if several amino acids are indeed used, the flux of each one will be small, making it difficult to quantitate fluxes and to identify the actual ammonium carriers.

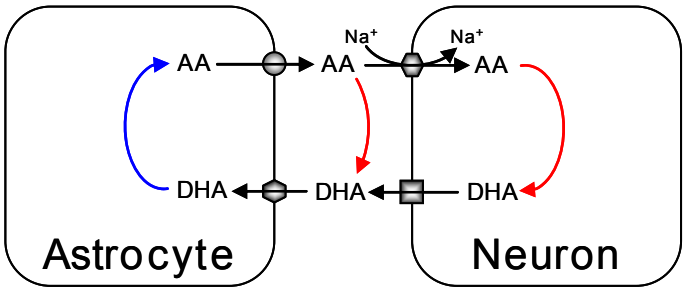

Figure 1.6 – Neuron-astrocyte interaction for vitamin C recycling in the nervous system. Vitamin C (ascorbic acid, AA) recycling associated with neuron-astrocyte interaction requires a specific AA uptake in neurons (⬡) and DHA uptake in astrocytes (⬡). SVCT2 (⬡) is expressed principally in neurons and mediates temperature- and sodium-dependent AA uptake. GLUT1 (⬡) is expressed in astrocytes and mediates glucose-DHA uptake. It has been postulated that intracellularly, AA is oxidized in neurons (in red) generating DHA, which may exit neurons through facilitated transport via GLUT1 or GLUT3 (▭). In the extracellular space AA may be oxidized (in red) to DHA, while providing extracellular antioxidant protection. DHA is incorporated into the astrocytes through GLUT1. Inside astrocytes, DHA is reduced (in blue) back to AA, which may be released and taken up again by neurons via SVCT2. This recycling model may work as an efficient system for the salvage of vitamin C by avoiding the irreversible hydrolysis of DHA produced by antioxidative protection of both the intracellular neuronal compartment and the extracellular *milieu* (adapted from Astuya *et al.,* 2005).

Anti-Oxidants in the Brain

The interactions between astrocytes and neurons are not restricted to central metabolism, but extend to other metabolic pathways, as is the case of the anti oxidative pathways of glutathione (GSH, Fig 1.5) and ascorbic acid (AA, vitamin C, Fig 1.6). Initially, neurons were considered to have less glutathione than astrocytes (Cooper, 1997), however in 1999 Dringen and coworkers (Dringen *et al.*, 1999) showed that astrocytes were able to supply neurons with precursors required for the synthesis of glutathione, and thereby neurons were able to attain similar intracellular levels of this anti-oxidant. It was proposed (Fig. 1.5.) by the same authors that astrocytes release to the extracellular space newly synthesized glutathione, which is cleaved by a γ-glutamyl transpeptidase to generate cysteinylglycine (Dringen *et al.*, 1997). This dipeptide is subsequently cleaved by the neuronal ectoenzyme aminopeptidase N and the amino acids cysteine and glycine generated are subsequently taken up and used as precursors for the synthesis of neuronal glutathione (Dringen *et al.*, 2001).

Vitamin C (Fig. 1.6.) has an active role in the protection against free radicals and has been suggested to be recycled between astrocytes and neurons.

Dehydroascorbate (DHA) in high concentration may be toxic. In response to this toxicity, astrocytes remove this molecule through GLUT1 and reduce it back to ascorbate (AA). Once released, ascorbate may either protect the extracellular milieu from free radicals or may be transported by the SVCT2 to neurons, where it exerts a protective role. Once oxidized, the DHA exits the neurons through the glucose transporters (GLUT1 or GLUT3), becoming available to be transported by astrocytes (Astuya *et al.*, 2005).

Ketone Bodies Metabolism

Recent evidence suggests that astrocytes might also supply neurons with significant amounts of ketone bodies like acetoacetate and 3-hydroxybutyrate from fatty acids or leucine. It has also been shown that glutamate increases astrocytic ketogenesis and that 3-hydroxybutyrate, like lactate, can replace glucose and preserve neuronal synaptic function. These findings suggest a more important role of ketone bodies in brain energy metabolism than thought thus far (for review Guzman and Blazquez, 2001).

Metabolic Differences Between Astrocytes and Neurons

As mentioned above, the metabolism of astrocytes and neurons interact with each other at several points, with metabolic trafficking occurring at these points. However, there are several metabolic features in the metabolism of each cell type, that although not directly associated with metabolic trafficking, impose restrictions on how the trafficking occurs. One of the most important features is the lack of pyruvate carboxylase in neurons (Yu *et al.*, 1983; Shank *et al.*, 1985; Cesar and Hamprecht, 1995). The lack of pyruvate carboxylase prevents neurons from using glycolytic substrates to increase, anaplerotic, the pools of the TCA cycle intermediates, thus rendering neurons dependent on the surrounding astrocytes for the supply of TCA cycle intermediate related metabolites (Schousboe *et al.*, 1997). This feature also places astrocytes virtually in control of the pool of glutamate, which can have serious repercussions. For example, inhibitors of the carbonic anhydrase can be used to treat epilepsy, because limiting the availability of bicarbonate may lead to a diminished flux through pyruvate carboxylase, which in turn may reduce the pool of glutamate, the main excitatory amino acid (Gamberino *et al.*, 1997).

Insofar as mitochondrial metabolism is concerned there are differences between the two cell types in the shuttling of the reducing equivalents from cytoplasm to the mitochondria. There are two ways of performing this shuttling in the brain: through the malate-aspartate shuttle or through the glycerol 3-phosphate shuttle. Of the two processes, the malate-aspartate shuttle is better known than the glycerol 3-phosphate shuttle which has been claimed to have little importance in the brain (Nguyen *et al.*, 2003). However, more studies are required given that this shuttling system seems to be differentially expressed in the different brain cells (McKenna *et al.*, 2006). In what concerns the malate-aspartate shuttle, astrocytes exhibit considerately lower levels of AGC1 protein (aralar1, the Ca^{2+}-sensitive aspartate-glutamate carrier) which appears to be the rate-limiting step of this shuttle (del Arco *et al.*, 2002), and also lower levels of activity of the malate-aspartate shuttle than neurons (Ramos *et al.*, 2003). Thus evidence, suggests that astrocytes do not shuttle their cytosolic reducing equivalents to the mitochondria, but probably use most of them to reduce pyruvate to lactate in agreement with their predominant glycolytic nature.

In the brain, glycogen is found exclusively in the glial compartment and accordingly the glycogenolytic enzyme, glycogen phosphorylase, is astrocyte-specific (for review Wiesinger *et al.*, 1997). Given the intermediate position of astrocytes between capillaries and neurons, glycogen functions as a glucose (and probably lactate) buffer, allowing not only the astrocytes themselves to survive a hypoglycaemic period, but also neurons by supplying them with glycogen-born lactate (Tekkok *et al.*, 2005).

Models for the Study of Brain Metabolism

The brain is a complex object of study. Apart from the highly heterogeneous cellular make-up, as described above, the mammalian brain is enclosed in a head composed of soft tissue and bone. From the inside, as from the outside, the brain is difficult to reach. The highly selective nature of the blood-brain barrier makes it difficult for substances to reach the brain. The *in vivo* model, i.e. the brain inside a living organism, has been used with some degree of success in metabolic studies (Bouzier *et al.*, 2000; Sibson *et al.*, 2001; Kanamori *et al.*, 2002; Merle *et al.*, 2002; de Graaf *et al.*, 2004; Xu *et al.*, 2004) but other organs like the liver usually interfere.

Also, the heterogeneous make-up of the brain increases the complexity of assigning a specific metabolism to a given compartment. To resolve these questions simpler models are used (Table 1.1).

Primary Cultures of Brain Cells

As described above the brain itself is composed of a myriad of cells which do not include the endothelial cells of the vascular system, the epithelial cells and/or many others. To study one particular cell type one has either to use a selective technique, which allows looking into the whole brain and register only the signals coming from the selected cell type, or one has to resort to the dissociation of the cerebral tissue, which then allows the use of several techniques to study the selected cell type.

Primary cultures of brain cells present several advantages over the other model systems. In contrast to slices or organotypic cultures, primary cultures allow the examination at precise developmental stages of a particular cell type and are less technically demanding. Cell lines are much easier to culture but their transformation and immortalization limit their ability to model non-neoplasic tissue. Primary cultures can be grown in a variety of ways, making them a very plastic model, like in aggregates, in monolayers, on microcarriers, immobilized in gel structures, etc. Also, primary cultures may be selectively enriched in specific cell populations, like astrocytes, oligodendrocytes, different kinds of neurons as glutamatergic, gabaergic. Pure primary cultures may be recombined to allow studying interaction of different cell types in co-cultures. However, this model system does present some

Table 1.1 – Experimental models for the study of the brain metabolism.

Model system	Pros	Cons
In vivo	• The brain itself	• It is too complex • Suffers interferences from other organs
Slices	• Retain most of the 3D structure • May be prepared from selected regions • Defined medium content	• May still be complex to analyse due to cellular composition
Primary cultures of brain cells	• Controlled cellular composition • Easily characterised biochemically	• Altered 3D structure • Possible metabolic changes • Heterogeneous populations • Finite cultures with low cellular yields
Cell lines	• Genetically homogeneous • Large cell yields	• Unknown relationship with original tissue • Possible metabolic alterations

disadvantages: by destroying the three-dimensional structure of the tissues, cells lose their natural contacts between each other, which may, ultimately, result in altered phenotypes. Moreover, the time spent in culture and the medium composition can also have repercussions on cell metabolism.

In this work primary cultures of astrocytes were used because this model system allowed studying astrocytic metabolism with different techniques, for example, cells can be cultured in static conditions, which can be easily coupled to high resolution NMR studies of cellular extracts. Also, furthermore cells may be immobilized in different matrices, which enable their use for metabolic studies with bioreactors under fully controlled conditions or for time-dependent *in vivo* NMR studies.

REFERENCES

Abbott N. J., Ronnback L. and Hansson E. (2006) Astrocyte-endothelial interactions at the blood-brain barrier. *Nat. Rev. Neurosci.* **7,** 41-53.

Abi-Saab W. M., Maggs D. G., Jones T., Jacob R., Srihari V., Thompson J., Kerr D., Leone P., Krystal J. H., Spencer D. D., During M. J. and Sherwin R. S. (2002) Striking differences in glucose and lactate levels between brain extracellular fluid and plasma in conscious human subjects: effects of hyperglycemia and hypoglycemia. *J. Cereb. Blood Flow Metab.* **22,** 271-279.

Anderson C. M. and Swanson R. A. (2000) Astrocyte glutamate transport: review of properties, regulation, and physiological functions. *Glia* **32,** 1-14.

Araque A., Parpura V., Sanzgiri R. P. and Haydon P. G. (1999) Tripartite synapses: glia, the unacknowledged partner. *Trends Neurosci.* **22,** 208-215.

Astuya A., Caprile T., Castro M., Salazar K., Garcia Mde L., Reinicke K., Rodriguez F., Vera J. C., Millan C., Ulloa V., Low M., Martinez F. and Nualart F. (2005) Vitamin C uptake and recycling among normal and tumor cells from the central nervous system. *J. Neurosci. Res.* **79,** 146-156.

Bouzier A. K., Thiaudiere E., Biran M., Rouland R., Canioni P. and Merle M. (2000) The metabolism of [3-^{13}C]lactate in the rat brain is specific of a pyruvate carboxylase-deprived compartment. *J. Neurochem.* **75,** 480-486.

Broer S. and Brookes N. (2001) Transfer of glutamine between astrocytes and neurons. *J. Neurochem.* **77,** 705-719.

Cammer W. and Tansey F. A. (1988) Carbonic anhydrase immunostaining in astrocytes in the rat cerebral cortex. *J. Neurochem.* **50,** 319-322.

Cammer W. and Zhang H. (1991) Comparison of immunocytochemical staining of astrocytes, oligodendrocytes, and myelinated fibers in the brains of carbonic anhydrase II-deficient mice and normal littermates. *J. Neuroimmunol.* **34,** 81-86.

Cesar M. and Hamprecht B. (1995) Immunocytochemical examination of neural rat and mouse primary cultures using monoclonal antibodies raised against pyruvate carboxylase. *J. Neurochem.* **64,** 2312-2318.

Chaudhry F. A., Reimer R. J. and Edwards R. H. (2002) The glutamine commute: take the N line and transfer to the A. *J. Cell Biol.* **157,** 349-355.

Chaudhry F. A., Reimer R. J., Krizaj D., Barber D., Storm-Mathisen J., Copenhagen D. R. and Edwards R. H. (1999) Molecular analysis of system N suggests novel physiological roles in nitrogen metabolism and synaptic transmission. *Cell* **99,** 769-780.

Clarke D. D. and Sokoloff L. (1994) Circulation and energy metabolism of the brain, in *Basic Neurochemistry - molecular, cellular and medical aspects,* 6th Edition (G.J. Siegel B. W. A., R.W. Albers, S. K. Fisher, and M. D. Uhler, ed.), p 637–670. Lippincott - Raven, New York.

Cooper A. J. L. (1997) Glutathione in the brain: disorders of glutathione metabolism., in *The Molecular and Genetic Basis of Neurological Disease* (R.N. Rosenberg S. B. P., S. DiMauro, R.L. Barchi and L.M. Kunk, ed.), pp 1195-1230. Butterworth-Heinemann, Boston.

Danbolt N. C. (2001) Glutamate uptake. *Prog. Neurobiol.* **65,** 1-105.

de Graaf R. A., Mason G. F., Patel A. B., Rothman D. L. and Behar K. L. (2004) Regional glucose metabolism and glutamatergic neurotransmission in rat brain *in vivo*. *Proc. Natl. Acad. Sci. U. S. A.* **101,** 12700-12705.

Dehnes Y., Chaudhry F. A., Ullensvang K., Lehre K. P., Storm-Mathisen J. and Danbolt N. C. (1998) The glutamate transporter EAAT4 in rat cerebellar Purkinje cells: a glutamate-gated chloride channel concentrated near the synapse in parts of the dendritic membrane facing astroglia. *J. Neurosci.* **18,** 3606-3619.

Deitmer J. W. (2001) Strategies for metabolic exchange between glial cells and neurons. *Respir. Physiol.* **129,** 71-81.

del Arco A., Morcillo J., Martinez-Morales J. R., Galian C., Martos V., Bovolenta P. and Satrustegui J. (2002) Expression of the aspartate/glutamate mitochondrial carriers aralar1 and citrin during development and in adult rat tissues. *Eur. J. Biochem.* **269,** 3313-3320.

Dermietzel R. and Spray D. C. (1998) From neuro-glue ('Nervenkitt') to glia: a prologue. *Glia* **24,** 1-7.

Dringen R., Kranich O. and Hamprecht B. (1997) The gamma-glutamyl transpeptidase inhibitor acivicin preserves glutathione released by astroglial cells in culture. *Neurochem. Res.* **22,** 727-733.

Dringen R., Pfeiffer B. and Hamprecht B. (1999) Synthesis of the antioxidant glutathione in neurons: supply by astrocytes of CysGly as precursor for neuronal glutathione. *J. Neurosci.* **19,** 562-569.

Dringen R., Gutterer J. M., Gros C. and Hirrlinger J. (2001) Aminopeptidase N mediates the utilization of the GSH precursor CysGly by cultured neurons. *J. Neurosci. Res.* **66,** 1003-1008.

Gamberino W. C., Berkich D. A., Lynch C. J., Xu B. and LaNoue K. F. (1997) Role of pyruvate carboxylase in facilitation of synthesis of glutamate and glutamine in cultured astrocytes. *J. Neurochem.* **69,** 2312-2325.

Giacobini E. (1961) Localization of carbonic anhydrase in the nervous system. *Science* **134,** 1524-1525.

Gladden L. B. (2004) Lactate metabolism: a new paradigm for the third millennium. *J. Physiol.* **558,** 5-30.

Gotoh J., Itoh Y., Kuang T. Y., Cook M., Law M. J. and Sokoloff L. (2000) Negligible glucose-6-phosphatase activity in cultured astroglia. *J. Neurochem.* **74,** 1400-1408.

Guzman M. and Blazquez C. (2001) Is there an astrocyte-neuron ketone body shuttle? *Trends Endocrinol. Metab.* **12,** 169-173.

Hertz L. and Dienel G. A. (2005) Lactate transport and transporters: general principles and functional roles in brain cells. *J. Neurosci. Res.* **79,** 11-18.

Kanamori K. and Ross B. D. (2005) Suppression of glial glutamine release to the extracellular fluid studied *in vivo* by NMR and microdialysis in hyperammonemic rat brain. *J. Neurochem.* **94,** 74-85.

Kanamori K., Ross B. D. and Kondrat R. W. (2002) Glial uptake of neurotransmitter glutamate from the extracellular fluid studied *in vivo* by microdialysis and ^{13}C NMR. *J. Neurochem.* **83,** 682-695.

Kasischke K. A., Vishwasrao H. D., Fisher P. J., Zipfel W. R. and Webb W. W. (2004) Neural activity triggers neuronal oxidative metabolism followed by astrocytic glycolysis. *Science* **305,** 99-103.

Kimelberg H. K. (2004) The problem of astrocyte identity. *Neurochem. Int.* **45,** 191-202.

Kvamme E., Torgner I. A. and Roberg B. (2001) Kinetics and localization of brain phosphate activated glutaminase. *J. Neurosci. Res.* **66,** 951-958.

Laming P. R., Kimelberg H., Robinson S., Salm A., Hawrylak N., Muller C., Roots B. and Ng K. (2000) Neuronal-glial interactions and behaviour. *Neurosci. Biobehav. Rev.* **24,** 295-340.

Marcaggi P. and Coles J. A. (2001) Ammonium in nervous tissue: transport across cell membranes, fluxes from neurons to glial cells, and role in signalling. *Prog. Neurobiol.* **64,** 157-183.

Martinez-Hernandez A., Bell K. P. and Norenberg M. D. (1977) Glutamine synthetase: glial localization in brain. *Science* **195,** 1356-1358.

McKenna M. C., Waagepetersen H. S., Schousboe A. and Sonnewald U. (2006) Neuronal and astrocytic shuttle mechanisms for cytosolic-mitochondrial transfer of reducing equivalents: current evidence and pharmacological tools. *Biochem. Pharmacol.* **71,** 399-407.

Merle M., Bouzier-Sore A. K. and Canioni P. (2002) Time-dependence of the contribution of pyruvate carboxylase versus pyruvate dehydrogenase to rat brain glutamine labelling from [1-^{13}C]glucose metabolism. *J. Neurochem.* **82,** 47-57.

Morgello S., Uson R. R., Schwartz E. J. and Haber R. S. (1995) The human blood-brain barrier glucose transporter (GLUT1) is a glucose transporter of gray matter astrocytes. *Glia* **14,** 43-54.

Nedergaard M., Ransom B. and Goldman S. A. (2003) New roles for astrocytes: redefining the functional architecture of the brain. *Trends Neurosci.* **26,** 523-530.

Nguyen N. H., Brathe A. and Hassel B. (2003) Neuronal uptake and metabolism of glycerol and the neuronal expression of mitochondrial glycerol-3-phosphate dehydrogenase. *J. Neurochem.* **85,** 831-842.

Nogradi A., Domoki F., Degi R., Borda S., Pakaski M., Szabo A. and Bari F. (2003) Up-regulation of cerebral carbonic anhydrase by anoxic stress in piglets. *J. Neurochem.* **85,** 843-850.

Pellerin L. and Magistretti P. J. (1994) Glutamate uptake into astrocytes stimulates aerobic glycolysis: a mechanism coupling neuronal activity to glucose utilization. *Proc. Natl. Acad. Sci. U. S. A.* **91,** 10625-10629.

Perea G. and Araque A. (2002) Communication between astrocytes and neurons: a complex language. *J. Physiol. Paris* **96,** 199-207.

Pfrieger F. W. (2002) Role of glia in synapse development. *Curr. Opin. Neurobiol.* **12,** 486-490.

Ramos M., del Arco A., Pardo B., Martinez-Serrano A., Martinez-Morales J. R., Kobayashi K., Yasuda T., Bogonez E., Bovolenta P., Saheki T. and Satrustegui J. (2003) Developmental changes in the Ca^{2+}-regulated mitochondrial aspartate-glutamate carrier aralar1 in brain and prominent expression in the spinal cord. *Brain Res. Dev. Brain Res.* **143,** 33-46.

Ransom C. B., Ransom B. R. and Sontheimer H. (2000) Activity-dependent extracellular K^+ accumulation in rat optic nerve: the role of glial and axonal Na^+ pumps. *J. Physiol.* **522,** 427-442.

Sakai R., Cohen D. M., Henry J. F., Burrin D. G. and Reeds P. J. (2004) Leucine-nitrogen metabolism in the brain of conscious rats: its role as a nitrogen carrier in glutamate synthesis in glial and neuronal metabolic compartments. *J. Neurochem.* **88,** 612-622.

Schousboe A., Westergaard N., Waagepetersen H. S., Larsson O. M., Bakken I. J. and Sonnewald U. (1997) Trafficking between glia and neurons of TCA cycle intermediates and related metabolites. *Glia* **21,** 99-105.

Shank R. P., Bennett G. S., Freytag S. O. and Campbell G. L. (1985) Pyruvate carboxylase: an astrocyte-specific enzyme implicated in the replenishment of amino acid neurotransmitter pools. *Brain Res.* **329,** 364-367.

Sibson N. R., Mason G. F., Shen J., Cline G. W., Herskovits A. Z., Wall J. E., Behar K. L., Rothman D. L. and Shulman R. G. (2001) *In vivo* ^{13}C NMR measurement of

neurotransmitter glutamate cycling, anaplerosis and TCA cycle flux in rat brain during. *J. Neurochem.* **76,** 975-989.

Silver I. A. and Erecinska M. (1997) Energetic demands of the Na^+/K^+ ATPase in mammalian astrocytes. *Glia* **21,** 35-45.

Slezak M. and Pfrieger F. W. (2003) New roles for astrocytes: regulation of CNS synaptogenesis. *Trends Neurosci.* **26,** 531-535.

Tekkok S. B., Brown A. M., Westenbroek R., Pellerin L. and Ransom B. R. (2005) Transfer of glycogen-derived lactate from astrocytes to axons via specific monocarboxylate transporters supports mouse optic nerve activity. *J. Neurosci. Res.* **81,** 644-652.

Thompson R. F. (1993) *The brain - a neuroscience primer*. W. H. Freeman and Company, New York.

Vannucci S. J., Maher F. and Simpson I. A. (1997) Glucose transporter proteins in brain: delivery of glucose to neurons and glia. *Glia* **21,** 2-21.

Waagepetersen H. S., Sonnewald U., Larsson O. M. and Schousboe A. (2000) A possible role of alanine for ammonia transfer between astrocytes and glutamatergic neurons. *J. Neurochem.* **75,** 471-479.

Walz W. (1989) Role of glial cells in the regulation of the brain ion microenvironment. *Prog. Neurobiol.* **33,** 309-333.

Wiesinger H., Hamprecht B. and Dringen R. (1997) Metabolic pathways for glucose in astrocytes. *Glia* **21,** 22-34.

Xu Y., Oz G., LaNoue K. F., Keiger C. J., Berkich D. A., Gruetter R. and Hutson S. H. (2004) Whole-brain glutamate metabolism evaluated by steady-state kinetics using a double-isotope procedure: effects of gabapentin. *J. Neurochem.* **90,** 1104-1116.

Yu A. C., Drejer J., Hertz L. and Schousboe A. (1983) Pyruvate carboxylase activity in primary cultures of astrocytes and neurons. *J. Neurochem.* **41,** 1484-1487.

Yudkoff M., Daikhin Y., Nelson D., Nissim I. and Erecinska M. (1996a) Neuronal metabolism of branched-chain amino acids: flux through the aminotransferase pathway in synaptosomes. *J. Neurochem.* **66,** 2136-2145.

Yudkoff M., Daikhin Y., Grunstein L., Nissim I., Stern J. and Pleasure D. (1996b) Astrocyte leucine metabolism: significance of branched-chain amino acid transamination. *J. Neurochem.* **66,** 378-385.

Zwingmann C., Richter-Landsberg C., Brand A. and Leibfritz D. (2000) NMR spectroscopic study on the metabolic fate of [3-^{13}C]alanine in astrocytes, neurons, and cocultures: implications for glia-neuron interactions in neurotransmitter metabolism. *Glia* **32,** 286-303.

CHAPTER 2

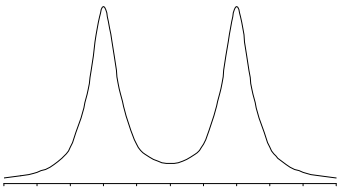

Ethanol Effect on Central Metabolism of Primary Astrocytes Studied by ^{13}C- and ^{31}P-NMR Spectroscopy

This chapter is published in:

Fonseca L. L., Alves P. M., Carrondo M. J. T. & Santos H. (2001) *J. Neurosci. Res.* **66**, 803-811.

Chapter | 2 | Contents

ABSTRACT

Nuclear magnetic resonance was used as the primary technique to investigate the effect of ethanol (40, 80, and 160 mM) on the levels of high-energy phosphates, glycolytic flux, anaplerotic and oxidative fluxes to the tricarboxylic acid (TCA) cycle, the contribution of the pentose phosphate pathway (PPP), and the uptake and release of amino acids on primary cultures of rat astrocytes. On line ^{31}P-NMR spectroscopy showed that long-term exposure to ethanol caused a drop in the levels of ATP and phosphocreatine. The ratio between the fluxes through the pyruvate dehydrogenase and pyruvate carboxylase reactions also decreased, whereas the glycolytic flux and the ratio between formation of lactate and glucose consumption increased when cells were exposed to acute doses of ethanol. Flux through the pentose phosphate pathway was not affected. The uptake of cysteine and the release of glutamine were stimulated by ethanol, whereas the release of methionine was inhibited. Moreover, the fractional enrichment in serine was enhanced. The changes in the amino acid metabolism are interpreted as a response to oxidative stress induced by ethanol.

INTRODUCTION

The impact of ethanol on central nervous system development and metabolism has become an increasingly important issue because of the detrimental effects of alcoholism in modern societies. In particular, in adult humans, ethanol intake causes behaviour changes that can go from mood alterations and anxiety relief (10–30 mM), to impairment of memory and motor control (>30 mM), and to narcosis (>80 mM) (Little, 1991). Chronic alcoholics are more tolerant and require higher concentrations of ethanol to exhibit these effects. During pregnancy, ethanol has deleterious consequences on the development of the foetal central nervous system due to depression of neurogenesis, delayed and aberrant neuronal migration, and altered formation of axonal and dendritic projections (Miller, 1992).

Cell membranes are particularly susceptible to ethanol toxicity. An immediate consequence is the increased fluidity, which is counterbalanced by the long term alteration of the lipid composition toward a higher cholesterol content and an increased ratio of saturated to unsaturated fatty acids (Leonard, 1987). Furthermore, almost all of the important physiopathological targets for ethanol in neural cells appear to be specific membrane proteins such as, ion channels, transporters, and neurotransmitter receptors (Diamond and Gordon, 1997).

Studies with cultures of astrocytes have shown that ethanol impairs cell proliferation (Guerri *et al.*, 1990) possibly by interfering with the stimulatory effect of trophic factors (Luo and Miller, 1996). Moreover, cell swelling, alterations of the cytoskeleton, increased production of reactive oxygen species, and depletion of glutathione have been reported (Renau-Piqueras *et al.*, 1989; Kimelberg *et al.*, 1993; Montoliu *et al.*, 1995).

The interpretation of experimental data on brain metabolism with living animals is complicated due not only to brain compartmentalization but also to interference of other organs. In this study, we used primary cultures of rat astrocytes to assess the effect of ethanol on different aspects of metabolism of this type of brain cells. Although a large volume of data is available on the effect of ethanol on whole brain

physiology, very little is known at the level of the impact on major metabolic pathways of individual nerve cell types (Guerri and Renau-Piqueras, 1997).

Nuclear magnetic resonance (NMR) spectroscopy comprises a very broad range of powerful techniques that allow the study of metabolism directly in living cells (Gadian, 1995). It is possible to perform interleaved acquisition of data from different nuclei in the same sample, reducing the experimental variability and enabling the probing of complementary aspects of cell physiology. In particular, in the case of ^{13}C-NMR, the isotopomer pattern analysis of metabolites enables the assessment of metabolic flux ratios through different and even competing pathways (Lapidot and Gopher, 1994; Bachelard, 1998; Alves *et al.*, 2000b). The inherent low sensitivity of this technique can be overcome by the use of high cell densities. For this purpose, various cell immobilization techniques can be applied that allow metabolic events to be monitored from several hours up to a few days (Alves *et al.*, 1996b; Barbotin *et al.*, 2001). An experimental set-up optimized in our group enabled us to monitor on line the energetic status of primary astrocytes and neurons when subjected to several metabolic insults (Alves *et al.*, 2000a).

In this study the same methodology was used to assess the effects of acute doses of ethanol on the metabolism of rat cortical astrocytes, namely by examining the levels of high-energy phosphates, glycolytic flux, anaplerotic and oxidative fluxes to the tricarboxylic acid (TCA) cycle, the contribution of the pentose phosphate pathway (PPP), and uptake and release of amino acids.

EXPERIMENTAL PROCEDURES

Materials

Dulbecco's modified Eagle's medium (DMEM), foetal bovine serum (FBS), phosphate-buffered saline (PBS) and trypsin-EDTA were purchased from GIBCO (Glasgow, UK). The ^{13}C labelled glucose and ethanol were from Isomed (Madrid, Spain). Culture dishes and flasks were obtained from Nunc (Roskilde, Denmark). Matrigel solution was from Serva (Heidelberg, Germany). CultiSpher S microcarriers were a generous gift from Dr. Kjell Nilsson (Percell, Lund, Sweden). Kits for analytical determinations

were from Boehringer-Mannheim Biochemicals (Germany). Other chemicals were of the purest grade available from regular commercial sources.

Cell Culture

Primary cultures of astrocytes were prepared from 1–2-day-old Wistar rats as described before (Richter-Landsberg and Besser, 1994; Alves *et al*., 1996a). After 4 weeks in culture, cells were either subcultured in 15 cm dishes or immobilized in 300 mm diameter BMG threads according to methodologies previously described (Alves *et al*., 1996a) or in CultiSpher microcarriers as described below. In every case cells were kept for another 5 days in the incubator.

Experiments with Monolayer Cultures

These experiments were designed to assess the effect of ethanol (final concentration 40, 80, and 160 mM) on glucose and amino acid metabolism. Confluent monolayers of astrocytes were used. The medium was removed, cells were washed once with PBS, and new medium was added (DMEM containing 10% FBS, 4 mM glutamine, 5 mM of ^{13}C-labeled glucose, and different concentrations of ethanol). Experiments were performed with [1-^{13}C]glucose, [2-^{13}C]glucose or [U-^{13}C6]glucose.

Due to the volatile nature of ethanol, culture dishes were placed in sealed containers (Luo and Miller, 1996). First, the bottom of each plastic container was covered with 400 mL of a solution containing phosphoric acid (80 mM final concentration) and ethanol at a concentration identical to that of the medium present in the culture dishes. Controls without ethanol were also prepared. To generate a 7% CO_2 atmosphere, 1.4 g of sodium carbonate was added immediately before sealing the containers. Cell cultures were incubated at 37°C different periods of time (4 and 24 hours for the experiments with 40 mM ethanol, 5, 10, 15, and 36 hours for the experiments with 80 mM ethanol, and 36 hours for the experiments with 160 mM ethanol). At the end of each incubation period, the medium from each dish was collected, an aliquot saved for measurement of glucose, lactate content, and LDH (L-lactate dehydrogenase, EC 1.1.1.27) activity, and the remaining medium was lyophilized. Cells were washed twice with ice-cold

solution of NaCl (9 g/L), dishes were placed in liquid nitrogen and 1 mL of cold 7% (v/v) perchloric acid was added to each plate. The resulting mixture was scraped off, the contents from four dishes were pooled and centrifuged (4,000 × g, 10 min, 4°C). The pellets were treated overnight with 0.1 M NaOH and the protein content was determined using the Pierce protein assay. The supernatants were neutralized and centrifuged and the resulting supernatant was lyophilized. For NMR spectroscopy analysis, the residues of lyophilized media and cell extracts were dissolved in D_2O containing 0.1% (v/v) dioxane, used as an internal concentration standard. Each experiment was repeated two or three times. Aliquots from some of these samples were used for amino acid quantification.

In Vivo NMR Studies

For *in vivo* NMR experiments astrocytes immobilized in BMG threads were transferred to a 10 mm NMR tube fitted with a perfusion insert (Alves *et al.*, 1996a; Flögel *et al.*, 1994). Typical amounts of biomass corresponded to 100 mg DNA per experiment. Cells were perfused at 1.5 mL/min with DMEM containing 0.5% FBS and 5 mM [1-^{13}C]glucose, at 37°C and continuously gassed with 95% O_2/5% CO_2 (Fig. 2.1).

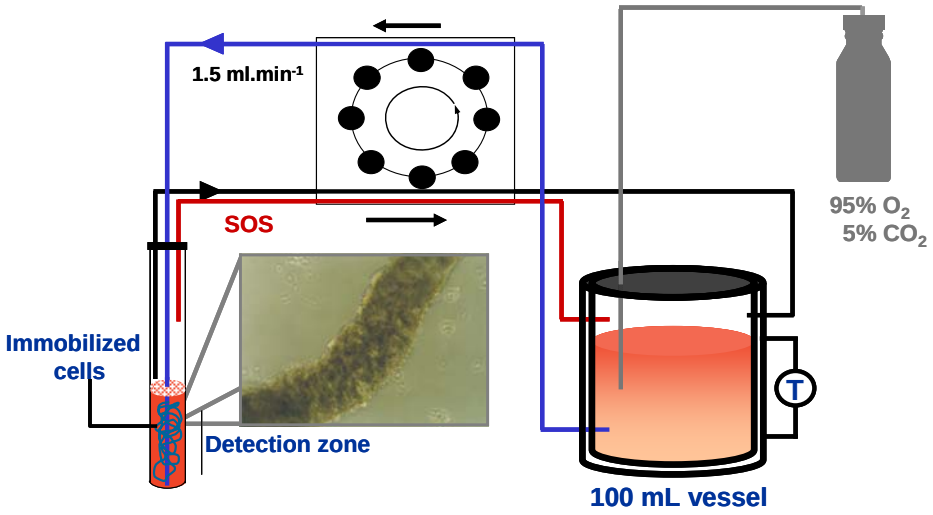

Figure 2.1 – Experimental set up for *in vivo* NMR analysis of astrocytes. Cells immobilized in BMG threads were placed in a 10 mm NMR tube and perfused with medium at a rate of 1.5 mL/min. The medium was maintained at 37°C and continuously gassed with a mixture of 95% O_2 and 5% CO_2.

Ethanol was added to the perfusion medium to obtain the desired final concentration and supplements were added whenever necessary to compensate for ethanol evaporation. In all the experiments ^{13}C- and ^{31}P-NMR spectra were acquired alternately before and after ethanol addition. Each experiment was repeated twice, using independent cell batches. ^{13}C-NMR was also used to evaluate ethanol metabolism. For this purpose, DMEM containing 0.5% FBS, 40 mM [2-^{13}C]ethanol and 5 mM glucose was used for cell perfusion during ≈24 hours. The ethanol concentration in the perfusion medium was determined using the area of the C2 resonance of ethanol calibrated with high-performance liquid chromatography (HPLC) measurements.

Experiments Performed in Spinner Vessels

To determine oxygen uptake and perform long-term (up to 72 hours) incubations with ethanol, astrocytes were immobilized in CultiSpher S microcarriers and grown in spinner vessels with DMEM containing 10% FBS. Spinners were inoculated with 3×10^7 cells and 3 g/L of microcarriers. Cells were allowed to attach for 2 hours, without agitation. After this time, agitation was started at low speed (40 rpm) and 24 hours later speed was increased to 50 rpm. Spinner vessels were kept in the incubator for 5–7 days, during which 50% of the culture medium was changed every 48 hours. Experiments were performed with DMEM containing 10% FBS, 5 mM glucose and 80 mM ethanol. At given time points, samples with or without beads were taken and analyzed for oxygen uptake or by ^{13}C-NMR. To assess the metabolism of ethanol by ^{13}C-NMR, [2-^{13}C]ethanol was used.

Spectroscopy

^{31}P- and ^{13}C-NMR spectra of astrocytes immobilized in BMG threads were acquired with a quadruple nuclei probe head (10 mm diameter) in a Bruker DRX500 operating at a frequency of 202.45 MHz and 125.77 MHz, respectively. Typically, ^{31}P spectra were acquired with 500 transients, a 66° flip angle, repetition time 2.1 sec, spectral width 9.0 kHz, data size 8 K; data were transformed using 20 Hz line broadening. Phosphocreatine and NTP in each experiment were estimated from the peak areas of PCr and γ-NTP and expressed as percentage of control conditions. Extracellular

and intracellular pH values were calculated from the chemical shift of inorganic phosphate (Pi) relative to phosphocreatine (PCr) at 0 ppm. Curves of the chemical shift vs. pH were obtained with DMEM at 37°C. ^{13}C spectra were acquired with 1,024 transients, a 60° flip angle, repetition time 1.54 sec and proton decoupling with wide-band alternating phase low-power technique for zero-residue splitting sequence (WALTZ). Data were processed with 10 Hz line broadening. Chemical shifts were referenced to the C1 signal of β-D-glucose at 96.8 ppm.

Glucose and lactate concentrations in the perfusion medium were quantified using enzyme kits in samples collected at several time points. These values were used to convert the integrated areas of the peaks to concentrations. Proton decoupled ^{13}C-NMR spectra of lyophilized culture medium samples and cellular extracts (pH 7.2) were acquired with 40 K data points using a 60° pulse angle and 31 kHz spectral width. Proton decoupling was applied during the acquisition using the WALTZ sequence. The total recycle delay and number of transients were 20.7 sec and 4,096. Spectra were recorded at a temperature of 300 K. Chemical shifts were reported relative to dioxane at 66.98 ppm. Assignments were made by comparison with chemical shifts found in the literature for metabolic intermediates (Cerdan *et al.*, 1990; Hassel *et al.*, 1994). The total amount of ^{13}C under a particular resonance was calculated by integration of the peaks and whenever necessary, with application of deconvolution routines. Dioxane was used as an internal concentration standard. Spin relaxation was examined using up to 31 sec of recycle delay and determined to be 98% for carboxyl carbons with the selected acquisition conditions. The isotopic enrichments were determined as described earlier, after evaluation of the total amounts of each metabolite (Badar-Goffer *et al.*, 1990).

Cell Quantification and Analytical Methods

The extent of cell lysis was assessed by determination of LDH released to the medium (Vassault, 1983). Total protein was determined using kit 23220 from Pierce (Rockford, IL). Glucose, lactate, glutamate, and glutamine were quantified in the culture medium using enzymatic assays from Boehringer-Mannheim Biochemicals (Germany): kits 716251, 139084, 139092 without and with asparaginase, respectively. Complete analysis of amino acids composition was done using the

Pico-Tag (Waters) method. Amino acids were derivatized by the phenyl-isothiocyanate method and quantified by HPLC. The Pico-Tag system consisted of a Nova-Pak C18 column (WAT 011695), a Waters 510 pump, an automatic injector Waters 717 and a tunable absorbance detector 486. Data acquisition was performed on a PC using software from Millenium.

DNA quantification was used to evaluate the amount of cells in each experiment whenever protein measurements were unreliable due to the proteinic nature of gel threads and microcarriers. Cells were washed with PBS, incubated in water for 30 min at 37°C and disrupted with three freeze-thaw cycles in liquid nitrogen. DNA was quantified with a method involving Hoechst 33258 staining (Rago *et al.*, 1990). A linear correlation between DNA and protein contents was observed using monolayer cultures and the conversion factor was 26.1±1.7 mg of protein per μg of DNA.

Ethanol was quantified by HPLC using a Shodex Sugar SH 1011 column from Waters at 50°C, sulfuric acid (0.01 M) as mobile phase. A linear correlation was found between the HPLC areas and the ethanol concentrations allowing for the calibration of the ^{13}C-NMR data.

Oxygen uptake was measured using a Clark-type electrode in a stirred temperature controlled chamber. All measurements were performed after calibration with water and medium, using nitrogen and air for 0% and 100% oxygen saturation, respectively. Results were handled assuming a molar concentration of dissolved oxygen at 37°C (assay temperature) of 214 μM.

Determination of Flux Ratios from Isotopomer Analysis

The ratio between pyruvate dehydrogenase (PDH, pyruvate dehydrogenase (lipoamide) complex, EC 1.2.4.1, EC 2.3.1.12, EC 1.8.1.4) and pyruvate carboxylase (PC, pyruvate carboxylase, EC 6.4.1.1) fluxes were evaluated by the ratio of the following glutamine isotopomers (Lapidot and Gopher, 1994):

$$\frac{\left[4,5\text{–}{}^{13}C_2\right]+\left[3,4,5\text{–}{}^{13}C_3\right]}{\left[1,2,3\text{–}{}^{13}C_3\right]+\left[2,3\text{–}{}^{13}C_2\right]} \qquad \text{(Eq 2.1)}$$

The ratio between fluxes via the pentose phosphate pathway and glycolysis was determined as (Mancuso *et al*., 1994):

$$\frac{5\times\left[1\text{–}^{13}C\right]\text{lactate}}{2\times\left[2\text{–}^{13}C\right]\text{lactate}} \qquad \text{(Eq 2.2)}$$

RESULTS

To evaluate the effect of ethanol on astrocytic metabolism several biochemical parameters were monitored: glucose consumption and lactate production rates, lactate to glucose ratio, ATP and PCr levels, intracellular pH, protein content, and protein to DNA ratio. Preliminary experiments showed that 24 hours exposure to 40 mM ethanol had no influence on these biochemical parameters when compared to controls (data not shown); therefore, results for 80 and 160 mM ethanol concentrations are reported here.

Effects on Amino Acid Metabolism

Analysis of the lyophilized medium resulting from 5–15 hours incubations of astrocyte monolayer cultures with [1-^{13}C]glucose showed that 80 mM ethanol induced the uptake of cysteine, inhibited the release of methionine and increased the fractional enrichment on C3 of serine without changing significantly the release of this amino acid (Fig. 2.2). Although no notable differences were found in the labelling patterns of glutamine in cultures exposed to 80 mM ethanol for more than 5 hours, the amount of this amino acid in the culture medium increased by approximately 50%, relative to the control cultures, at the end of a 15 hours exposure. Uptake and release of other amino acids were not affected.

Effects on Glycolysis

Long exposure times (36 hours) and high ethanol concentrations (80 mM and 160 mM) were also imposed using monolayer cultures of astrocytes. The labelled substrate ([U-^{13}C]glucose or [2-^{13}C]glucose) was supplied at time 24 hours after the start of the incubation with ethanol so that potential alterations on astrocytic

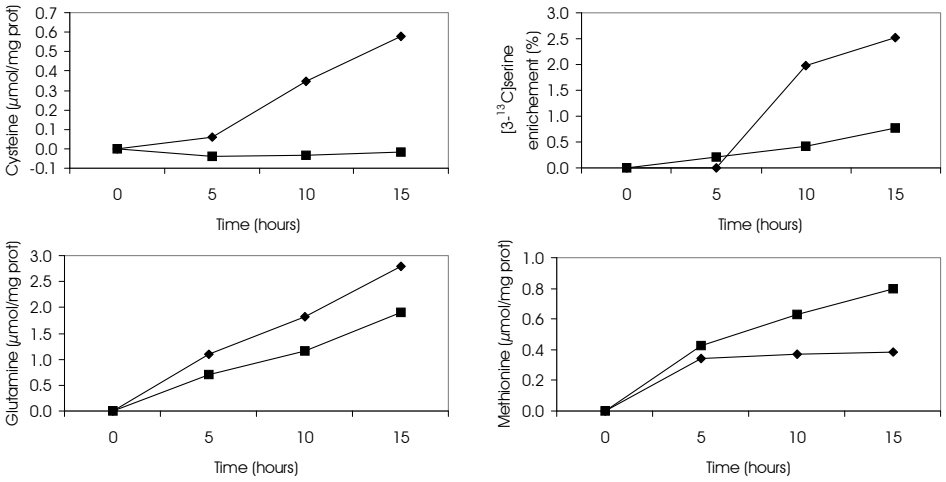

Figure 2.2 – Total amounts of cysteine consumed, glutamine and methionine released, and percentage of ^{13}C enrichment of serine in the culture medium of cortical astrocytes after 5, 10 and 15 hours of incubation with 5 mM [1-^{13}C]glucose without (control, ■) or with 80 mM ethanol (◆) .

metabolism were evaluated during the last 12 hours of the 36 hours incubation period. A typical ^{13}C-NMR spectrum of the culture medium after incubation with [U-^{13}C]glucose is shown in Figure 2.3 where incorporation of label in glutamine, alanine and lactate is clearly visible. The presence of 80 mM ethanol did not affect either glucose consumption (1.2±0.1 µmol/h/mg of protein) and lactate production rates (1.8±0.2 µmol/h/mg of protein) or the ratio between lactate produced and glucose consumed (1.5±0.1) (Fig. 2.4). Conversely, when ethanol concentration was increased to 160 mM the glucose uptake and lactate release rates increased by 18 and 35%, respectively and the amount of lactate produced per glucose consumed increased by approximately 14%. The percentage of labelled lactate in the total lactate pool was 85±6% in controls as well as in cells challenged with ethanol. No statistically significant cell lysis was detected during the experiments.

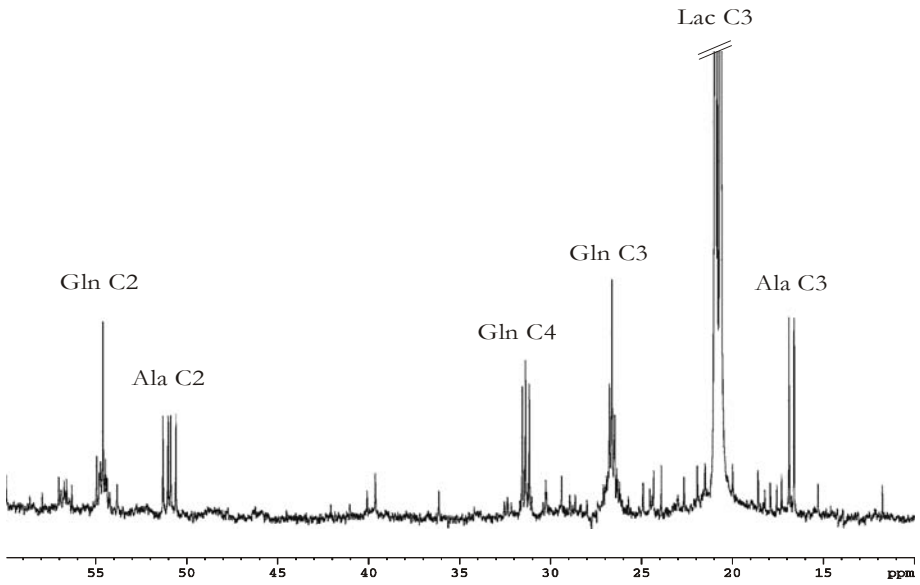

Figure 2.3 – ^{13}C-NMR spectrum of lyophilized medium collected from astrocytes monolayers exposed to ethanol (160 mM) for 36 hours. The initial medium contained 5 mM unlabeled glucose and was replaced by identical medium containing 5 mM of [U-^{13}C]glucose 24 hours after the start of contact with ethanol.

Effects on the Metabolic Fluxes Through Pyruvate Dehydrogenase and Pyruvate Carboxylase

The multiple patterns of resonances C2 and C4 in glutamine released by monolayer cultures of astrocytes exposed to 80 mM ethanol (bottom) and control (top), and derived from the metabolism of [U-^{13}C6]glucose are shown in Figure 2.4. Analysis of the isotopomer populations (Table 2.1) showed that ethanol reduced the PDH to PC flux ratio in a concentration dependent manner (Fig. 2.4) and that this reduction was due to a decrease in the flux through PDH rather than an effect on the flux through PC (Fig. 2.5, Table 2.1). This drop in the flux through PDH was evaluated from the extent of labelling on C2 of glutamine, which remained essentially the same, in control and in ethanol exposed cells, and from the labelling on C4 that was significantly affected. Ethanol reduced by 32% ($P < 0.03$) the ratio between the C4-doublet in [4,5-$^{13}C_2$]glutamine and the singlet due to [4-^{13}C]glutamine, whereas the ratio between the areas of the C2-doublet in [2,3-$^{13}C_2$]glutamine and the singlet

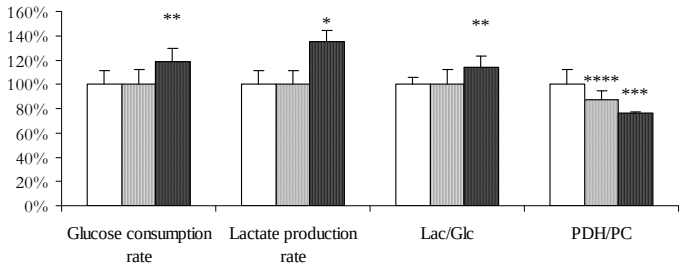

Figure 2.4 – Ethanol effects on glucose consumption rate, lactate production rate, glucose to lactate ratio and pyruvate dehydrogenase to pyruvate carboxylase flux ratio determined in monolayers cultures of astrocytes. Values are relative to the respective controls assumed to be 100. * $P<0.001$; ** $P<0.01$; *** $P<0.04$; **** $P>0.1$. Bar colour code White, control; grey, 80 mM ethanol; black, 160 mM ethanol.

due to [2-^{13}C]glutamine was reduced by 13% ($P > 0.8$). In control conditions the flux ratio between PDH and PC was approximately 2.3.

Effects on the Pentose Phosphate Pathway Activity

The analysis of the labelling pattern in lactate derived from the metabolism of [2-^{13}C]glucose showed that the PPP activity relative to glycolysis remained within the control levels of 4.5±1.0% when monolayer cultures of astrocytes were exposed to 80 mM ethanol for 36 hours.

Table 2.1 – Isotopomer populations (nmol/mg protein) of individual carbons of glutamine released by cortical astrocytes (36 hours exposure to ethanol 160 mM or to control conditions). The initial medium contained 5 mM unlabeled glucose and 24-hours after incubation with ethanol it was replaced by identical medium containing 5 mM of [U-^{13}C]glucose.

Glutamine Isotopomers	Control	Ethanol
2-^{13}C	46	40
2,3-$^{13}C_2$	124	126
1,2-$^{13}C_2$	80	91
1,2,3-$^{13}C_3$	42	46
4-^{13}C	14	16
4,5-$^{13}C_2$	329	276
3,4-$^{13}C_2$	0	0
3,4,5-$^{13}C_3$	110	61

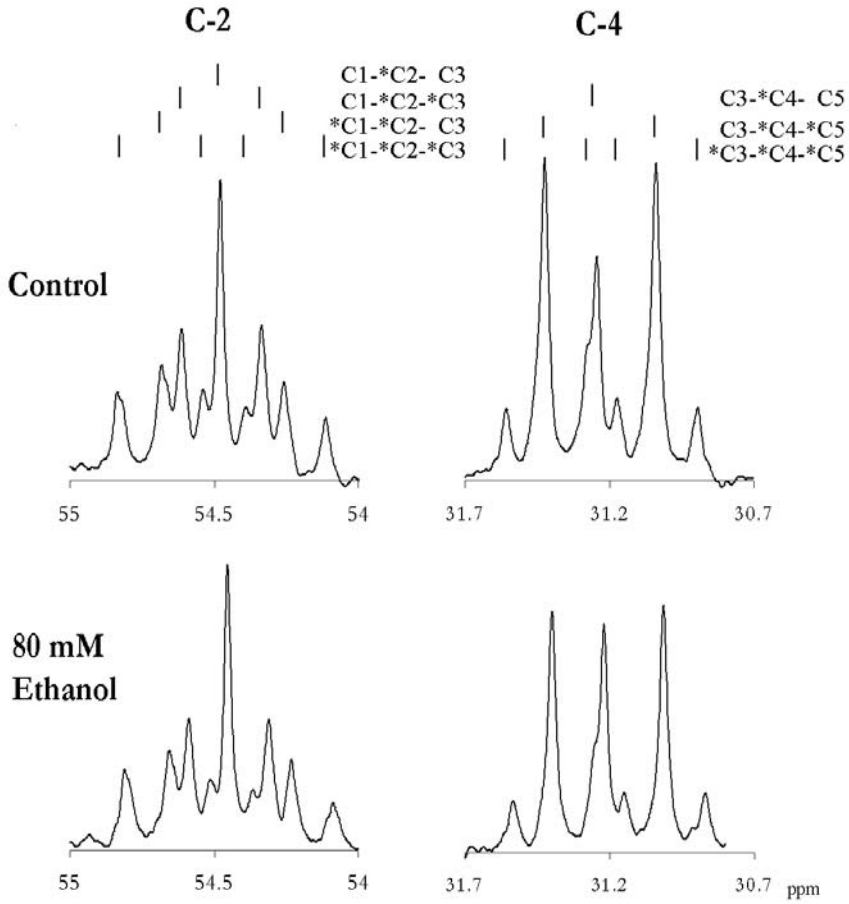

Figure 2.5 – Expanded view of multiplet resonances of glutamine carbons 2 and 4 taken from ^{13}C-NMR spectra of lyophilized medium of astrocytes in control conditions (top) and exposed to 80 mM ethanol for 36 hours. The initial medium contained 5 mM unlabeled glucose and was replaced by identical medium containing 5 mM of [U-^{13}C]glucose at time 24 hours after the start of incubation with ethanol.

Effects on the Energy Level

To evaluate the effect of ethanol on the energetic status as well as on glucose metabolism of astrocytes, *on line* ^{31}P and ^{13}C-NMR spectra of cells immobilized in BMG threads and perfused with medium containing 80 mM ethanol were acquired alternately and consecutively for a period of 60 hours; in control experiments cells were perfused with medium without ethanol. A sequence of ^{31}P-NMR spectra is shown on Figure 2.6. The decrease of PCr and ATP resonances with time was clearly apparent. The time dependency of pH and the levels of PCr and ATP are shown on

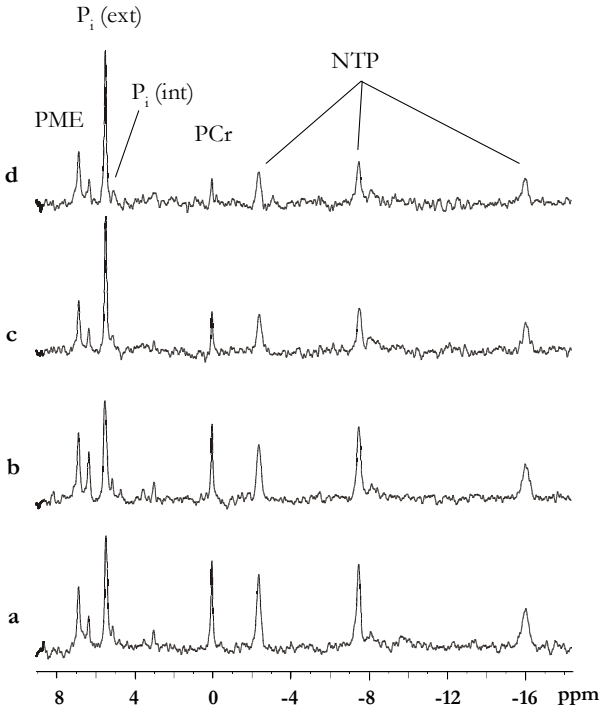

Figure 2.6 – Effect of 80 mM ethanol on the high-energy phosphate compounds of astrocytes immobilised in BMG threads. ^{31}P-NMR spectra were obtained before (a), 24 h (b), 48 h (c) and 60 h (d) after addition of 80 mM ethanol. Assignments: PME, phosphomonoesters; Pi(int), intracellular inorganic phosphate; Pi(ext), extracellular inorganic phosphate; PCr, phosphocreatine; NTP, nucleoside triphosphate.

Figure 2.7. The level of phosphocreatine decreased steadily (1.0±0.1% per hour) whereas ATP remained constant for about 18 hours, dropping thereafter at a rate of 1.2±0.2% per hour. The addition of ethanol did not affect the intracellular pH, which was approximately 7.2.

The increase of phosphatidylcholine and phosphatidylethanolamine (resonances at 6.4 and 6.8 ppm, respectively) observed during the first 24 hours could not be definitely correlated with the presence of ethanol because this trend was not apparent in duplicates of this experiment. The glucose uptake rate and lactate production were evaluated in the same cells using on line ^{13}C-NMR and 5 mM [1-^{13}C]glucose in the perfusion medium, (Fig. 2.8). For the period of time studied (up

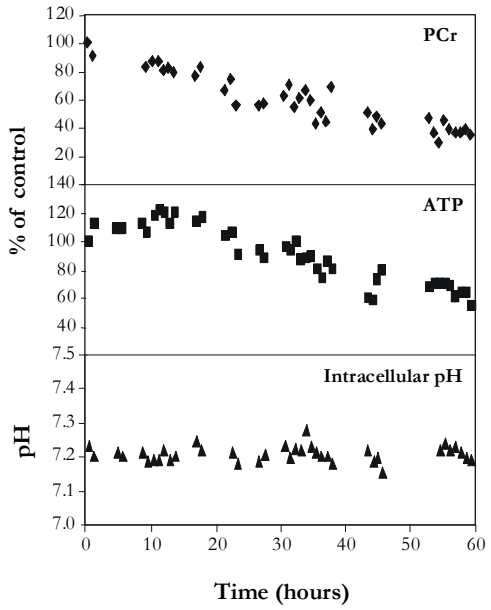

Figure 2.7 – Effects of ethanol (80 mM) on the energetic status of primary astrocytes immobilised in BMG threads. Time-dependency of intracellular pH (bottom) and levels of PCr (top) and ATP (middle). Areas of the PCr and γ-ATP resonances were measured and are expressed as a percentage of control conditions.

to 60 hours), ethanol (80 mM) did not affect these parameters confirming results reported above for monolayer cultures (Fig. 2.4).

Effects on the Oxygen Consumption Rate

Because exposure to 80 mM ethanol had a clear influence on the energetic status (Fig. 2.7) and on the PDH to PC ratio of astrocytes (Fig. 2.4), oxygen uptake rates were measured as well. No significant changes were observed (Table 2.2) in cells exposed to ethanol when compared to control cultures for the exposure times examined (up to 48 hours). The lower oxygen consumption determined at time zero

Table 2.2.- Oxygen uptake rates (μmol.h^{-1}.mg protein^{-1}) determined in primary cultures of astrocytes immobilized in microcarriers and exposed to 80 mM ethanol for different periods of time.

		Incubation time (h)		
		0	24	48
Oxygen uptake rate	Control	1.00±0.03	1.47±0.11	1.43±0.20
	Ethanol	1.01±0.04	1.47±0.19	1.50±0.20

for both control and ethanol exposed cells was interpreted as a metabolic response to medium replacement.

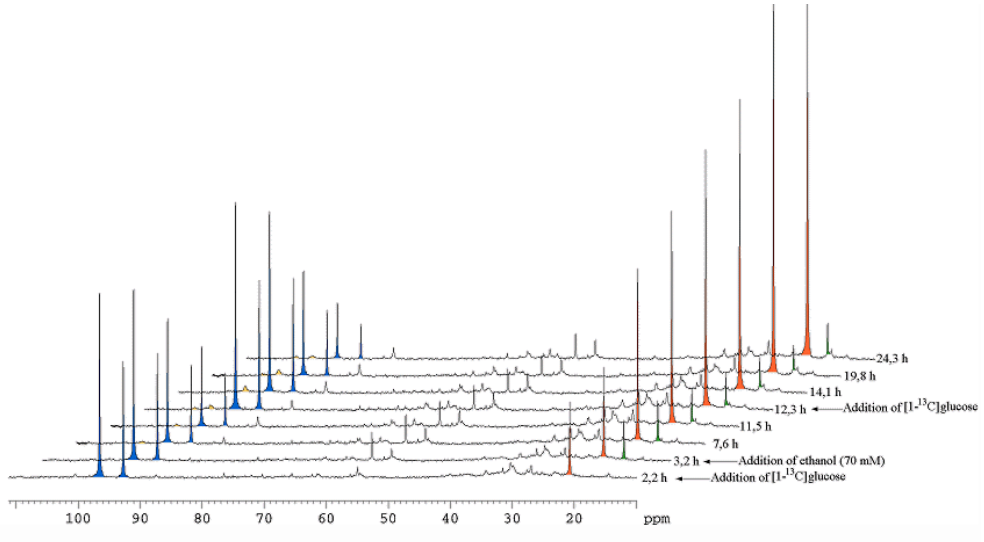

Figure 2.8 – Sequence of ^{13}C-NMR spectra of immobilized primary astrocytes, exposed to ethanol (80 mM). Cells were supplied with two pulses of [1-^{13}C]glucose (at 2.2h and 12.3h) and ethanol (3.2h). In Yellow is show the build up of labelled ^{13}C in the glycogen pool, in blue consumption of the glucose, in red the production of [3-^{13}C]lactate and in green the level of ethanol (natural abundance).

Catabolism of [2-^{13}C]ethanol

The capacity of astrocytes to metabolize ethanol was assessed by ^{13}C-NMR using [2-^{13}C]ethanol in the culture medium. No detectable incorporation of label was found in spectra acquired on line with cells immobilized in BMG threads and perfused with medium containing 40 mM [2-^{13}C]ethanol for a period of 24 hours. Results obtained with cells cultured in microcarriers using spinner vessels also showed that 80 mM [2-^{13}C]ethanol was not metabolized while in contact with the cells for up to 72 hours (data not shown). In these experiments ethanol metabolism was evaluated based on the assumption that any metabolized labelled ethanol ([2-^{13}C]ethanol) would lead to an increase in the ^{13}C enrichment in the astrocytic end products of metabolism.

DISCUSSION

The effect of ethanol on astrocytes is a very important issue, because these cells are responsible not only for the normal development of the central nervous system but also for the maintenance of normal neuronal physiology and survival (Guerri and Renau-Piqueras, 1997). At concentrations up to 40 mM, and for exposure times up to 24 hours, ethanol showed no effect on astrocytic metabolism, as assessed by the glucose consumption and lactate production rates, ATP and PCr levels, and intracellular pH. Conversely, exposure to higher concentrations of ethanol (80 mM for 15 hours) affected the amino acid metabolism of astrocytes. Ethanol stimulated cysteine uptake, glutamine release, increased fractional enrichment on C3 of serine and inhibited methionine release without affecting the release of either serine or glycine (Fig. 2.2). Chronic ethanol consumption has been associated with an increased content of cytochrome P450 2E1 (Montoliu *et al.*, 1994; Tindberg and Ingelman-Sundberg, 1996) and in the formation of reactive oxygen species (Montoliu *et al.*, 1994), which, in turn, can lead to the depletion of endogenous antioxidants, such as glutathione (Montoliu *et al.*, 1995). Under these circumstances the synthesis of glutathione needs to be enhanced, which can only be accomplished at the expense of glutamate, cysteine and glycine. According to Dringen and Hamprecht (1996) astrocytes can use several amino acids as precursors of these three amino acids. In particular, serine is used as a precursor for glycine in glutathione synthesis. Therefore, the observed increase in the metabolic flux through the serine pathway and in the cysteine uptake (Fig. 2.2) could be associated with the ethanol-induced depletion of glutathione. On the other hand, the inhibition in the release of methionine could be related to the function of this amino acid as a donor of the SH group for the synthesis of cysteine. Although recent studies suggest that methionine cannot be used by astrocytes as a cysteine precursor for the synthesis of glutathione (Kranich *et al.*, 1998), this observation, on

its own, does not preclude the presence of a metabolic pathway for the conversion of methionine to cysteine.

Ethanol at 80 mM concentration slightly decreased the PDH to PC flux ratio, but a higher ethanol concentration caused a clear flux reduction through the PDH reaction. This result correlates with the observed increase in the ratio of lactate produced/glucose consumed, suggesting a stimulation of the conversion of pyruvate to lactate rather than to acetyl-CoA. It is known that in brain mitochondria, the calcium steady-state concentration is maintained by an electrogenic uniporter and a Na1/Ca21 antiporter (Rottenberg and Scarpa, 1974; Crompton *et al*., 1978). Although the uniporter is not affected by pharmacological concentrations of ethanol (Rottenberg and Marbach, 1991, 1992), the Na1/Ca21 antiporter is stimulated, and thus, exposure to ethanol leads to the reduction of the steady-state concentration of calcium in the mitochondrial matrix (Li *et al*., 1995). Because several NAD-linked dehydrogenases of the mitochondrial matrix, namely, the PDH, isocitrate dehydrogenase, and 2-oxoglutarate dehydrogenase are activated by calcium (Hansford, 1985; Mc-Cormack *et al*., 1990), it is possible that the observed reduction of the PDH activity *in vivo* is a reflection of the activation by ethanol of the Na1/ Ca21 antiporter and consequent reduction of brain mitochondrial calcium.

The depression of the PDH activity induced by ethanol is also accompanied by the enhancement of glucose consumption and lactate release in an attempt to maintain the cell energetic charge; however, the logical decrease of the oxygen uptake rate was not observed for 80 mM ethanol and higher doses were not examined for this purpose. It is conceivable that ethanol induced the expression of enzymes such as cytochrome P450 2E1, capable of consuming oxygen. Also, it should be noted, that only the metabolism of glucose and amino acids were probed here, and potential effects on the metabolism of other substrates present in the medium were not investigated. The PCr and ATP level in astrocytes was considerably affected by the long-term exposure to ethanol, the observed stimulation of glycolysis being insufficient to compensate for the higher energy demand in the presence of this stressing agent. It is interesting to compare this finding with the remarkable capacity showed by identical cultures of astrocytes to maintain the levels of ATP and PCr when subjected to several hours under hypoxia

(Alves *et al*., 2000a). Mild conditions (40 mM ethanol, 5 hours), caused no significant changes in the energetic status of primary astrocytic cultures. Preliminary results obtained for primary cultures of cortical neurons also showed no effects on the energetic status when these cells were subjected to 80 mM of ethanol up to 15 hours (data not shown). Denays *et al*. (1993), however, reported a small transient increase in the PCr level in rat brain 60–130 min after injection of a single dose of ethanol (equivalent to 21 mM of ethanol in the blood). This discrepancy may be merely due to the different experimental models used in the two studies. It is possible that the effect observed by those authors is not caused by phenomena at the cellular level but at a higher level of hierarchy of the brain such as cell–cell interactions (e.g., astrocyte–neuron) or organ interactions (e.g., liver– brain). Interestingly, Desmoulin *et al*. (1987) reported ethanol effects similar to ours (drop in ATP levels and maintenance of the intracellular pH) in livers of fed rats perfused with 70 mM of ethanol. Although there are reports of ethanol metabolism to acetaldehyde by the catalase-H_2O_2 system in brain homogenate (Aragon *et al*., 1992) and of conversion of ethanol to acetate in astrocytes (Wickramasinghe, 1987; Montoliu *et al*., 1995), we failed to detect ^{13}C-labeled species derived from [2-^{13}C]ethanol. Montoliu *et al*. (1995) showed that in astrocytes, ethanol induces the expression of cytochrome P450 2E1 that uses ethanol as substrate (for review see Lieber, 1997). It is likely that the sensitivity limitations of the NMR technique did not allow for the detection of the low levels expected for eventual ethanol catabolites. Also, it is worth mentioning that the effects of ethanol *in vivo* are not only due to the presence of this substance, but also to the presence of the main catabolite, acetaldehyde, which has been shown to reach concentrations of 50 μM in the blood of humans after an intoxicating dose of ethanol (Majchrowicz and Mendelson, 1970; Westcott *et al*., 1980). In summary, high doses of ethanol caused stimulation of the glycolytic flux, a depression of the flux to the TCA cycle via pyruvate dehydrogenase and a drop in the energetic charge of astrocytes. Furthermore, the alterations observed on amino acid release and uptake suggest an enhancement of the glutathione demand, which is compatible with an ethanol-induced response to oxidative stress.

ACKNOWLEDGEMENTS AND WORK CONTRIBUTIONS

I am grateful to Dr. Paula Chicau, ITQB, Oeiras for the amino acid determination.

REFERENCES

Alves P.M., Fonseca L.L., Peixoto C.C., Almeida A.C., Carrondo M.J.T., Santos H. (2000a). NMR studies on energy metabolism of immobilized primary neurons and astrocytes during hypoxia, ischemia and hypoglycemia. *NMR Biomed.* **13,** 438–448.

Alves P.M., Nunes R., Zhang C., Maycock C.D., Sonnewald U., Carrondo M.J.T., Santos H. (2000b). Metabolism of [3-^{13}C]malate in primary cultures of mouse astrocytes. *Dev. Neurosci.* **22,** 456–462.

Alves P.M., Flögel U., Brand A., Leibfritz D., Carrondo M.J.T., Santos H., Sonnewald U. (1996a). Immobilization of primary astrocytes and neurons for on-line monitoring of biochemical processes by NMR. *Dev. Neurosci.* **18**, 478–483.

Alves P.M., Moreira J.L., Rodrigues J.M., Aunins J.G., Carrondo M.J.T. (1996b). Two-dimensional vs. three-dimensional culture systems: effects on growth and productivity of BHK cells. *Biotechnol. Bioeng.* **52**, 429–432.

Aragon C.M., Rogan F., Amit Z. (1992). Ethanol metabolism in rat brain homogenates by a catalase-H2O2 system. *Biochem. Pharmacol.* **44**, 93–98.

Bachelard H. (1998). Landmarks in the application of ^{13}C-magnetic resonance spectroscopy to studies of neuronal/glial relationships. *Dev. Neurosci.* **20**, 277–288.

Badar-Goffer R.S., Bachelard H.S., Morris P.G. (1990). Cerebral metabolism of acetate and glucose studied by ^{13}C-NMR spectroscopy. *Biochem. J.* **282**, 133–139.

Barbotin J.N., Portais J.C., Alves P.M., Santos H. (2001). NMR and immobilized cells. In: Wijffels R, editor. Immobilized cells. Springer lab manual. Springer-Verlag. p 123–138.

Cerdan S., Kunnecke B., Seeling J. (1990). Cerebral metabolism of [1,2-^{13}C]acetate as detected by *in vivo* and *in vitro* ^{13}C NMR. *J. Biol. Chem.* **265**, 12916 – 12926.

Crompton M., Moser R., Ludi H., Carafoli E. (1978). The interrelations between the transport of sodium and calcium in mitochondria of various mammalian tissues. *Eur. J. Biochem.* **82**, 25–31.

Denays R., Chao S.L., Mathur-Devré R., Jeghers O., Frühling J., Noël P., Ham H.R. (1993). Metabolic changes in the rat brain after acute and chronic ethanol intoxication: a ^{31}P-NMR spectroscopy study. *Magn. Reson. Med.* **29**, 719 –723.

Desmoulin F., Cozzone P.J., Canioni P. (1987). Phosphorus-31 nuclear magnetic resonance study of phosphorylated metabolites compartmentation, intracellular pH and phosphorylation state during normoxia, hypoxia and ethanol perfusion, in the perfused rat liver. *Eur. J. Biochem.* **162**, 151–159.

Diamond I., Gordon A.S. (1997). Cellular and molecular neuroscience of alcoholism. *Physiol. Rev.* **77**, 1–20.

Dringen R., Hamprecht B. (1996). Glutathione content as an indicator for the presence of metabolic pathways of amino acids in astroglial cultures. *J. Neurochem.* **67**, 1375–1381.

Flögel U., Willker W., Leibfritz D. (1994). Regulation of intracellular pH in neuronal and glial tumor cells, studied by multinuclear NMR spectroscopy. *NMR Biomed.* **7**, 157–166.

Gadian D.G. (1995). NMR and its applications to living systems. London: Oxford University Press.

Guerri C., Renau-Piqueras J. (1997). Alcohol, astroglia, and brain development. *Mol. Neurobiol.* **15**, 65– 81.

Guerri C., Saez R., Sancho-Tello M., Martin de Aquilera E., Renau-Piqueras J. (1990). Ethanol alters astrocyte development: a study of critical periods using primary cultures. *Neurochem. Res.* **15**, 559 –565.

Hansford R.G. (1985). Relation between mitochondrial calcium transport and control of energy metabolism. *Rev. Physiol. Biochem. Pharmacol.* **102**, 1–72.

Hassel B., Sonnewald U., Unsgard G., Fonnum F. (1994). NMR spectroscopy of cultured astrocytes: effects of glutamine and the gliotoxin fluorocitrate. *J. Neurochem.* **62**, 2187–2194.

Kimelberg H.K., Cheema M., O'Connor E.R., Tong H., Goderie S.K., Rossman P.A. (1993). Ethanol-induced aspartate and taurine release from primary astrocyte cultures *J. Neurochem.* **60**, 1682–1689.

Kranich O., Drigen R., Sandberg M., Hamprecht B. (1998). Utilization of cysteine and cysteine precursors for the synthesis of glutathione in astroglial cultures: preference for cystine. *Glia* **22**, 11–18.

Lapidot A., Gopher A. (1994). Cerebral metabolic compartmentation. Estimation of glucose flux via carboxylase/pyruvate dehydrogenase by ^{13}C NMR isotopomer analysis of D-[U-^{13}C]glucose metabolites. *J. Biol. Chem.* **269**, 27198 –27208.

Leonard B.E. (1987). Ethanol as a neurotoxin. *Biochem. Pharmacol.* **36**, 2055–2059.

Li H.L., Moreno-Sanchez R., Rottenberg H. (1995). Alcohol inhibits the activation of NAD-linked dehydrogenases by calcium in brain and heart mitochondria. *Biochim. Biophys. Acta* **1236**, 306 –316.

Lieber C.S. (1997). Cytochrome P-4502E1: its physiological and pathological role. *Physiol. Rev.* **77**, 517–544.

Little H.J. (1991). Mechanisms that may underlie the behavioral effects of ethanol. *Prog. Neurobiol.* **36**, 171–194.

Luo J., Miller M.W. (1996). Ethanol inhibits basic fibroblast growth factor mediated proliferation of C6 astrocytoma cells. *J. Neurochem.* **67**, 1448–1456.

Majchrowicz E., Mendelson J.H. (1970). Blood concentrations of acetaldehyde and ethanol in chronic alcoholics. *Science* **168**, 1100 –1102.

Mancuso A., Sharfstein S.T., Tucker S.N., Clark D.S., Blanch H.W. (1994). Examination of primary metabolic pathways in a murine hybridoma with carbon-13 NMR spectroscopy. *Biotechnol. Bioeng.* **44**, 563–585.

McCormack J.G., Halestrap A.P., Denton R.M. (1990). Role of calcium ions in regulation of mammalian intramitochondrial metabolism. *Physiol. Rev.* **70**, 391– 425.

Miller M.W. (1992). The effects of prenatal exposure to ethanol on cell proliferation and neuronal migration. In: Miller M, editor. Development of the central

nervous system: effects of alcohol and opiates. New York: Alan R. Liss. p 47–69.

Montoliu C., Sancho-Tello M., Azorin I., Burgal M., Valles S., Renau-Piqueras J., Guerri C. (1995). Ethanol increases cytochrome P4502E1 and induces oxidative stress in astrocytes. *J. Neurochem.* **65**, 2561–2570.

Montoliu C., Valles S, Renau-Piqueras J, Guerri C. (1994). Ethanol-induced oxygen radical formation and lipid peroxidation in rat brain: effect of chronic alcohol consumption. *J. Neurochem.* **63**, 1855–1862.

Rago R., Mitchen J., Wilding G. (1990). DNA fluorometric assay in 96-well tissue culture plates using Hoescht 33258 after cell lysis by freezing in distilled water. *Anal. Biochem.* **191**, 31–34.

Renau-Piqueras J., Zaragoza R., De Paz P., Baguena-Cervellera R., Megias L., Guerri C. (1989). Effects of prolonged ethanol exposure on the glial fibrillary acidic protein-containing intermediate filaments of astrocytes in primary culture: a quantitative immunofluorescence and immunogold electron microscopic study. *J. Histochem. Cytochem.* **37**, 229 –240.

Richter-Landsberg C., Besser A. (1994). Effects of organotins on rat brain astrocytes in culture. *J. Neurochem.* **63**, 2202–2209.

Rottenberg H., Marbach M. (1991). Alcohol stimulates Na1/Ca21 exchange in brain mitochondria. *Life Sci.* **48**, 987–994.

Rottenberg H., Marbach M. (1992). The effect of alkanols on Ca21 transport in brain mitochondria. *Cell Calcium* **13**, 41– 47.

Rottenberg H., Scarpa A. (1974). Calcium uptake and membrane potential in mitochondria. *Biochemistry* **13**, 4811– 4817.

Tindberg N., Ingelman-Sundberg M. (1996). Expression, catalytic activity, and inducibility of cytochrome P450 2E1 (CYP2E1) in the rat central nervous system. *J. Neurochem.* **67**, 2066 –2073.

Vassault A. (1983). Lactate dehydrogenase: UV-method with pyruvate and NADH. In: Bergmeyer HU, Bergmeyer J, Grassl M, editors. Methods of enzymatic analysis, Vol. III. Weiheim: VerlagChemie. p 118–126.

Westcott J.Y., Weiner H., Shultz J., Myers R.D. (1980). *In vivo* acetaldehyde in the brain of the rat treated with ethanol. *Biochem. Pharmacol.* **29**, 411–417.

Wickramasinghe S.N. (1987). Neuroglial and neuroblastoma cell lines are capable of metabolizing ethanol via an alcohol-dehydrogenase independent pathway. *Alcohol Clin. Exp. Res.* **11**, 234 –237.

CHAPTER 3

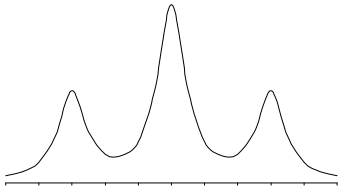

Cultures of Rat Astrocytes Challenged with a Steady Supply of Glutamate: a New Model to Study Flux Distribution in the Glutamate-Glutamine Cycle

This chapter is published in:

Fonseca L. L., Monteiro M. A., Alves P. M., Carrondo M. J. T. & Santos H. (2005) *Glia* **51**, 286-296.

Chapter | 3 | Contents

ABSTRACT

Glutamate metabolism in astrocytes was studied using an experimental set-up that simulates the role of neurons (glutamate producers and glutamine consumers) by the addition of glutaminase to the culture medium. Thereby, a steady supply of glutamate was imposed at the expense of glutamine, and the stress intensity was manipulated by changing the glutaminase concentration. Glutamate supply rates in the range 8 to 23 nmol/min/mg of protein were examined. When the glutamate supply rate exceeded the uptake rate of this amino acid, a transient increase in the extracellular concentration of glutamate was observed. In response to this stress, the fluxes through the glutamate transporter and glutamine synthetase were considerably increased and the extracellular concentration of glutamate was eventually restored to a low level. The increased levels of glutamine synthetase were demonstrated by immunoblotting analysis. The effect on glutamate metabolism of the transaminase inhibitor, AOAA, and of NH_4Cl was also investigated. The accumulation of glutamate caused a concomitant reduction in the levels of phosphocreatine, phosphoethanolamine and phosphocholine without affecting the ATP pool. It was shown that glutamine synthetase is a key element in the control of glutamate metabolism in astrocytic cultures. The metabolic fate of glutamate depended greatly on the time of endurance to the challenge: in naive cells, glutamate was primarily metabolized through the transaminase pathway, while in well-adapted cells glutamate was converted almost exclusively through glutamine synthetase.

INTRODUCTION

Glutamate is the main excitatory neurotransmitter in the mammalian central nervous system (Fonnum, 1984). Synaptic glutamate concentration is determined by the equilibrium between pre-synaptic release, diffusion, binding and uptake. When this balance is pathologically shifted towards increasing glutamate concentrations, neuronal cells die through a process of excitotoxicity, which is due to excessive or prolonged activation of the receptors for this neurotransmitter (for review see (Doble, 1999)).

Astrocytes play a key role in the process of preventing neuronal cell death by excitotoxicity. Glutamate is rapidly taken up by these cells due to the presence of specific transporter proteins (GLAST and GLT-1) that couple the transport of glutamate to the translocation of sodium and potassium at the expense of their transmembrane gradients (Gegelashvili and Schousboe, 1997). Intracellularly, glutamate is converted to glutamine by glutamine synthetase (EC 6.3.1.2; GS) (Norenberg and Martinez-Hernandez, 1979) or metabolised to α-ketoglutarate by the action of glutamate dehydrogenase (EC 1.4.1.2; GDH) or one of the transaminases (EC 1.6.1.X; TA). In addition, glutamate can be diverted to the synthesis of proteins and glutathione.

Glutamine derived from glutamate is released by astrocytes, subsequently taken up by neurons and converted back to glutamate. The glutamate-glutamine cycle plays a very important physiological role since it allows for the maintenance of a low intra-synaptic concentration of glutamate while enabling neurons to be supplied with the metabolic precursor of this neurotransmitter in a harmless form. Given the lack of anaplerotic enzymes needed for the *de novo* synthesis of glutamate in neurons, glutamate must be converted to glutamine in astrocytes to prevent depletion of the glutamate pool in the brain (Hertz, 2004).

Previous studies on glutamate metabolism have provided a wide range of values for the ratio between the fluxes to glutamine (via glutamine synthetase) and to α–ketoglutarate (via glutamate dehydrogenase and transaminases) (Westergaard *et al.*, 1995). For example, Farinelli and Nicklas (1992) found that 70% of the supplied

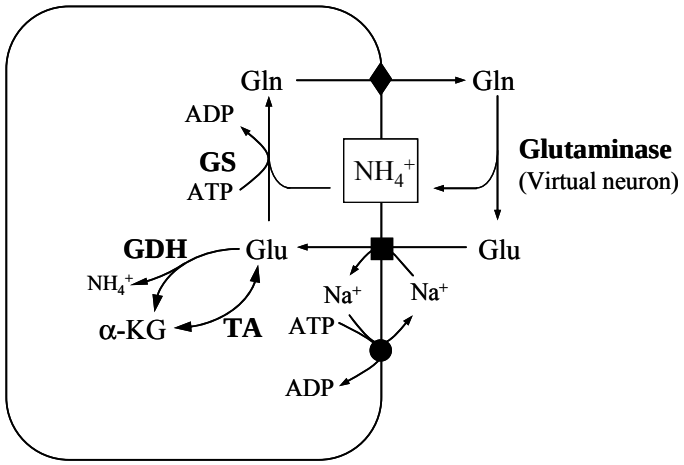

Figure 3.1 – Schematic representation of the reactions included in the experimental model of the glutamine-glutamate cycle. Glutamate is transported by high affinity transporters (GLAST and GLT-1 (■) at the expense of sodium and potassium gradients generated by Na+/K+ATPase (●). Glutamate can be metabolised to α-ketoglutarate by glutamate dehydrogenase (GDH) or by transaminases (TA), or converted to glutamine by glutamine synthetase (GS) at the expense of ATP. Glutamine may exit the cell through several transporters (◆). *In vivo*, neurons continuously uptake glutamine and release glutamate in response to an action potential at the pre-synaptic element. In this model, glutaminase plays the role of neurons, and ensures a steady supply of glutamate.

glutamate (50 μM) was directly converted to glutamine by rat primary cortical astrocytes. This contrasts with the percentage of 30% observed by Sonnewald *et al*. (1993) upon supplying 0.5 mM glutamate to mice cortical astrocytes. These results were later reconciled by McKenna *et al*. (1996) who proposed that the metabolic fate of glutamate depends on the external concentration of this amino acid. *In vivo* data, however, indicate that the flux through glutamine synthetase in the intact brain is even higher than the glutamate supply from the glutamate-glutamine cycle since there is *de novo* synthesis of glutamate in astrocytes (Gruetter *et al*., 1998; Shen *et al*., 1999; Shen *et al*., 1998; Sibson *et al*., 1997).

Providing that *in vivo* astrocytes have to endure a continuous neuronal supply of glutamate, we deemed important to assess the metabolism of glutamate in rat astrocytes subjected to a steady supply of glutamate. To mimic the role of neurons as glutamine consumers and glutamate producers, glutaminase (EC 3.5.1.2; Glnase) was added to the incubation medium (Fig. 3.1). Our work showed that astrocytes responded to the imposed stress by increasing the flux through glutamine synthetase up to the point where produced glutamate was fully converted to

glutamine in steady state conditions. The fate of glutamate was highly dependent on the time of exposure to glutamate. It is also shown that glutamate reduced the cell energetic level and affected lipid metabolism.

EXPERIMENTAL PROCEDURES

Cell Culture

Primary cultures of astrocytes were prepared from 1- to 2-day-old Wistar rats as described before (Richter-Landsberg and Besser, 1994). After 4 weeks in culture at 37°C with 7% CO_2 atmosphere, the cells were either subcultured in 15 cm culture dishes (Nunc, Roskilde, Denmark) or immobilized in 300 μm diameter basement membrane gel (BMG; Serva, Heidelberg, Germany) threads according to methodologies described previously (Alves *et al*. 1996). In every case cells were kept for another 5 days in the incubator under the conditions mentioned above. Cells were cultured in DMEM (GIBCO, Glasgow, U.K.) with 10% FBS (GIBCO) and 100 U/mL of penicillin/streptomycin (GIBCO), which was changed twice per week.

Glutaminase Reaction

Glutaminase activity used throughout this work is a side reaction catalyzed by L-asparaginase (EC 3.5.1.1; Roche Diagnostics GmbH, Mannheim, Germany). DMEM does not contain asparagine and we verified that the rate of glutamate production by this enzyme was proportional to the concentration of enzyme in DMEM containing 3-4 mM glutamine. Therefore, we are confident that the reaction catalysed in DMEM upon addition of L-asparaginase is the hydrolysis of glutamine to glutamate and ammonia. Hereafter this activity will be designated glutaminase.

Metabolic Studies

Incubations with glutaminase were performed in 15 cm culture dishes with 30 mL of DMEM containing 10% FCS, 2 g/L of glucose and 100 U/mL of penicillin/streptomycin. Glutaminase was added to obtain the desired rate of glutamate supply (between 0.038 and 0.110 enzyme units) and in some experiments

1 mM aminooxyacetic acid (AOAA) or 10 mM of NH_4Cl were added simultaneously with glutaminase. Control experiments without addition of glutaminase were also performed. Samples of the incubation medium (120 μL) were taken every 2 to 3 hours for the determination of external glutamate, glutamine, and glutamate supply rate; the total volume withdrawn from each plate never exceeded 5% of the initial volume of the plate. For the analysis of the intracellular content of glutamate and glutamine, one plate was randomly selected at a given time point, the supernatant was removed and the cells washed twice with a cold solution of NaCl (9 g/L). The dishes were immediately placed in liquid nitrogen and the cells extracted with ice-cold ethanol (70%). The extracts were centrifuged (12,000 g for 30 min at 4°C), the supernatants saved and the pellets washed in ice-cold ethanol (70%) and centrifuged again. Both supernatant solutions were pooled together and freeze-dried. Solid residues were suspended in 500 μL of PBS and analysed for their content in glutamate and glutamine. The pellets were boiled for a few minutes in 1 mL of 35 mM Tris (pH 6.8) with 2% SDS; to ensure complete protein dissolution 1 mL of 35 mM Tris (pH 6.8) containing 8% ureia was added to each sample. Protein solutions were used to determine the total protein content and to measure the levels of glutamine synthetase by Western blot. Experiments were repeated at least three times, using independent cell batches and yielding comparable metabolic profiles.

In Vivo NMR Studies

For *in vivo* NMR experiments, astrocytes immobilized in BMG threads were transferred to a 10-mm NMR tube fitted with a perfusion insert (Alves *et al.*, 1996; Flögel *et al.*, 1994). Typical amounts of biomass corresponded to 100 μg DNA per experiment. Cells were perfused at 1.5 mL/min with DMEM containing 0.5 % FBS and 2 g/L of glucose, at 37°C and continuously gassed with $95\%O_2/5\%CO_2$. After a period of data acquisition under control conditions (approximately 12 hours), glutaminase was added to obtain the desired rate of supply of glutamate. ^{31}P NMR spectra were subsequently acquired consecutively every 20 minutes up to approximately 48 hours. Each experiment was repeated twice with independent cell batches.

Spectroscopy

^{31}P-NMR spectra of astrocytes immobilized in BMG threads were acquired with a quadruple nuclei probe head (10-mm diameter) in a Bruker DRX500 operating at a frequency of 202.45 MHz. A width at half-height of 15 Hz for the water signal could be routinely obtained. Typically, ^{31}P-NMR spectra were acquired with 512 transients, a 66° flip angle, repetition time 2.1 s, spectral width 9.0 kHz, data size 8 K; data were zero filled to 16 K and transformed using 20 Hz line broadening. Phosphocreatine and ATP in each experiment were estimated from the peak areas of PCr and γ-ATP and expressed as percentage of control conditions. Extracellular and intracellular pH values were calculated from the chemical shift of inorganic phosphate (Pi) relative to phosphocreatine at 0 ppm. Curves of the chemical shift versus pH were obtained with DMEM at 37°C.

Glutamine Synthetase Quantification by Western Blot

For SDS-PAGE, protein samples (10 µL) in 35 mM Tris with 1% SDS and 4 M urea were mixed with the same volume of sample buffer (80 mM Tris HCl (pH 6.8) with 2% SDS, 10% glycerol, 0.1 M dithiothreitol and 0.001% bromophenol blue). SDS PAGE was carried out on 8% polyacrylamine gels with a 3.8% stacking gel accordingly to Laemmli (1970) for 1 hour in running buffer (25 mM Tris (pH 8.3) with 192 mM glycine and 0.1% SDS) at 180 V and 14°C. Protein transfer onto nitrocellulose membrane (Amersham Biosciences, UK) was done using a semi-dry system (Bio-Rad) for 1 h at 2 mA/cm^2, with all components imbibed in transfer buffer (25 mM Tris (pH 8.3) with 192 mM glycine and 20% methanol). Membranes were blocked with 5% (w/v) skim milk powder (Merck) in TBS (0.05 M Tris (pH 8.0) with 0.138 M NaCl and 0.0027 M KCl, Sigma) for 1 h following an incubation with 1:500 goat polyclonal IgG anti glutamine synthetase (Santa Cruz Biotechnology, USA) in TBS with 0.2% Tween and 0.5% skim milk powder over night. Finally the membranes were incubated with 1:5000 donkey anti-goat IgG conjugated with horseradish peroxidase (Santa Cruz Biotechnology, USA) in TBS with 0.2% Tween and 2% skim milk powder for 1 h. All incubations were performed at room temperature with orbital agitation and between incubations the membranes were washed 3 times with 0.2% Tween in TBS for 5 min. Detection was performed with ECL plus Western Blotting Detection System (Amersham Biosciences,

UK) and the membranes were used to impress a photographic film (Kodak X-OMAT LS, Sigma). Samples containing glutamine synthetase showed a band with an apparent weight between 40 and 50 kDa, which was absent when the membranes were not incubated with goat polyclonal IgG anti-glutamine synthetase. Quantification was performed with an algorithm developed in our lab in MATLAB™ (The MathWorks, Inc) that numerically integrates band volume. The amount of protein in a given band was expressed as the ratio between the respective volume and the average volume of bands in control samples. Gel to gel variations were accounted for by running in each gel a control (sample without addition of glutaminase) and expressing the volume of each band relative to the volume of the control sample in the same gel.

Cell Quantification and Analytical Methods

The extent of cell lysis during the experiments was assessed by determination of lactate dehydrogenase (LDH, EC 1.1.1.27) released to the medium as previously described (Vassault, 1983). The incubation of cells with glutaminase did not affect the extent of LDH release. Total protein was determined using the kit 23220 from Pierce (Rockford, Md, USA). Glutamate, glutamine, glucose and lactate were quantified in the culture medium or in extracts using an YSI 2700 Select system (YSI Life Sciences, USA) under the standard operation conditions advised by the supplier. Glutamate and glutamine determinations were performed immediately after sampling. Determination of the glutamate supply rate was performed by incubation of the samples of culture medium at 37ºC and quantification of glutamate as a function of time.

DNA quantification was used to evaluate the amount of cells when immobilized in BMG threads since protein measurements were not reliable due to the proteinaceous nature of the BMG. Cells were washed with PBS, incubated in water for 30 minutes at 37ºC and disrupted with three freeze-thaw cycles in liquid nitrogen. DNA was quantified according to previously described methods involving Hoechst 33258 staining (Fonseca *et al.*, 2001; Kissane and Robins, 1958; Rago *et al.*, 1990). A linear correlation between DNA and protein content was observed using monolayer cultures: a ratio of 19.5 mg of protein per mg of DNA was obtained.

Model for Data Analysis

A mathematical model (Eq. 3.1-3.4) taking into account the reactions involved in the metabolism of glutamate in astrocytes (Fig. 3.1) was developed to allow the calculation of the relevant fluxes.

$$\frac{\partial[Glu_{ext}]}{\partial t} = \mathbf{GInase} - \mathbf{GluT} \qquad \text{(Eq. 3.1)}$$

$$\frac{\partial[Glu_{int}]}{\partial t} = \mathbf{GluT} - \mathbf{GS} - \mathbf{GDHTA} \qquad \text{(Eq. 3.2)}$$

$$\frac{\partial[Gln_{int}]}{\partial t} = \mathbf{GS} - \mathbf{GInT} \qquad \text{(Eq. 3.3)}$$

$$\frac{\partial[Gln_{ext}]}{\partial t} = \mathbf{GInT} - \mathbf{GInase} \qquad \text{(Eq. 3.4)}$$

GInase, **GluT**, **GS**, and **GInT** represent the fluxes through glutaminase, glutamate transporter, glutamine synthetase, and glutamine transporter, respectively. GDHTA designates the flux of glutamate towards α-ketoglutarate (TCA cycle). The time courses for glutamate and glutamine (intra and extracellular pools) and the glutamate supply rate (glutaminase activity) were fitted to polynomial functions with the Spline Toolbox supplied with MATLAB™ using the least-square method with up to 2 knots. First-order time derivatives of these functions were used to replace the derivatives in equations 3.1-3.4, thus rendering an analytical solution to the given set of equations as functions of the 4 variables (**GluT**, **GS**, **GInT**, and **GDHTA**).

$$\frac{\partial[NH_4^+]}{\partial t} = \mathbf{GInase} \qquad \text{(Eq. 3.5)}$$

$$\frac{\partial[NH_4^+]}{\partial t} = \mathbf{GInase} - \mathbf{GS} \qquad \text{(Eq. 3.6)}$$

$$\frac{\partial[NH_4^+]}{\partial t} = \mathbf{GInase} - \mathbf{GS} + \mathbf{GDHTA} \qquad \text{(Eq. 3.7)}$$

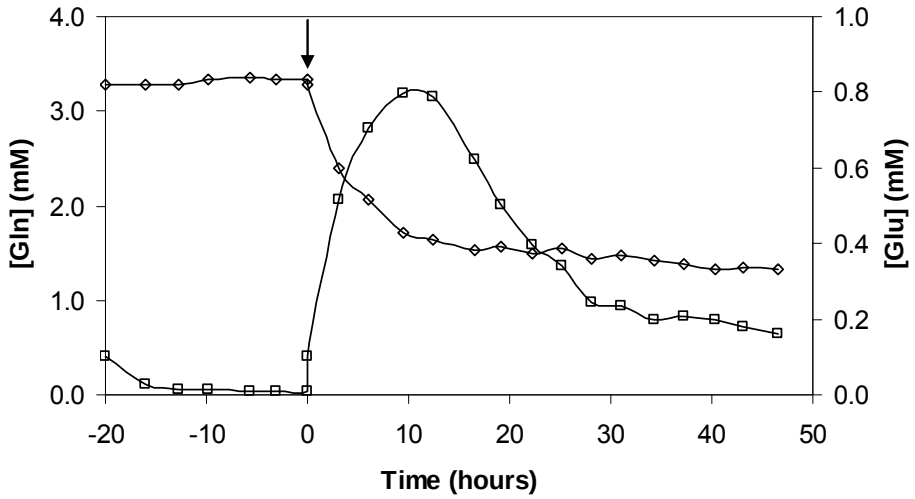

Figure 3.2 – Extracellular concentrations of glutamate (□) and glutamine (◇) before and after the addition of glutaminase to a culture of astrocytes. During the first 20 hours the culture was under control conditions. After addition of glutaminase to the medium at time zero (indicated by the arrow), glutamate was accumulated and subsequently consumed while glutamine decreased until reaching a steady state level of 1.3 mM.

Simulations of the ammonium concentration were performed using the above-calculated fluxes. Three different scenarios, in respect to the set of reactions assumed to be involved in the metabolism of ammonium, were tested. In hypothesis 1, glutaminase is the only enzyme involved (Eq. 3.5); hypothesis 2 considers glutaminase and glutamine synthetase (Eq. 3.6); and hypothesis 3 considers glutaminase, glutamine synthetase, and glutamate dehydrogenase (Eq. 3.7). The concentrations determined within these three scenarios were compared with the experimental results. Throughout the manuscript, the expression "glutamate supply rate" refers to the activity of glutaminase divided by the total biomass, hence this "rate" has the units of a metabolic flux.

Statistics

Two-tailed Student's t-tests, assuming unequal variances, were used to determine whether there were any significant differences between groups of samples under different experimental conditions. A level of $p < 0.02$ was considered statistically significant.

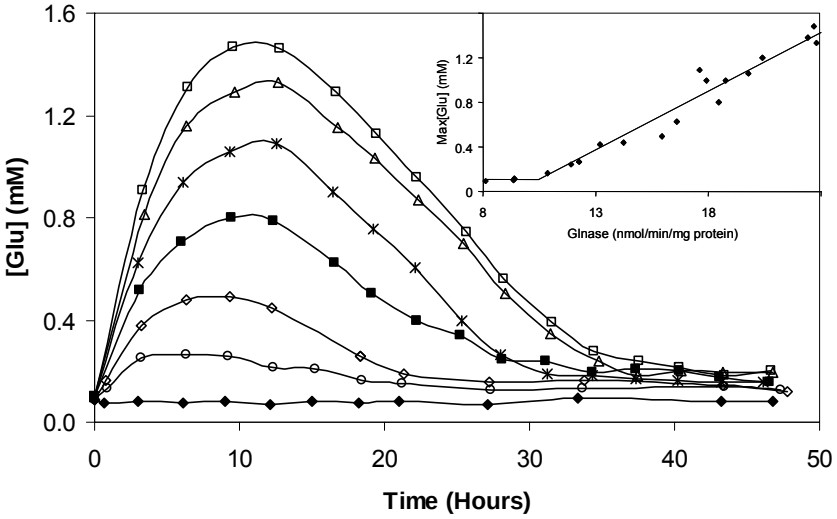

Figure 3.3 – Time courses for the concentration of extracellular glutamate in astrocytes exposed to several glutamate supply rates (from bottom to top, 8.1; 12.2; 14.3; 18.5; 20.4; 22.0; 22.8 nmol/min/mg protein). The insert shows the relationship between the maximum attained glutamate concentration and the glutamate supply rate imposed in the same culture. Glutamate supply rates lower than ≈10 nmol/min/mg protein did not lead to glutamate accumulation.

RESULTS

Effect of Different Rates of Glutamate Supply

Glutamate metabolism in cultured rat astrocytes was studied using glutaminase in the incubation medium to mimic the presence of neurons. Upon addition of glutaminase to a culture of astrocytes, an immediate increase in the extracellular concentration of glutamate was observed (Fig. 3.2). The concentration of glutamate reached a maximum, subsequently decreasing to values of the order of 150 to 200 μM (Fig. 3.2). Concomitantly, the extracellular concentration of glutamine decreased and reached a near-steady state concentration. Prior to glutaminase addition (control conditions) no variation in the concentration of extracellular glutamine and glutamate were observed. This profile was reproduced (Fig. 3.3) as long as the imposed rate of glutamate supply was greater than ≈10 nmol/min/mg

of protein (insert in Fig. 3.3). The maximum extracellular concentration of glutamate was directly dependent on the rate of glutamate supply.

Extracellular and Intracellular Profiles of Glutamate and Glutamine

The intracellular concentrations of glutamate and glutamine and the extracellular concentrations of glutamate, glutamine, and ammonia were measured in several experimental conditions to be used for the calculation of the relevant metabolic fluxes. Astrocytes were incubated in control conditions (no glutaminase or any another compound; Fig. 3.4 A & E), with glutaminase alone (Fig. 3.4 B, F, I & L) or with glutaminase and either 1 mM AOAA (an inhibitor of transaminases; Fig. 3.4 C, G, J & M) or 10 mM NH_4Cl (Fig. 3.4 D, H, K & N). Addition of glutaminase drastically changed the profiles of intra and extracellular glutamate, glutamine, and ammonium (Fig. 3.4 B & F vs. A & E). The level of extracellular glutamate, which was very low in the absence of glutaminase (Fig. 3.4 A), increased notably upon addition of this enzyme, while extracellular glutamine was consumed and ammonium produced (Fig. 3.4 B). After some time, the extracellular concentrations of glutamate, glutamine and ammonium tended to stabilize, regardless of the fact that glutaminase continued to consume glutamine and to produce glutamate and ammonium at the same rate. The action of glutaminase provoked an increase in the levels of intracellular glutamine, which changed from 0.13 in the control (Fig. 3.4 E) to approximately 0.33 μmol/mg of protein (Fig. 3.4 F). On the other hand, the glutamate content had an initial, sharp increase to 0.6 μmol/mg of protein, and subsequently decreased slowly to approximately 0.16 μmol/mg of protein (Fig. 3.4 F).

Glutaminase activity remained constant throughout the duration of the experiments, resulting in a stable supply of glutamate as depicted by the red line in Fig. 3.4 I, J & K (for simplicity the experimental points were not shown).

Effect of AOAA

Addition of AOAA (1 mM) had a small effect on the extracellular profiles of glutamate, glutamine and ammonium (compare Fig. 3.4 B and Fig. 3.4 C) but

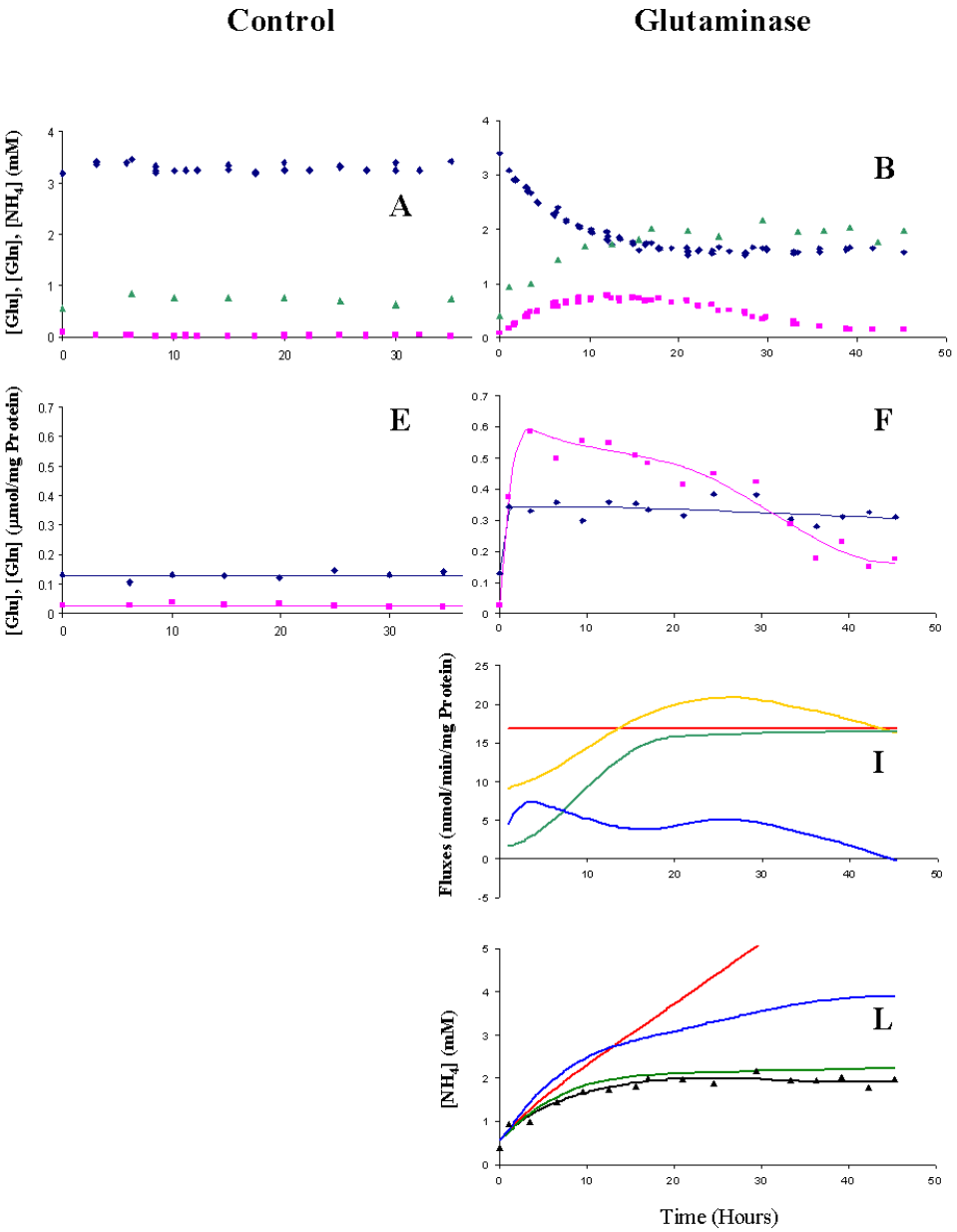

Figura 3.4 – Metabolic profiles of extracellular glutamate, glutamine and ammonium (A, B, C & D), intracellular glutamate and glutamine (E, F, G & H), time profiles of calculated fluxes (I, J & K) and simulated and experimental ammonium concentrations (L, M & N) in astrocyte cultures subjected to control conditions (A & E), glutaminase (B, F, I & L), glutaminase and 1 mM AOAA (C, G, J & M) or glutaminase and 10 mM NH_4Cl (D, H, K & N). Graphs A to H: glutamate (■), glutamine (◆), ammonium (▲).Graphs I to K: glutamate supply rate by glutaminase (—), glutamate uptake (—),flux through glutamine synthetase (—) and flux to

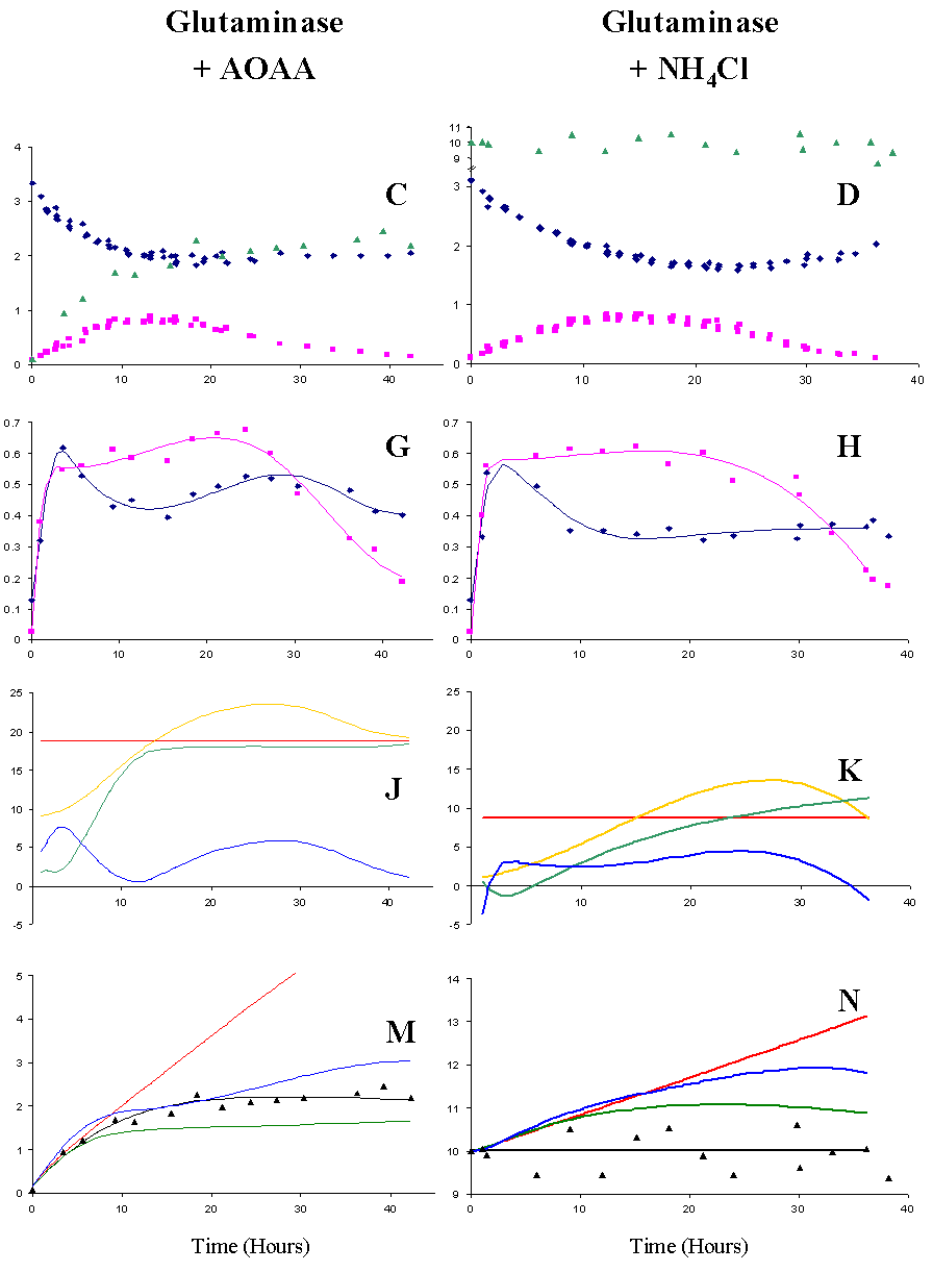

α-ketoglutarate (—). Graphs L to N: experimental values of ammonium concentration (▲) and best fit to the experimental data (—). Coloured lines represent the calculated ammonium concentrations on the basis of three scenarios: i) ammonium is produced by glutaminase and no consumption reaction is considered (—); ii) ammonium is produced by the action of glutaminase and consumed by glutamine synthetase (—); iii) ammonium is produced by glutaminase and glutamate dehydrogenase and consumed by glutamine synthetase (—).

clearly changed the intracellular profiles of glutamate and glutamine (Fig. 3.4 G). The addition of the inhibitor resulted in a greater intracellular accumulation of glutamate for a longer period of time, and a different profile for glutamine accumulation with higher intracellular levels of this amino acid. The intracellular content of glutamine peaked initially to around 0.6 μmol/mg of protein, a feature not observed in the absence of AOAA, and then dropped to values similar to those obtained in the absence of AOAA.

Effect of Ammonium Chloride

When astrocytes were exposed to glutaminase and 10 mM NH_4Cl, the levels of extracellular glutamate were similar to those obtained with glutaminase alone (compare Fig. 3.4 B & D). However, cells subjected to NH_4Cl endured a significantly lower glutamate supply rate (see calculation of fluxes below), which was due to an inhibition of glutaminase caused by the presence of NH_4Cl, an end-product of the reaction catalysed by this enzyme. The profile of extracellular glutamine was generally similar to that observed in the presence of glutaminase alone, except for the increase in the glutamine level towards the end of the experiment. The ammonium concentration in the medium did not vary significantly (Fig. 3.4 D). The intracellular profiles (Fig. 3.4 H) were generally similar to those observed in the presence of AOAA.

Calculation of Metabolic Fluxes

The results obtained for the extra (Fig. 3.4 B, C & D) and intracellular (Fig. 3.4 F, G & H) concentrations of glutamate, glutamine and ammonia, were used as input data for the calculation of the relevant fluxes considered in the model system depicted in Fig. 3.1. The time course of glutamate uptake and the fluxes associated with glutamate metabolism are shown in Fig. 3.4 I, J & K. Upon addition of glutaminase to the medium (Fig. 3.4 I), cells consumed glutamate at a rate of 9.0 nmol/min/mg of protein, significantly lower than the imposed rate of supply (16.8 nmol/min/mg of protein), resulting in the extracellular accumulation of glutamate. During the initial 13 hours the transport capacity of astrocytes increased until reaching the imposed rate of glutamate supply; as a consequence the

extracellular glutamate accumulation ceased. From this point onwards, further increasing the transport capacity resulted in a decrease of the external concentration of glutamate. Concomitantly, during the first 7.5 hours, intracellular glutamate was primarily metabolised to α-ketoglutarate in detriment of the flux via GS. However, the GS flux increased steadily, and eventually becoming the predominant glutamate-consuming pathway. Towards the end of the time period examined, the glutamate conversion to α-ketoglutarate had a negligible contribution to glutamate consumption.

The addition of 1 mM AOAA resulted in a steeper increase of the flux through GS, but otherwise the flux pattern was generally similar to that observed in the absence of inhibitors (Fig. 3.4 J).

The addition of 10 mM NH_4Cl led to inhibition of glutaminase, hence these cells were exposed to a lower glutamate supply (8.8 nmol/min/mg of protein). However, the accumulation of glutamate in the extracellular medium was similar to that found in cells exposed to glutaminase alone, because the glutamate transport capacity was clearly inhibited by NH_4Cl. Actually, the initial glutamate transport capacity of cells exposed to NH_4Cl was about 1.0 nmol/min/mg of protein while a value of 9.0 was obtained for cells exposed to glutaminase alone or in the presence of AOAA. The GS flux was lower than in cells not exposed to NH_4Cl even at similar extracellular concentrations of glutamate. Also, the increase in this flux was notably slower. Contrary to the other cases, the GS flux reached values higher than the imposed rate of glutamate supply (Fig. 3.4 K).

Relative Contributions of the Alternative Routes Directing Glutamate to the TCA Cycle

The fluxes calculated above were used to predict the concentrations of ammonium (Fig. 3.4 L, M & N) on the basis of the three different scenarios described in the Experimental Procedures. The first hypothesis results in a large overestimation of the ammonium concentration in all three cases examined (red lines in Fig. 3.4 L, M & N), therefore, it is not adequate. On the other hand, hypothesis 2 generates a profile that matches the experimental results obtained for astrocytes incubated with

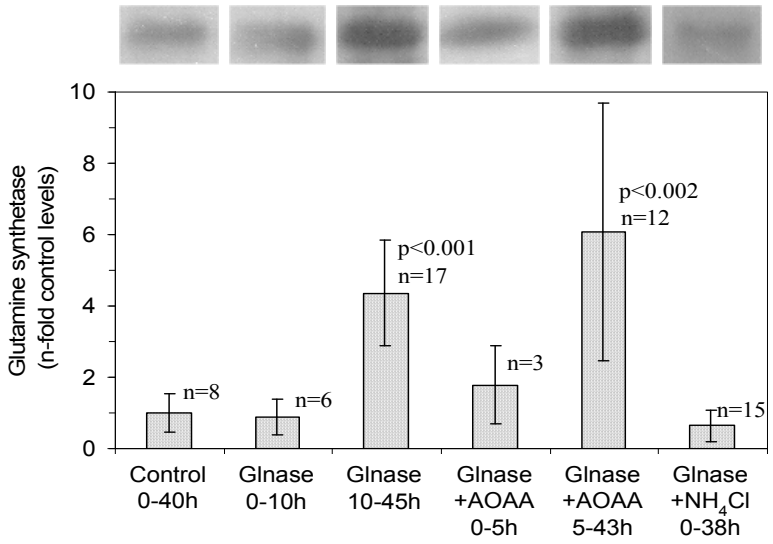

Figure 3.5 – Glutamine synthetase levels determined by Western blot analysis in extracts of astrocyte cultures incubated with glutaminase for less than 10 hours (Glnase 0-10 h), or more than 10 hours (Glnase 10-45 h), glutaminase plus 1 mM AOAA for less than 5 hours (Glnase+AOAA 0-5 h) or more (Glnase+AOAA 5-43 h), and glutaminase plus 10 mM NH_4Cl (Glnase+NH_4Cl 0-38 h). Results are expressed as n-fold of control levels; p is the statistic significance level compared with the control.

glutaminase alone (Fig. 3.4 L). In the case where astrocytes were incubated with glutaminase and AOAA (Fig. 3.4 M) the experimental results fall between the values predicted by hypotheses 2 and 3. All three scenarios led to a substantial overestimation of the experimental results obtained for astrocytes incubated with glutaminase and NH_4Cl (Fig. 3.4 N).

Levels of Glutamine Synthetase by Immunoblotting

Western blot analysis of cell extracts showed a statistically significant ($p<0.002$) increase in the level of GS in the cell groups exposed to glutaminase alone and to glutaminase and AOAA, after 10 and 5 hours of exposure, respectively. No statistically significant differences were found between cells in control conditions, cells exposed to glutaminase alone for less than 10 hours, cells exposed to glutaminase and AOAA for less than 5 hours, or cells exposed to glutaminase and NH_4Cl (Fig. 3.5).

Table 3.1 – Glucose uptake rate, lactate release rate, and ratio between glucose uptake and lactate release rates in rat astrocyte cultures exposed to a steady supply of glutamate generated by glutaminase activity.

	Glutamate supply rate (nmol/min/mg protein)	Glucose uptake rate (nmol/min/mg protein)	Lactate release rate (nmol/min/mg protein)	Lac/Glc
Control	0	8.9 ± 0.3	17.2 ± 2.1	1.9 ± 0.3
GInase	16.8 ± 3.1	13.1 ± 2.1§	22.6 ± 3.6§	1.7 ± 0.1
GInase + AOAA	18.8 ± 3.6	15.4 ± 0.8§	31.1 ± 1.4§,‡	2.0 ± 0.1‡
GInase + NH_4Cl	8.8 ± 1.8	15.1 ± 1.0§	25.8 ± 1.2§	1.7 ± 0.1

§ Statistically different from control values ($p<0.001$)
‡ Statistically different from glutaminase values ($p<0.001$)

Glucose Uptake and Lactate Release

Results obtained for glucose uptake and lactate release rates are presented in Table 3.1. Glucose uptake and lactate release rates were significantly higher ($p<0.001$) in all cell groups exposed to glutaminase as compared to control conditions.

Levels of Phosphorylated Metabolites by *in Vivo* ^{31}P NMR

Phosphocholine, phosphoethanolamine, phosphocreatine and ATP as well as the intracellular pH were determined by ^{31}P NMR directly in immobilized astrocytes (Fig. 3.6). In the bottom spectrum, acquired while cells were perfused with control medium, the resonances of phosphocholine, phosphoethanolamine, inorganic phosphate (extra and intracellular), phosphocreatine and ATP were easily detected. In the upper spectrum, acquired after the addition of glutaminase and when glutamate reached the highest level (540 μM), it is apparent a strong reduction of

Table 3.2 – Levels of phosphorylated metabolites determined by *in vivo* ^{31}P-NMR in rat astrocytes subjected to a steady supply of glutamate or in control conditions (prior to the addition of glutaminase).

	[Glu] (μM)	PC (%)[a]	PE (%)[a]	Phosphocreatine (%)[a]	ATP (%)[a]	Intracellular pH
Control	6 ± 11	100 ± 3	100 ± 10	100 ± 5	100 ± 5	7.23 ± 0.02
Max[Glu][b]	540 ± 29	53 ± 4	60 ± 6	22 ± 4	111 ± 5	7.09 ± 0.02

PC, Phosphocholine; PE, Phosphoethanolamine.
[a] Values are expressed as a percentage of control values.
[b] Values determined at the maximum of glutamate accumulation.

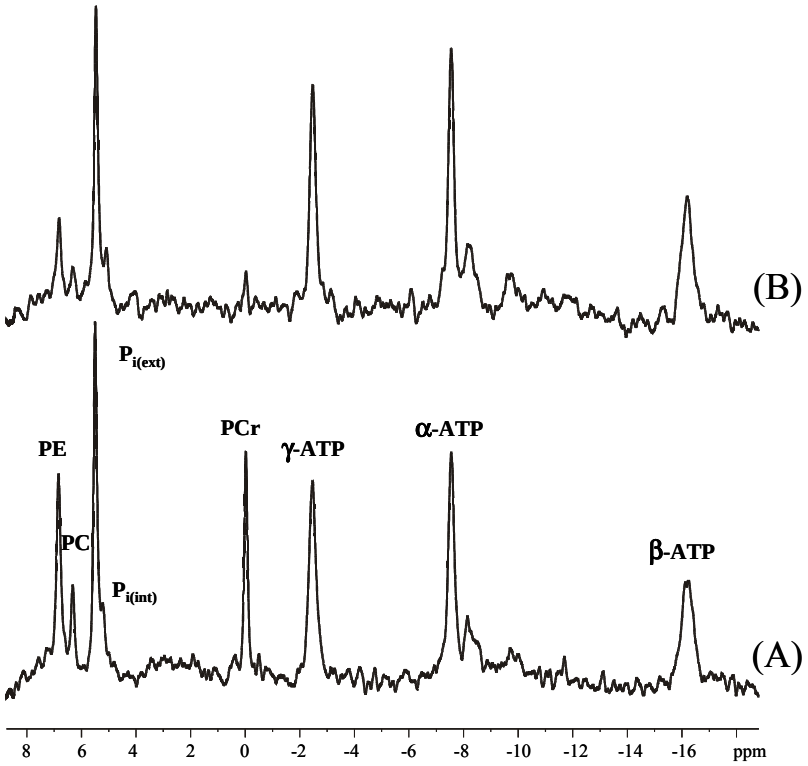

Figure 3.6 – ^{31}P-NMR spectra of astrocytes immobilized in biomembrane gel threads perfused with DMEM. **A:** spectrum acquired under control conditions; **B:** spectrum acquired at the maximum level of glutamate accumulation (540 μM) after addition of glutaminase. Assignments: PE, phosphoethanolamine; PC, phosphocholine; Pi, inorganic phosphate; ext, extracellular; int, intracellular; PCr, phosphocreatine

the phosphocreatine resonance, a slight reduction in both phosphocholine and phosphoethanolamine, a small increase in the ATP resonances, and a down-field shift of the resonance due to the intracellular inorganic phosphate (intracellular acidification). These changes are summarized in Table 3.2.

*D*ISCUSSION

Neuronal activity, which involves a continuous release of glutamate, can only be sustained under normal conditions if the extracellular levels of this amino acid are kept low (Shaw *et al.*, 1995). This desideratum is achieved in the brain through the glutamate-glutamine cycle. Thus far, glutamate metabolism has been studied in astrocytic cultures incubated with specific concentrations of this amino acid

(Farinelli and Nicklas, 1992; McKenna *et al.*, 1996; Sonnewald *et al.*, 1993). Here, we used an experimental approach that mimics the actual glutamate-glutamine cycle in the brain, where glutamate is continuously released by neurons and recycled to glutamine in astrocytes. In this model system, the glutamate-releasing role of neurons is performed by glutaminase, added to the incubation medium; in this way, astrocytes are subjected to a continuous supply of glutamate as in the brain.

At glutamate supply rates lower than ≈10 nmol/min/mg of protein, astrocytes were able to take up all the glutamate, but at higher supply rates, glutamate accumulated in the extracellular space up to around 10 hours, decreasing afterwards (Fig. 3.3). The maximum level of extracellular glutamate increased with the imposed rate of supply, but astrocytes were able to respond efficiently to this stress by increasing the rate of glutamate uptake in a short time.

During the initial period of adaptation, glutamate removal was ensured primarily by conversion to α-ketoglutarate, but the glutamate flux through GS increased notably (about 9 fold), thus becoming the major glutamate-metabolising pathway (Fig. 3.4 I). Furthermore, the increase in the flux via GS was associated with an increase in the level of GS (Fig. 3.5). Our results also suggest that there was a direct correlation between the extent of GS activation and the intensity of the imposed stress, at least within the range of glutamate supply rates examined (Fig. 3.3).

Glutamine synthetase activity has been shown to increase during postnatal development (Virgili *et al.*, 1990); in contrast, a strong reduction in GS is observed in pure cultures of astrocytes prepared from rat brains in various stages of development (Stanimirovic *et al.*, 1999). Glutamine synthetase, however, was up-regulated in astrocytes co-cultured with neurons (Mearow *et al.*, 1990). These findings suggest that GS activity in pure cultures of astrocytes does not represent the *in vivo* activity of this enzyme (Stanimirovic *et al.*, 1999). It is possible that the enzymes required to metabolise glutamate are down regulated due to lack of challenge during the culture preparation. When challenged with a steady supply of glutamate in the experimental set-up used here, astrocytes recovered their natural capacity to metabolise this amino acid, primarily through conversion to glutamine. Our results corroborate the view of other authors (Stanimirovic *et al.*, 1999) that,

although cultured astrocytes lose their *in vivo* phenotype, they still retain the ability to up regulate GS activity.

Most studies on glutamate metabolism in astrocytes (Farinelli and Nicklas, 1992; McKenna *et al*., 1996; Schousboe *et al*., 1993; Sonnewald *et al*., 1993; Sonnewald *et al*., 1997) were performed with short-time incubations (up to 2 hours); our work shows that after 2 hours of exposure to glutamate the flux through GS was only 12% of that attained at the end, and the conversion of glutamate to α-ketoglutarate was the prevalent pathway for glutamate utilization (Fig. 3.4 I). Furthermore, the level of GS remained low during the first 10 hours of exposure to glutamate, a result reflecting the long time required for up-regulation of this enzyme (Fig. 3.5). Thus, if cells are challenged for only a few hours with increasing concentrations of glutamate it is expected that the relative contribution of the flux to the TCA cycle will increase accordingly, as reported by McKenna *et al*. (1996). Our experimental model system shows that the fate of glutamate is largely dependent on the activation of GS rather than on the extracellular concentration of glutamate. In fact, the flux towards the TCA did not change considerably for most of the experiment (30 hours), despite the range of exogenous glutamate concentrations experienced by the culture (0-780 μM) over that time period. Moreover, when the concentrations of glutamate and glutamine reached a steady state (no further change in the extracellular concentration of glutamate or glutamine), the flux of glutamate to the TCA cycle became negligible as compared to the flux through GS. In conclusion, the results on flux distribution obtained in experiments with short-incubation times should be regarded with caution since they may not represent adequately the behaviour of astrocytes in the brain.

The mathematical model used to rationalize the experimental data also allowed for the calculation of the flux distribution through transaminases and glutamate dehydrogenase. In cells incubated with glutaminase alone, glutamate was channelled to the TCA cycle exclusively via the transaminases pathway (Fig. 3.4 L), but the model also shows that when the transaminase inhibitor AOAA was used, the flux distribution was shifted towards the glutamate dehydrogenase pathway (Fig. 3.4 M). This result is in agreement with the higher ratio between lactate release and

glucose uptake rates observed in the presence of the inhibitor AOAA (Table 3.1). Interestingly, the total flux to the TCA cycle did not change appreciably. A notable acceleration of the flux through GS was induced by the presence of the inhibitor (compare Fig. 3.4 J & I), which was accompanied by a decrease in the time required to enhance the level of GS (Fig. 3.5). It appears that the presence of AOAA exerted an extra pressure for the up-regulation of GS.

The glutamate/glutamine cycle is a generally accepted picture of the interaction between astrocytes and neurons to deal with glutamate toxicity; however, the process that shuttles the nitrogen produced in neurons and needed by astrocytes is poorly understood. Branched-chain amino acids and alanine (as opposed to ammonium) have been proposed as candidates for moving nitrogen between neurons and astrocytes (Lieth *et al.*, 2001; Waagepetersen *et al.*, 2000; Yudkoff *et al.*, 1996). The cell system used in this work is able to recycle efficiently glutamate, but leads to the production of ammonium by glutaminase. Interestingly, ammonium in the medium reaches a steady state at a concentration of approx. 2 mM, indicating that astrocytes are able to utilize this nitrogen source. Contradictory results appear in the literature concerning the effects of ammonium on glutamate metabolism: Huang *et al*. (1994) have shown that chronic exposure to ammonium results in increased glutamine synthesis; on the other hand, other authors observed little or no increase in the formation of glutamine, and reported a reduction of the oxidative metabolism of glutamate (Yu *et al.*, 1984). Therefore, we investigated the effect of 2 mM ammonium on astrocytes with the experimental set-up used in this study. No changes were observed in the profiles of extracellular glutamate and glutamine in comparison with experiments carried out without ammonium; furthermore, glutaminase was not inhibited by this level of ammonium (results not shown). Also, it was deemed interesting to study the effect of ammonium on the metabolism of astrocytes. At a concentration of 10 mM, ammonium caused a reduction of about 50% in the activity of glutaminase and hence the rate of glutamate supply decreased to 8.8 nmol/min/mg of protein (compare Fig. 3.4 I & K). At this low rate of glutamate supply, astrocytes incubated with glutaminase alone did not accumulate glutamate (Fig. 3.3); in contrast, cells treated with ammonium showed a profile of glutamate accumulation (Fig. 3.4 D) similar to that of cells

exposed to a 2 fold higher glutamate supply rate, which evidences the inhibitory effect of ammonium in glutamate uptake. *In vivo* as well as *in vitro* models for hyperammonemia have shown a reduction at the level of transcription as well as expression of genes encoding the glutamate transporters GLAST and GLT-1 (Chan and Butterworth, 1999; Chan *et al.*, 2000). Ammonium also affected the profile of the flux through GS (Fig. 3.4 K); moreover, the glutamate-dependent enhancement of the level of GS observed in the absence of ammonium, was suppressed (Fig. 3.5). This result shows that the observed stimulation of the GS activity was not due to an increase in the amount of protein, but to other regulatory factors. It is worth noting that, for incubation periods longer than 24 hours the flux through GS outweighed the glutamate supply rate (Fig. 3.4 K), leading to an increase in the extracellular glutamine synthesized from glutamate derived from the TCA cycle (Fig. 3.4 D). This unexpected result is interpreted as being part of a strategy for ammonium detoxification.

According to the model proposed by Pellerin and Magistretti (1994), the glutamate-glutamine cycle is coupled to the glycolytic pathway. Our results corroborate this model insofar as glucose uptake rates are stimulated in the presence of glutamate (Table 3.1). This stimulation is justified by the fact that glutamate metabolism is very expensive from the energetic point of view mainly for two reasons: the transport of glutamate is fuelled by sodium and potassium gradients, which are built by the Na^+/K^+ ATPase at the expense of ATP; also, the conversion of glutamate to glutamine is an ATP-consuming process. The ATP content of astrocytes did not change appreciably upon glutaminase addition, but a drastic reduction in the level of PCr was observed (Table 3.2). This suggests an increased energy demand, but the level of ATP is maintained at the expense of the PCr pool, as observed in response to short times under ischemia (Alves *et al.*, 2000). Decreased PCr /ATP ratios in astrocytes challenged with glutamate in a discontinuous experimental set-up have been reported earlier (Sonnewald *et al.*, 1997).

Perhaps more interesting was the clear reduction in the level of phosphocholine and phosphoethanolamine, two precursors in the synthesis of phospholipids. In mouse neocortical neurons, glutamate induces the production of the unusual lipids N-acylethanolamine and N-acylphosphatidylethanolamine (Hansen *et al.*, 1995),

which are also found in mammalian tissues undergoing degenerative changes (Schmid *et al.*, 1990). Therefore, it is conceivable that similar glutamate-induced processes could occur in astrocytes that would account for the drop observed in the pools of precursors.

In conclusion, data presented here show that astrocytes adapted efficiently to a constant supply of glutamate by increasing glutamate uptake and GS activity up to levels similar to the imposed glutamate supply rate. The metabolic fate of glutamate depended greatly on the time of endurance to the challenge: in naïve cells, glutamate was primarily metabolised through the transaminase pathway, while in well-adapted cells glutamate was converted almost exclusively through GS. The evidence and conclusions presented herein confirm that the experimental set-up developed in this work to study glutamate metabolism, constitutes a more representative model of the *in vivo* condition than other systems using cultures of astrocytes with single additions of glutamate.

Acknowledgements and Work Contributions

I am grateful to Dr. Cristina Peixoto and to Dr. Victor Sousa, ITQB, Oeiras for the enlightening discussions and endless suggestions on the improvement of the quality of the Western Blots.

References

Alves P.M., Flögel U., Brand A., Leibfritz D., Carrondo M.J.T., Santos H., Sonnewald U. (1996). Immobilization of primary astrocytes and neurons for on-line monitoring of biochemical processes by NMR. *Dev. Neurosci.* **18**, 478-483.

Alves P.M., Fonseca L.L., Peixoto C.C., Almeida A.C., Carrondo M.J.T., Santos H. (2000). NMR studies on energy metabolism of immobilized primary neurons and astrocytes during hypoxia, ischemia and hypoglycemia. *NMR. Biomed.* **13**, 438-48.

Chan H., Butterworth R.F. (1999). Evidence for an astrocytic glutamate transporter deficit in hepatic encephalopathy. *Neurochem. Res.* **24**, 1397-401.

Chan H., Hazell A.S., Desjardins P., Butterworth R.F. (2000). Effects of ammonia on glutamate transporter (GLAST) protein and mRNA in cultured rat cortical astrocytes. *Neurochem. Int.* **37**, 243-8.

Doble A. (1999). The role of excitotoxicity in neurodegenerative disease: implications for therapy. *Pharmacol. Ther.* **81**, 163-221.

Farinelli S.E., Nicklas W.J. (1992). Glutamate metabolism in rat cortical astrocyte cultures. *J. Neurochem.* **58**, 1905-15.

Flögel U., Willker W., Leibfritz D. (1994). Regulation of intracellular pH in neuronal and glial tumour cells, studied by multinuclear NMR spectroscopy. *NMR Biomed.* **7**, 157-166.

Fonnum F. (1984). Glutamate: a neurotransmitter in mammalian brain. *J. Neurochem.* **42**, 1-11.

Fonseca L.L., Alves P.M., Carrondo M.J.T., Santos H. (2001). Effect of ethanol on the metabolism of primary astrocytes studied by ^{13}C- and ^{31}P-NMR spectroscopy. *J. Neurosci. Res.* **66**, 803-11.

Gegelashvili G., Schousboe A. (1997). High affinity glutamate transporters: regulation of expression and activity. *Mol. Pharmacol.* **52**, 6-15.

Gruetter R., Seaquist E.R., Kim S., Ugurbil K. (1998). Localized *in vivo* ^{13}C-NMR of glutamate metabolism in the human brain: initial results at 4 tesla. *Dev. Neurosci.* **20**, 380-8.

Hansen H.S., Lauritzen L., Strand A.M., Moesgaard B., Frandsen A. (1995). Glutamate stimulates the formation of N-acylphosphatidylethanolamine and N-acylethanolamine in cortical neurons in culture. *Biochim. Biophys. Acta* **1258**, 303-8.

Hertz L. (2004). Intercellular metabolic compartmentation in the brain: past, present and future. *Neurochem. Int.* **45**, 285-96.

Huang R., Kala G., Murthy R.K., Hertz L. (1994). Effects of chronic exposure to ammonia on glutamate and glutamine interconversion and compartmentation in homogeneous primary cultures of mouse astrocytes. *Neurochem. Res.* **19**, 257-65.

Kissane J.M., Robins E. (1958). The fluorimetric measurement of deoxyribonucleic acid in animal tissues with special reference to the central nervous system. *J. Biol. Chem.* **233**, 184-188.

Laemmli U.K. (1970). Cleavage of structural proteins during the assembly of the head of bacteriophage T4. *Nature* **227**, 680-5.

Lieth E., LaNoue K.F., Berkich D.A., Xu B., Ratz M., Taylor C., Hutson S.M. (2001). Nitrogen shuttling between neurons and glial cells during glutamate synthesis. *J. Neurochem.* **76**, 1712-23.

McKenna M.C., Sonnewald U., Huang X., Stevenson J., Zielke H.R. (1996). Exogenous glutamate concentration regulates the metabolic fate of glutamate in astrocytes. *J. Neurochem.* **66**, 386-93.

Mearow K.M., Mill J.F., Freese E. (1990). Neuron-glial interactions involved in the regulation of glutamine synthetase. *Glia* **3**, 385-92.

Norenberg M.D., Martinez-Hernandez A. (1979). Fine structural localization of glutamine synthetase in astrocytes of rat brain. *Brain Res.* **161**, 303-10.

Pellerin L., Magistretti P.J. (1994). Glutamate uptake into astrocytes stimulates aerobic glycolysis: a mechanism coupling neuronal activity to glucose utilization. *Proc. Natl. Acad. Sci. U.S.A.* **91**, 10625-9.

Rago R., Mitchen J., Wilding G. (1990). DNA fluorometric assay in 96-well tissue culture plates using Hoescht 33258 after cell lysis by freezing in distilled water. *Anal. Biochem.* **191**, 31-34.

Richter-Landsberg C., Besser A. (1994). Effects of organotins on rat brain astrocytes in culture. *J. Neurochem.* **63**, 2202-9.

Schmid H.H., Schmid P.C., Natarajan V. (1990). N-acylated glycerophospholipids and their derivatives. *Prog. Lipid Res.* **29**, 1-43.

Schousboe A., Westergaard N., Sonnewald U., Petersen S.B., Huang R., Peng L., Hertz L. (1993). Glutamate and glutamine metabolism and compartmentation in astrocytes. *Dev. Neurosci.* **15**, 359-66.

Shaw P.J., Forrest V., Ince P.G., Richardson J.P., Wastell H.J. (1995). CSF and plasma amino acid levels in motor neuron disease: elevation of CSF glutamate in a subset of patients. *Neurodegeneration* **4**, 209-16.

Shen J., Petersen K.F., Behar K.L., Brown P., Nixon T.W., Mason G.F., Petroff O.A., Shulman G.I., Shulman R.G., Rothman D.L. (1999). Determination of the rate of the glutamate/glutamine cycle in the human brain by *in vivo* ^{13}C NMR. *Proc. Natl. Acad. Sci. U.S.A.* **96**, 8235-40.

Shen J., Sibson N.R., Cline G., Behar K.L., Rothman D.L., Shulman R.G. (1998). ^{15}N-NMR spectroscopy studies of ammonia transport and glutamine synthesis in the hyperammonemic rat brain. *Dev. Neurosci.* **20**, 434-43.

Sibson N.R., Dhankhar A., Mason G.F., Behar K.L., Rothman D.L., Shulman R.G. (1997). *In vivo* ^{13}C NMR measurements of cerebral glutamine synthesis as evidence for glutamate-glutamine cycling. *Proc. Natl. Acad. Sci. U.S.A.* **94**, 2699-704.

Sonnewald U., Westergaard N., Petersen S.B., Unsgard G., Schousboe A. (1993). Metabolism of [U-^{13}C]glutamate in astrocytes studied by ^{13}C NMR spectroscopy: incorporation of more label into lactate than into glutamine demonstrates the importance of the tricarboxylic acid cycle. *J. Neurochem.* **61**, 1179-82.

Sonnewald U., Westergaard N., Schousboe A. (1997). Glutamate transport and metabolism in astrocytes. *Glia* **21**, 56-63.

Stanimirovic D.B., Ball R., Small D.L., Muruganandam A. (1999). Developmental regulation of glutamate transporters and glutamine synthetase activity in astrocyte cultures differentiated *in vitro*. *Int. J. Dev. Neurosci.* **17**, 173-84.

Vassault A. (1983). Lactate dehydrogenase: UV-method with pyruvate and NADH. In: Bergmeyer HU, Bergmeyer J, Grassl M, editors. Methods of enzymatic analysis. Weiheim: VerlagChemie. p 118-126.

Virgili M., Barnabei O., Contestabile A. (1990). Regional maturation of neurotransmitter-related and glial markers during postnatal development in the rat. *Int. J. Dev. Neurosci.* **8**, 159-66.

Waagepetersen H.S., Sonnewald U., Larsson O.M., Schousboe A. (2000). A possible role of alanine for ammonia transfer between astrocytes and glutamatergic neurons. *J. Neurochem.* **75**, 471-9.

Westergaard N., Sonnewald U., Schousboe A. (1995). Metabolic trafficking between neurons and astrocytes: the glutamate/glutamine cycle revisited. *Dev. Neurosci.* **17**, 203-11.

Yu A.C., Schousboe A., Hertz L. (1984). Influence of pathological concentrations of ammonia on metabolic fate of ^{14}C-labeled glutamate in astrocytes in primary cultures. *J. Neurochem.* **42**, 594-7.

Yudkoff M., Daikhin Y., Grunstein L., Nissim I., Stern J., Pleasure D. (1996). Astrocyte leucine metabolism: significance of branched-chain amino acid transamination. *J. Neurochem.* **66**, 378-85.

CHAPTER 4

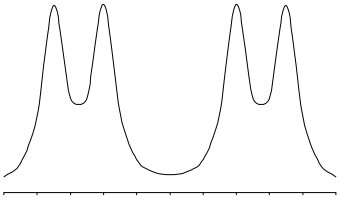

Lactate Recycling Through the Plasma Membrane of Astrocytes and Neurons as Detected by (^{13}C, ^{2}H) NMR

Results in this chapter were submitted for publication as:

Fonseca L. L., Sierra A., Santos H. & Cerdán S (2006) J. Cereb. Blood Flow Metab.

Chapter | 4 | Contents

ABSTRACT

We investigated the recycling of lactate between extracellular space and the cytosolic pool of pyruvate through the monocarboxylate transporters of the plasma membrane and the lactate dehydrogenase. For this purpose, primary cultures of astrocytes and neurons were incubated in Krebs Ringer bicarbonate buffer containing 50% $^{2}H_2O$ and [3-^{13}C]lactate (1 to 20 mM). Samples of incubation medium were collected at different times points and analyzed by ^{13}C-NMR to determine the deuteration kinetics of [3-^{13}C]lactate. A mathematical model was developed to analyse the time courses of lactate deuteration, which accounted for: (i) the bidirectional lactate transport in and out of the cells, (ii) the intracellular interconversion between lactate and pyruvate catalyzed by lactate dehydrogenase, and (iii) the pyruvate consumption. Results demonstrate that lactate recycling occurs in both cell types and increases with higher extracellular concentrations of lactate. In the same conditions astrocytes showed to have a higher lactate recycling activity than neurons, which was due to the differences in the reaction rates of the lactate dehydrogenase isozymes. Lacate dehydrogenase was the rate limiting step of lactate recycling process and favoured the neuronal pyruvate consumption and the glial lactate production. The use of ^{13}C-NMR spectroscopy to detect deuteration in the geminal and vicinal positions of a carbon-13 labelled precursor proved to be a powerful technique to study hydrogen turnover, providing complementary information to the conventional ^{13}C NMR method used to elucidate carbon turnover.

INTRODUCTION

Lactate metabolism in brain cells is the cross road linking the glycolytic pathways to the tricarboxylic acid cycles of astrocytes and neurons. In the astrocyte-neuron lactate shuttle hypothesis (ANLSH) assumes that lactate is produced by astrocytes and consumed by neurons (Pellerin and Magistretti, 1994). In agreement with this theory, astrocytes and neurons express differently the isozymes and the transporters required to metabolize lactate. Lactate transport is ensured in the mammalian brain by the family of monocarboxylate transporters (MCT's) (Bergersen *et al.,* 2002). In mouse it has been shown that astrocytes express only MCT1 and neurons MCT2 (Pierre *et al.,* 2000). Similar evidences, obtained with rats, suggest that neurons only express MCT2 but astrocytes may express both MCT1 and MCT2 (Gerhart *et al.,* 1998; Hanu *et al.,* 2000). Transport kinetic studies performed on MCT-expressing *Xenopus laevis* oocytes suggest that MCT1 and MCT2 favour the transport of lactate outwards or inwards, respectively (Broer *et al.,* 1997; Broer *et al.,* 1998; Broer *et al.,* 1999), thus supporting the ANLSH. More recently MCT4 was shown to be expressed in rat brain and characterized as being a transporter optimized for lactate release (Dimmer *et al.,* 2000). This transporter shows a differential expression pattern in the brain, and it has been shown to be present in astrocytes and absent in neurons (Bergersen *et al.,* 2001; Rafiki *et al.,* 2003).

Lactate dehydrogenase (LDH) has also been shown to be differently expressed in neurons and astrocytes (Bittar *et al.,* 1996; Laughton *et al.,* 2000). Astrocytes express LDH-5, the same isozyme expressed in muscle cells and thought to favour lactate formation, while neurons express LDH-1, the heart type isozyme thought to favour lactate consumption.

Lactate consumption and production has been shown to occur in cultures of astrocytes or neurons but, to our knowledge, recycling of this metabolite has never been investigated, probably because this is a difficult process to measure. By using [3-^{13}C]lactate and replacing 50% of the water ($^{1}H_2O$) in the incubation medium by $^{2}H_2O$ it became possible to follow lactate recycling (Rodrigues *et al.,* 2005). In this technique, the transported [3-^{13}C]lactate is metabolized to [3-^{13}C]pyruvate, which in

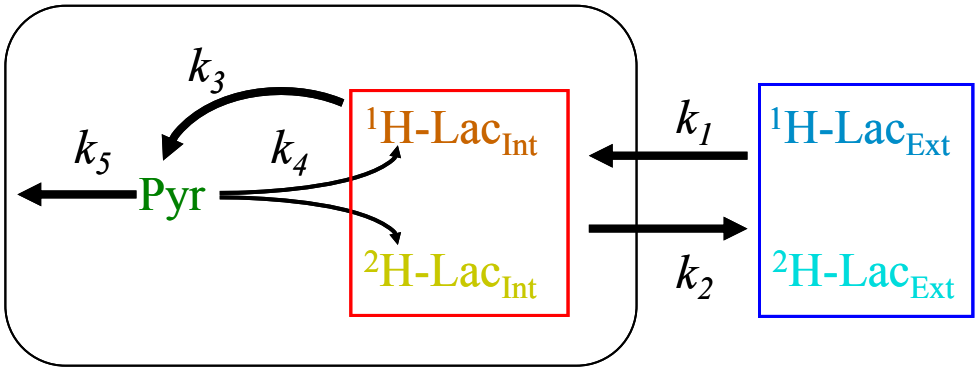

Figure 4.1 – Model of lactate recycling. The model assumes that all reactions follow first-order kinetics. k_1 and k_2 characterize the in and outwards transport of lactate by the monocarboxylate transporters (MCT's); k_3 and k_4 characterize the redox reaction between pyruvate and lactate catalyzed by the lactate dehydrogenase (LDH) and site of ^{1}H-^{2}H exchange; k_5 characterizes the consumption of pyruvate.

turn can be either further oxidized in the mitochondria or reduced back to lactate and subsequently released by the cell (Fig. 4.1). In the presence of 50% ^2H_2O, half of the reduced pyruvate is deuterated ([2-^{2}H,3-^{13}C]lactate) and once released this lactate molecule is easily detected and distinguished from the [3-^{13}C]lactate by ^{13}C NMR (Garcia-Martin *et al.,* 2002). The results of this study show that lactate recycling does occurs in both cell types and provide a model to interpret the mechanism. Lactate recycling is shown to proceed to a larger extent in astrocytes than in neurons, and the reason for this difference appears to be due to the different kinetic properties of the LDH isozymes, since MCT kinetics were found to be similar. In neurons the LDH equilibrium favoured the formation of pyruvate while in astrocytes favoured the formation of lactate.

Experimental Procedures

Materials

Dulbecco's modified Eagle's medium (DMEM), foetal bovine serum (FBS), horse serum (HS) and phosphate-buffered saline (PBS) were purchased from GIBCO (Glasgow, U.K.). Kits for analytical determinations were from Roche (Mannheim, Germany). Sodium [3-^{13}C]L-Lactate (98% ^{13}C) was purchased from Cambridge Isotope Laboratories, Inc. (Andover, MA, USA) and the ^2H_2O (>99.92%) was obtained

from Apollo Scientific (Cheshire, UK). Other chemicals were of the purest grade available from regular commercial sources.

Cell Culture

Primary cultures of cortical astrocytes were prepared from newborn (up to 2-day-old) Wistar rats. In short, the cortices were removed and cleaned from the meninges. The tissue obtained was minced, ressuspended with a pipette and vortexed for 1 minute. The resulting suspension was passed through a 80 μm filter and the cells seeded in poly-lysine coated 8 cm plate with 10 mL of DMEM containing 10% FBS, 10% HS, 10 mM HEPES, 2.5 μg/mL of fungizone and 100 U/mL of penicillin/streptomycin. Plates were maintained in a humidified incubator chamber at 37°C with 5% CO_2. After one week in culture cells were transferred to DMEM with 5% FBS, 5% HS, 10 mM HEPES, 2.5 μg/mL of fungizone and 100 U/mL of penicillin/streptomycin. Confluent cultures were obtained and used for experiments after two weeks in culture.

Primary cultures of cortical neurons were prepared from embryos of Wistar rats with 17 days of gestation. In short, after removal of the embryos, the brains were removed, cleaned, and the cortical areas collected in a PBS solution with 6 mM glucose and 1% BSA. The tissue obtained was minced and ressuspended with a pipette. The suspension was passed through a 80 μm filter and the cells seeded at 1.3×10^6 cells/mL in poly-lysine coated 8 cm plates with 10 mL of culture medium (DMEM with 15 mM HEPES, 2.5 μg/mL of fungizone, 100 U/mL of penicillin/streptomycin, 5 ng/mL Na_2SeO_4, 5 μg/mL insulin, 5 μg/mL transferrin, 6.3 ng/mL progesterone and 100 μM putrescine) containing 5% FBS, 5% HS. The plates were maintained in a humidified incubator chamber at 37°C with 5% CO_2. After 24 hours of culture, the cells were transferred to culture medium without serum and maintained for 6 more days in culture. Cytosine β-D-arabinofuranoside (10 μM) was added to the culture medium 48 hours before the experiments.

Recycling Experiments

When ready for use, the plates with the primary cultures of brain cells were washed with 5 mL of PBS and incubated with 12 mL of Krebs Ringer bicarbonate buffer (119 mM NaCl, 24 mM HEPES, 4.7 mM KCl, 1.2 mM $MgSO_4$, 1.2 mM KH_2PO_4 and 1.3 mM $CaCl_2$, pH 7.4) in 50% ^2H_2O, containing different concentrations of [3-^{13}C]lactate (5 and 10 mM for neurons and 1, 5, 10 and 20 mM for astrocytes). Samples of 600 μL of medium were taken at 0, 3, 6, 12, 24 and 48 hours of incubation. After measuring the pH, each sample was heat inactivated by incubation at 80°C for 20 minutes, and centrifuged at 10,000×g for 10 minutes. The supernatant solutions were saved and frozen until NMR analysis. At the end of the 48 hour period, after collection of the last sample, cells were washed and treated with perchloric acid. The cell extracts were centrifuged at 10,000×g and 4°C for 20 min and the acid insoluble precipitate used to measure the total protein content.

Substrate Switching Experiments

Substrate switching experiments in astrocytes were carried out in cultured prepared as described in Chapter 4. Glucose and lactate determination were quantified in the culture medium using an YSI 2700 Select system (YSI Life Sciences, USA) under the standard operation conditions advised by the supplier.

^{13}C NMR Spectroscopy

Broad band proton decoupled ^{13}C NMR spectra of the medium samples were obtained at 11.7 Tesla with a Bruker Avance 500 WB spectrometer operating at 125.76 MHz. Spectra were acquired at 300 K, with 60° pulses and 7 s recycle time, covering a 30 kHz sweep width. Spectra resulted from the sum of 700 FIDs, with 64k points and zero-filled to 256k points prior to Fourier transformation. Broad band proton decoupling was gated on during acquisition only. Chemical shifts were calibrated with the resonance of a 10% (v/v) dioxane solution (67.4 ppm) placed in a coaxial capillary. Quantification of the areas of the multiplets was achieved by deconvolution using a MATLAB™ program written for this purpose. Deconvolution was performed by minimizing the difference between the acquired spectrum and a

simulated spectrum resulting from the sum of Pearson type VII functions (van Winden *et al.,* 2001).

Cell Quantification and Analytical Methods

Total protein was determined using kit 23220 from Pierce (Rockford, Md, USA). Lactate was quantified in the culture medium using a spectrophotometric enzymatic assay from Boehringer (Mannheim, Germany) kit 139084.

Mathematical Model for Data Analysis

A mathematical model was used to describe lactate recycling and the associated kinetic processes (Fig. 4.1), which were modelled as having first-order kinetics ($\Phi_x = k_x$ [Substrate]). The model assumes three metabolite pools (extracellular and intracellular lactate, and intracellular pyruvate), of which lactate can be found in two forms (protonated and deuterated); two opposite transport reactions associated with the activity of the MCT, characterized by the rate-constants k_1 and k_2; two opposite reactions associated with the LDH activity and characterized by the rate-constants k_3 and k_4; and one reaction for pyruvate consumption with the rate-constant k_5. The following equations were used to describe the lactate recycling:

$$\frac{\partial[^1\text{H-Lac}_{\text{Ext}}]}{\partial t} = -[^1\text{H-Lac}_{\text{Ext}}]\cdot k_1 + [^1\text{H-Lac}_{\text{Int}}]\cdot k_2 \cdot \frac{V_i}{V_e} \qquad \text{(Eq. 4.1)}$$

$$\frac{\partial[^2\text{H-Lac}_{\text{Ext}}]}{\partial t} = -[^2\text{H-Lac}_{\text{Ext}}]\cdot k_1 + [^2\text{H-Lac}_{\text{Int}}]\cdot k_2 \cdot \frac{V_i}{V_e} \qquad \text{(Eq. 4.2)}$$

$$\frac{\partial[^1\text{H-Lac}_{\text{Int}}]}{\partial t} = [^1\text{H-Lac}_{\text{Ext}}]\cdot k_1 \cdot \frac{V_e}{V_i} - [^1\text{H-Lac}_{\text{Int}}]\cdot k_2 - [^1\text{H-Lac}_{\text{Int}}]\cdot k_3 + [\text{Pyr}]\cdot k_4 \cdot (1-\text{Pd}) \qquad \text{(Eq. 4.3)}$$

$$\frac{\partial[^2\text{H-Lac}_{\text{Int}}]}{\partial t} = [^2\text{H-Lac}_{\text{Ext}}]\cdot k_1 \cdot \frac{V_e}{V_i} - [^2\text{H-Lac}_{\text{Int}}]\cdot k_2 - [^2\text{H-Lac}_{\text{Int}}]\cdot k_3 + [\text{Pyr}]\cdot k_4 \cdot \text{Pd} \qquad \text{(Eq. 4.4)}$$

$$\frac{\partial[\text{Pyr}]}{\partial t} = ([^1\text{H-Lac}_{\text{Int}}] + [^2\text{H-Lac}_{\text{Int}}])\cdot k_3 - [\text{Pyr}]\cdot k_4 - [\text{Pyr}]\cdot k_5 \qquad \text{(Eq. 4.5)}$$

where [^{1}H-Lac$_{Ext}$] and [^{1}H-Lac$_{Int}$] represent the extra- and intracellular concentrations of [3-^{13}C]lactate; [^{2}H-Lac$_{Ext}$] and [^{2}H-Lac$_{Int}$] are the extra and intracellular concentrations of [3-^{13}C, 2-^{2}H]lactate; [Pyr] is the intracellular concentration of [3-^{13}C]pyruvate; $k_{1\text{-}5}$ are the first-order kinetic constants associated to the five

reactions (Fig. 4.1); V_i and V_e are the volumes of the intra and extracellular compartments; and Pd is the probability of deuteration.

Since the transport reactions are associated with a change in compartments and the intra and extracellular compartments have different volumes it was necessary to correct the fluxes by converting intracellular concentrations into extracellular and vice-versa. This was achieved by multiplying the concentrations by the ratio between the volumes (V_i/V_e and V_e/V_i) of both compartments. The amount of protonated or deuterated lactate formed from pyruvate was determined by the probability of deuteration (Pd), hence the corresponding fluxes from pyruvate to lactate characterized by k_4 (eq. 4.3 and 4.4) were multiplied by either (1-Pd) or Pd. It was assumed that the intracellular volumes of astrocytes and neurons are the same and equal to 5.14 µL/mg protein (Bender *et al.,* 1997), the initial concentration of pyruvate was 0.143 mM, and the initial concentration of intracellular lactate was 1.32 mM. It was also assumed that both intra and extracellular lactate were, initially, 100% protonated. The probability of deuteration (Pd) was 0.5, due to the presence of 50% ^2H_2O in the incubation medium. The space of possible solutions was restricted to solutions where neither the concentration of pyruvate nor intracellular lactate were able to attain values higher than the initial values.

Statistics

Results were presented as mean ± standard deviation. Two-tailed Student's t-tests, assuming unequal variances, were used to determine whether there were significant differences between groups of samples under different experimental conditions. A level of $p < 0.05$ was considered statistically significant. All experiments were repeated three times in cell cultures prepared from different animals.

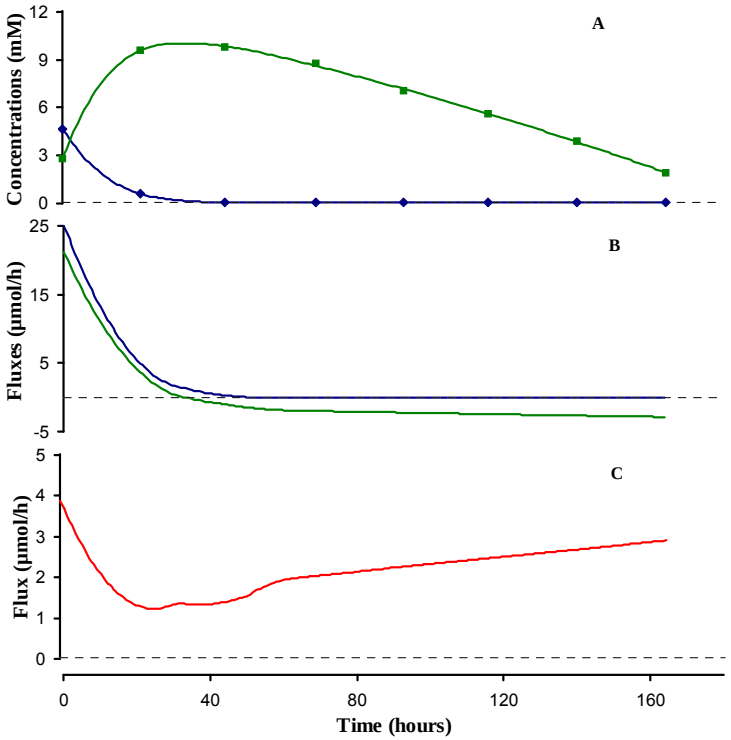

Figure 4.2 – Glucose and lactate metabolism of a primary culture of astrocytes in a T-flask. In **A**, the time course of the concentrations of glucose (◆) and lactate (■) in the culture medium (DMEM containing 10% FBS, 1% penicillin/streptomycin). In **B**, the time course of the fluxes of glucose consumption (in pyruvate units —) and of lactate release (—). In C, the time course of pyruvate oxidation (—) in the same culture.

RESULTS

Lactate Metabolism in Primary Astrocytes

To study the metabolism of lactate in astrocytes a pulse of glucose was supplied to a primary culture of astrocytes and the lactate production was followed. The astrocytes rapidly consumed the supplied glucose (5 mM) and 20 hours later less than 1 mM was left (Fig. 4.2). Concomitantly, there was the production of lactate with the usual lactate to glucose ratio of 1.65 ± 0.05 (during the first 20 hours). This production was only sustained while glucose was present in the medium. After glucose exhaustion, cells switched to the consumption of lactate (from 40 hours onwards). By assuming that the metabolism of glucose results in the production of

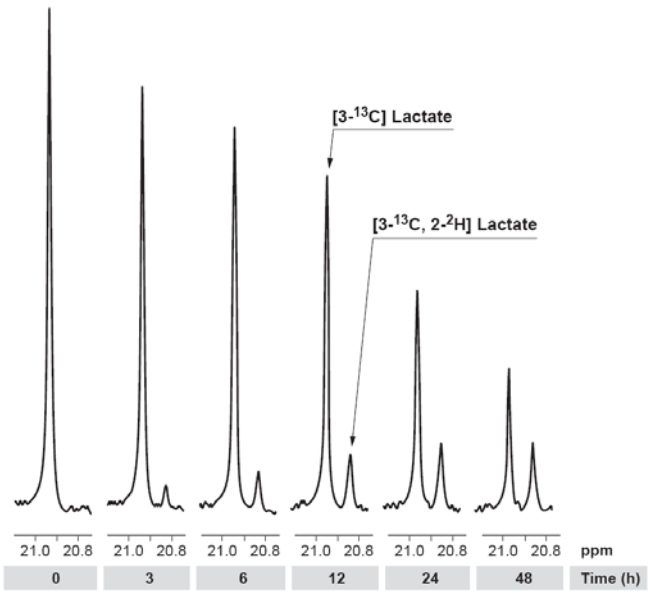

Figure 4.3 – Time course for the deuteration of lactate. Astrocytes were incubated with Krebs buffer containing 50% $^{2}H_2O$. Samples were taken at different time points and analyzed by ^{13}C NMR. Representative spectra of samples of the same culture of astrocytes are shown.

2 pyruvate molecules, which can either be reduced to lactate or oxidized, and that the pyruvate concentration within the cells does not change with time, it is possible to calculate the fluxes contributing to the pyruvate pool:

$$\frac{d[Pyr]}{dt} = 2 \cdot F_{Glycolysis} - F_{Lactate} - F_{Pyr\,ox} = 0 \qquad \text{(Eq 4.6)}$$

$$F_{Pyr\,ox} = 2 \cdot F_{Glycolysis} - F_{Lactate} \qquad \text{(Eq 4.7)}$$

From equation 4.6 it is possible to determine the flux of pyruvate oxidation ($F_{Pyr\ ox}$, Eq 4.7), as the difference between the glycolytic flux ($F_{Glycolysis}$) and the production of lactate (F_{Lacate}). Figure 4.2 graph B shows the calculated fluxes and it is clear that when glucose was exhausted cells went through a period where the oxidation of pyruvate was low. Eventually cells increased their capacity for lactate metabolization and the flux of pyruvate oxidation increased to values similar to the ones found in the presence of glucose. Pyruvate oxidation between 0 and 20 hours (during glucose consumption), and between 60 and 160 hours (during lactate consumption) were 2.3 ± 0.8 and 2.5 ± 0.3 µmol/h, respectively. Given, as shown, that the astrocytes are capable of switching the carbon source from glucose to lactate it was deemed interesting to study lactate metabolism in brain cells.

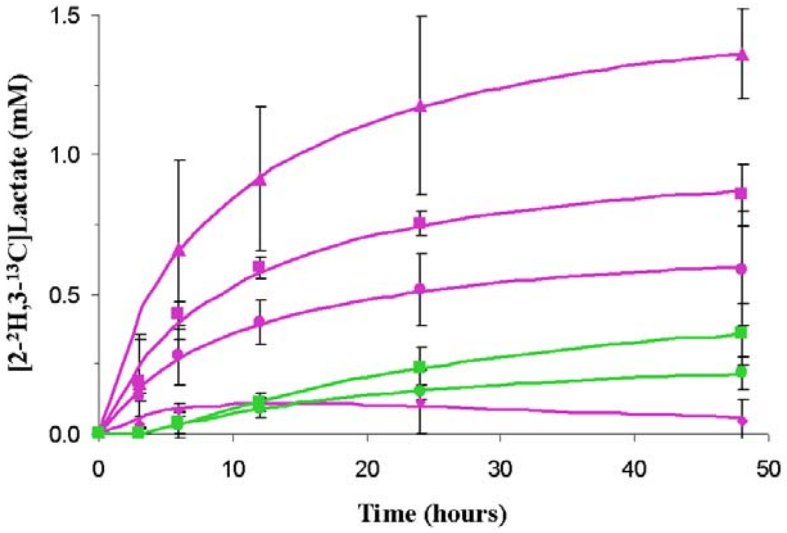

Figure 4.4 – Lactate recycling in astrocytes and neurons. Astrocytes (——) and neurons (——) were incubated with 1 mM (◆), 5 mM (●,●), 10 mM (■,■) and 20 mM (▲) [3-^{13}C]lactate and the amounts of released [2-^{2}H,3-^{13}C]lactate determined. Data points are averages of three experiments.

Lactate Recycling in Brain Cells

A representative time course of lactate deuteration obtained from a culture of rat astrocytes incubated with 5 mM [3-^{13}C]lactate up to 48 hours is shown in figure 4.3. It is possible to observe how [3-^{13}C]lactate (20.92 ppm) was consumed and simultaneously there was production of [3-^{13}C, 2-^{2}H]lactate (20.82 ppm), which shows unambiguously that pyruvate recycling occurs even during lactate consumption. Similar experiments with different concentrations of lactate performed in both astrocytes and neurons showed that recycled lactate increased with increasing concentrations of lactate (Fig. 4.4). Astrocytes are also shown to be more active in lactate recycling than neurons (Fig. 4.4). Control experiments performed in exactly the same conditions, but without cells, showed no production of [3-^{13}C, 2-^{2}H]lactate. Also, measurements of the extracellular pH were performed and showed no time dependent variations.

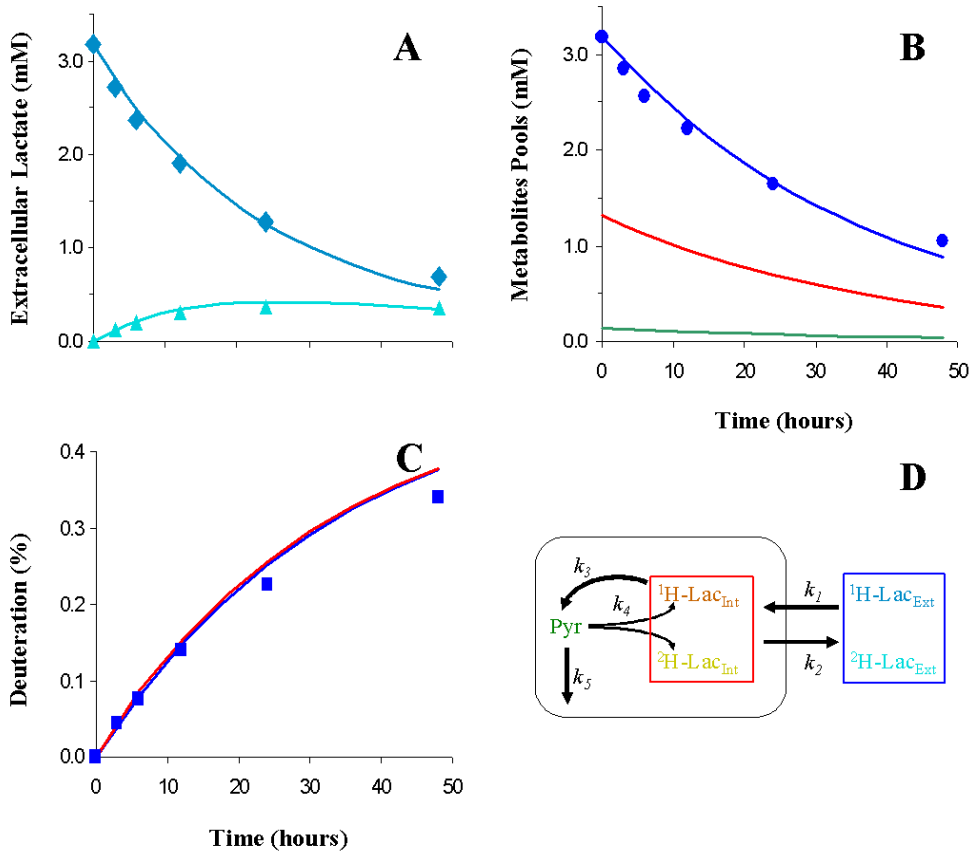

Figure 4.5 – Results obtained by fitting the data presented in **A** to the mathematical model described in Experimental Procedures. In **A**, the points represent experimental concentrations of protonated and deuterated extracellular lactate (◆ - [3-^{13}C]lactate; ▲ - [2-^{2}H,3-^{13}C]lactate) and the lines are the best fits obtained from the model (— [3-^{13}C]lactate; — [2-^{2}H,3-^{13}C]lactate). In **B**, the total concentrations of extracellular lactate (—), intracellular lactate (—) and pyruvate (—) obtained from the model and the experimental values for the total extracellular lactate (●) are shown. In **C**, the percentage of deuteration in extracellular (—) and intracellular (—) lactate obtained from the model as well as the experimentally obtained percentage of deuteration of the extracellular lactate (■) are shown. In **D**, scheme of the lactate recycling pathway.

Modelling the Lactate Recycling in Brain Cells

To extract information on the reactions behind these results (Figs. 4.3 and 4.4) a mathematical model was developed which included the transport reactions of the MCT, the LDH reactions and the reaction of consumption of pyruvate (Fig. 4.1). The results obtained with this modelling approach are illustrated in Figure 4.5 for the data obtained from an incubation of cortical astrocytes with 5 mM of [3-^{13}C]lactate.

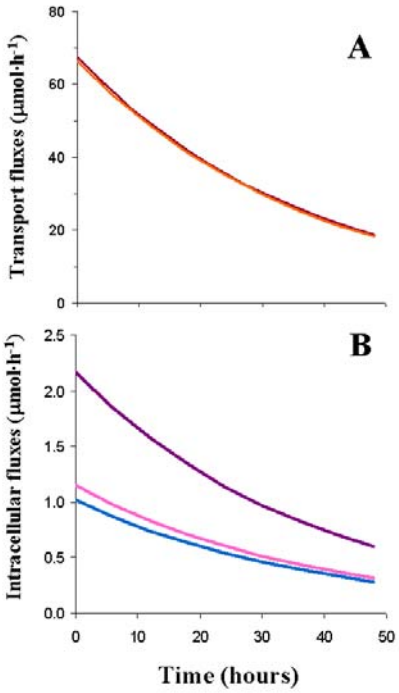

Figure 4.6 – Calculated fluxes obtained from the best fit of the data presented in Fig. 5.4. A to the model described in the Experimental Procedures. In **A,** the calculated fluxes of transport of lactate (—— - uptake; —— - release). In **B**, the calculated fluxes for the conversion of lactate into pyruvate (——), conversion of pyruvate into lactate (——) and pyruvate consumption (——).

Given the kinetics observed (Fig. 4.5 A) and the low number of parameters involved, the reactions were modelled as having first-order kinetics. The model allowed a satisfactory simulation of the results obtained (Fig. 4.5 A). However, several assumptions had to be made. First, the initial intracellular concentrations of lactate (1.32 mM) and pyruvate (0.143 mM) at time t=0 were set to same fixed values in all preparation to get consistent results from the different experiments. Similarly, and because there was no information on the variations of the intracellular concentrations, these were not allowed to increase above the initial values. These restrictions are apparent in Figure 4.5 B, where the intracellular concentration of lactate and pyruvate decrease with the extracellular lactate concentration throughout the time course of the experiment. These assumptions led to a similar percentage of deuteration of intracellular and extracellular lactate (Fig. 4.5 C). The values assumed for the initial concentration of intracellular lactate (1.32 mM) and

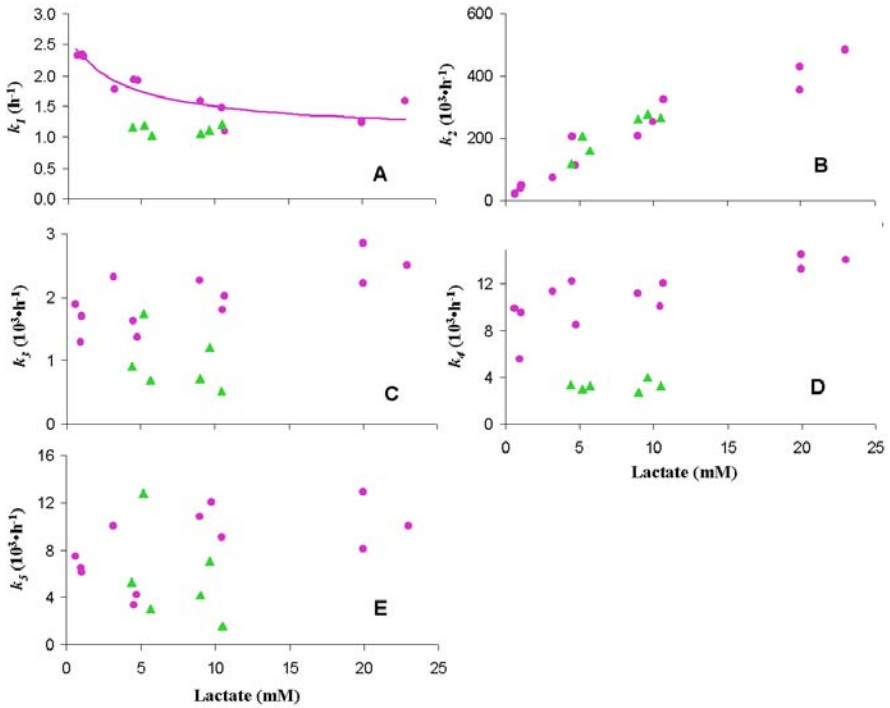

Figure 4.7 – Plots of the first-order kinetic constants obtained from best fits to the model described in Experimental Procedures as a function of the initial extracellular lactate concentration used in cultures of astrocytes (●) and neurons (▲).

pyruvate (0.143 mM) were obtained from best fits to the data and chosen because they were within the reported physiological values (Pryce *et al.,* 1970; McKenna *et al.,* 1995). Figure 4.6 shows the time course of the fluxes (see Fig. 4.1) calculated by the model for the data presented in Fig. 4.5. It is clear that the transport fluxes (Fig. 4.6 A) are at least one order of magnitude higher than the intracellular fluxes. Moreover, the transport fluxes were 65 times higher than the overall consumption of lactate (pyruvate consumption flux, Φ_5). This flux distribution, with transport fluxes being much larger than the metabolic steps, was similar for all experiments in both cell types, indicating that lactate recycling is not limited by transport but rather by the activity of the lactate dehydrogenase.

Characterization of the Observed Kinetics

Several rate-constants were determined by fitting to the model, described, the time courses obtained for both cultures systems with different concentrations of extracellular lactate. Plots of these rate-constants *versus* the initial extracellular concentration of lactate are shown in Figure 4.7. The results obtained for the first-order rate-constant of lactate uptake, k_1 (Fig. 4.7 A), in astrocytes, show a slight decrease with increasing concentrations of lactate while it remained constant for neurons. Additionally, the results obtained for k_1 in astrocytes fitted the function:

$$k_1 = \frac{V_{\max}}{K_m + [Lactate]} + const \qquad \text{Eq (4.8)}$$

with a K_m of 3.76 mM. The rate-constant of release of lactate, k_2 (Fig. 4.7 B), increased linearly with the concentration of lactate regardless of the cell type examined. In astrocytes the rate-constants of lactate oxidation and pyruvate reduction, k_3 and k_4, showed a small tendency to increase (Fig. 4.7 C and D). However, given the dispersion of the results it is unlikely that these rate-constants are significantly dependent on the concentration of lactate. In neurons, k_3 and k_4 showed no correlation with the concentration of lactate. Interestingly, it can be seen that k_3 and k_4 refer to the steps of the lactate recycling pathway in which the difference between astrocytes and neurons is more pronounced. The rate-constant of pyruvate consumption, k_5 (Fig. 4.7 E), showed also to be independent of the lactate concentration in both astrocytes and neurons. In order to clarify the differences between the two cell types the means of the rate-constants were calculated and expressed relative to the astrocytes values (Table 4.2). Table 4.2

Table 4.2.- Means of the rate-constants obtained for astrocytes and neurons with 5 and 10 mM extracellular lactate and expressed relative to the astrocyte values.

	Astrocytes (%)	Neurons (%)	Significance (p)
k_1[a]	100±18	81±5	0.15
k_2[a]	100±22	103±4	0.82
k_3	100±20	51±24	0.004
k_4	100±13	30±4	0.0001
k_5	100±37	66±46	0.2

[a] Only the results obtained with 10 mM lactate were averaged, due to the lactate concentration dependency of the parameter in question.

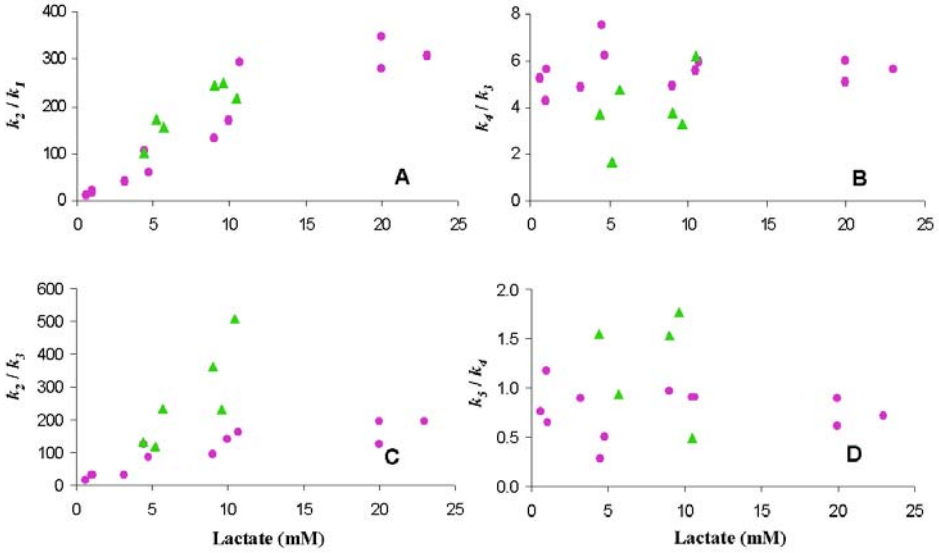

Figure 4.8 – Plots of the ratios k_2/k_1 (A), k_4/k_5 (B), k_2/k_3 (C) and k_5/k_4 (D) as function of the initial extracellular lactate concentration in cultures of astrocytes (●) and neurons (▲).

shows clearly that in fact the steps catalyzed by the LDH are the ones that best distinguish astrocytes and neurons. These results indicate that it is the slower activity of the neuronal pyruvate reduction the factor responsible for the reduced neuronal lactate recycling (Fig. 4.4). It is also clear that the lactate transport properties of astrocytes and neurons are quite similar.

Determination of the Equilibrium Constants and Flux Partition Ratios

To characterize better the lactate recycling pathway the equilibrium constants of the MCT (k_2/k_1) and LDH (k_4/k_3) steps were calculated (Fig. 4.8 A&B). Moreover the flux partition ratios of lactate and pyruvate were also calculated (Fig. 4.8 C&D). The

Table 4.3 – Means of the equilibrium constants and of the flux partition ratios obtained for astrocytes and neurons with 5 and 10 mM extracellular lactate and expressed relative to the astrocyte values.

	Astrocytes (%)	Neurons (%)	Significance (p)
k_2/k_1[a]	100±43	120±9	0.47
k_4/k_3	100±17	67±26	0.03
k_5/k_4	100±34	170±65	0.04
k_2/k_3[a]	100±27	281±106	0.05

[a] Only the results obtained with 10 mM lactate were averaged, due to the lactate concentration dependency of the parameter in question.

flux partition ratios allow to compare quantitatively fluxes out of a given metabolic pool and were determined using equations 4.9 and 4.10. The means of these rate-constant ratios were calculated as before (Table 4.3).

$$\frac{\Phi_2}{\Phi_3} = \frac{k_2 \cdot [\text{Lac}_{\text{Int}}]}{k_3 \cdot [\text{Lac}_{\text{Int}}]} = \frac{k_2}{k_3} \qquad \text{(Eq. 4.9)}$$

$$\frac{\Phi_5}{\Phi_4} = \frac{k_5 \cdot [\text{Pyr}]}{k_4 \cdot [\text{Pyr}]} = \frac{k_5}{k_4} \qquad \text{(Eq. 4.10)}$$

Given that k_2 numerically outweighs k_1, the equilibrium between intra and extracellular lactate (Fig. 4.8 A) was mainly determined by k_2, and hence k_2/k_1 increased linearly with the initial concentration of extracellular lactate. The equilibrium-constant of the reaction catalyzed by LDH (k_4/k_3, Fig. 4.8 B) was shown to be independent of the extracellular lactate concentration. As before the transport properties were similar in both cell types, but neurons showed to have a 67% smaller LDH equilibrium constant than astrocytes, indicating that the neuronal LDH equilibrium is displaced to the production of pyruvate while in astrocytes the lactate formation is favoured. In accordance with the previous results the flux partition ratio of pyruvate, k_5/k_4 (Fig. 4.8 D), showed no dependence with the concentration of lactate. Moreover, these results show that astrocytes recycle more pyruvate than what they consume ($k_5/k_4<1$), while neurons consume more pyruvate than what they recycle ($k_5/k_4>1$). The analysis of the flux partition ratio of lactate k_2/k_3 shows that in both cell types the fluxes through MCT were two orders of magnitude greater than the fluxes through LDH, thus confirming the observation made in respect to Figure 4.6. In neurons this difference was more pronounced due to the lower LDH fluxes found in these cells (see k_3 and k_4, Fig 4.7 C&D).

Statistical Analysis of the Results

A statistical analysis was performed to assess the possible linear dependence of the rate-constants obtained and their ratios with the initial extracellular concentration of lactate. To do so the slope and correlation factor of a linear regression were compared with the mean and the variation coefficient (Table 4.4).

The rate-constant of lactate uptake, k_1, in neurons showed very low correlation factor and variation coefficient, indicative of the independence of this rate-

constant from the initial lactate concentration. In contrast, the rate-constant of lactate release k_2, in both, astrocytes and neurons showed to be highly correlated with the initial concentration of lactate, as revealed by the high correlation factors. All intracellular rate-constants, k_{3-5}, showed low correlation factors, indicating that these rate-constants are independent of the initial concentration of lactate. Contrary to all the intracellular rate-constants, the rate-constant of pyruvate consumption, k_5, showed a high variation coefficient in neurons. This, however, does not seem to be indicative of a linear dependence of this rate-constant on the extracellular lactate; it may rather be solely the consequence of a higher degree of dispersion of this rate-constant results. Similarly to the results obtained for the rate-constants, the ratios of the rate-constants seem to be also independent of the initial concentration of lactate in both cell types, with the exception of the transport equilibrium, k_2/k_1. In agreement with the statistical analysis of the rate-constant of lactate release, k_2, the k_2/k_1 ratio was also linearly dependent on the initial concentration of lactate.

Effect of Glucose, Lactate and Glutamate on the Kinetics of Lactate Metabolism

The same model was used to study the effect of the presence of glucose (5 mM) or

Table 4.4 – Statistical analysis of the rate-constants and their ratios obtained from the mathematical model used to describe the lactate recycling pathway in primary cultures of astrocytes and neurons.

	Astrocytes				Neurons			
	Slope[a]	Correl[c]	Mean	VC[e]	Slope[a]	Correl[c]	Mean	VC[e]
k_1	n.a.	n.a.	n.a.	n.a.	0±14×10^{-3}[a]	0.00	**1.1±0.1**[d]	**0.06**
k_2	**19.0±1.7×10^{3}**[a]	**0.93**	211±158×10^{3}[d]	0.75	**22±5×10^{3}**[a]	**0.83**	214±63×10^{3}[d]	0.30
k_3	42±12[a]	0.54	**2.0±0.5×10^{3}**[d]	**0.24**	-69±79[a]	**0.16**	**1.0±0.4×10^{3}**[d]	0.47
k_4	246±62[a]	0.61	**11±3×10^{3}**[d]	**0.23**	28±80[a]	**0.03**	**3.3±0.4×10^{3}**[d]	0.13
k_5	204±98[a]	**0.30**	**8.3±3.0×10^{3}**[d]	**0.36**	-655±689[a]	**0.18**	**5.7±4.0×10^{3}**[d]	0.70
k_2/k_1	**14.8±1.7×10^{3}**[b]	**0.88**	148±127	0.86	**19±5×10^{3}**[b]	**0.80**	190±57	0.30
k_4/k_3	8±32×10^{-3}[b]	**0.01**	**5.6±0.8**	0.15	0.29±0.25[b]	0.24	3.9±1.5	0.39
k_5/k_4	0±0.01[b]	**0.00**	**0.8±0.2**	0.31	-0.04±0.11[b]	**0.04**	**1.3±0.5**	0.42
k_2/k_3	**7.0±1.3**[b]	**0.75**	101±65	0.65	**47±16**[b]	**0.69**	263±148	0.56

n.a. not applicable; [a] ($h^{-1}\cdot mM^{-1}$); [b] (mM^{-1}); [c] Linear correlation (r^2);
[d] (h^{-1}); [e] Variation coefficient

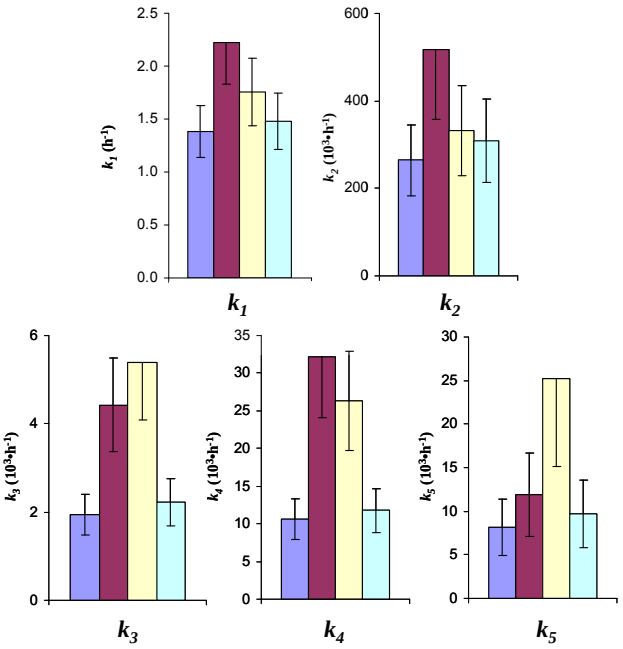

Figure 4.9 – Effects of co-incubation with 5 mM glucose (■), or 500 µM of glutamate (■) and of pre-incubation for 3 days with 10 mM lactate (■) on the first-order rate-constants (k_1, k_2, k_3, k_4 and k_5) determined from best fits to the model, for incubations with an initial concentration of [3-^{13}C]lactate of 10 mM. Control values are also plotted (■) for reference.

glutamate (500 µM) and the effect of a pre-incubation of 3 days with media containing 10 mM of lactate (without glucose) in astrocytes (Fig 4.9). All effects were studied as described above but for a single concentration of lactate (10 mM). As it can be seen in Figure 4.9, co-incubation with glucose (5 mM) increased the rate-constants of both reactions catalyzed the LDH and of both transport steps mediated by the MCT. Also noteworthy is the fact that the increments in k_4 and k_2 were higher than the increments in k_3 and k_1, thus showing a preference for an increased release of lactate rather than an increase in the uptake. Glucose, however, showed no effect on the first-order rate-constant of pyruvate consumption. Given that astrocytes seem to require some time to adapt to lactate consumption (Fig 4.2), these cells were supplied with culture media containing 10 mM of lactate (without glucose), 3 days before the study of the kinetic properties of the lactate recycling pathway. In these astrocytes, no significant differences were found in the lactate transport process. However, the rate-constants of both reactions coupled to the LDH

and of pyruvate consumption were increased. Co-incubation with glutamate (500 μM) had no effect on the recycling of lactate.

DISCUSSION

Transport and metabolism of lactate are the key components in the hypothesis of metabolic coupling between astrocytes and neurons. It has been shown that both LDH and MCT isoforms are differentially and selectively distributed in these brain cells; moreover, the distribution and kinetic properties of these isoforms support the astrocyte-neuron lactate shuttle hypothesis (Pellerin and Magistretti, 2004). The results obtained in the present study show that the rate-constants determined for MCT were similar in neurons and astrocytes, but the same does not hold true for the LDH equilibrium. In neurons the LDH equilibrium was more displaced towards the production of pyruvate than in astrocytes. Additionally, neurons showed lower values for the two rate-constants associated with the LDH reaction than astrocytes, thus resulting in a slower responding equilibrium. Moreover, the flux partitioning at the level of pyruvate clearly distinguishes the two cell types. While neurons consumed more pyruvate than what they recycled back to lactate, astrocytes recycled more pyruvate than what they consumed. These conclusions are in agreement with the proposed model of lactate shuttling between astrocytes and neurons and it does suggest that the distinctive behaviour of neurons and astrocytes in respect to the fate of pyruvate is mainly due to differences at the level of the LDH isoforms rather than to differences of the expressed MCT's. In fact, the transport properties of both cell types under the same conditions were similar, despite the different MCT isoform expressed. However, given the lower K_m of the neuronal lactate uptake system (Broer *et al.,* 1999), it is possible that *in vivo* the neuronal transporter outweighs its astrocytic counterpart. In any case no differences between neurons and astrocytes were found as far as the release of lactate is concerned.

The presence of glucose altered the flux distribution in the astrocytes. In fact glucose increased the rates of the LDH and of MCT in both directions, which may be due to an increased flux of glycolytic unlabeled pyruvate to lactate. This view is corroborated also by the fact that the increases were higher in the rate-constants of

the reactions involved in the production and release of lactate This is indicative of a shift of the equilibrium-constants, compatible with an increased flux of release of unlabeled lactate. As shown, astrocytes were capable of switching from glucose to lactate consumption. However this adaptation was not instantaneous, but it rather took some time to occur (24 to 36 hours). Afterwards, astrocytes showed an effective consumption of pyruvate, similar to the one found during glucose utilization. Similar observations have been made in C6 glioma cells by Bouzier and collaborators, (1998) who found that these cells had values of net 3-carbon unit entry in the same range for both glucose or lactate consumption (350 and 265±95 nmol/h/mg of protein, respectively). Also similar was the 75% yield of glucose conversion into lactate. Culturing the astrocytes for 3 days in media with 10 mM lactate and without glucose, before measuring lactate recycling, allowed the cells to adapt to this substrate. This adaptation resulted in a faster equilibrium at the level of the LDH and in an increased rate of consumption of pyruvate. However, it did not change the rates of transport of lactate in either direction.

The simple model developed in this work, allowed retrieving useful information out of the experimental data. Nevertheless, some assumptions had to be made to reduce the space of possible solutions. While the assumption of first-order kinetics was valid for the intracellular reactions, it was not satisfactory for the transport reactions as evidenced by the dependence of the calculated rate constants on the extracellular lactate concentration (Fig. 4.7). This differentiated behaviour was probably due to the different range of substrate concentrations experienced by the enzymes and transporters. In intracellular reactions the changes in substrate concentrations are small and probably within the range of the K_m of the enzymes, thus allowing the first-order kinetics to be a good linear approximation of the Michaelis-Menten kinetics. In the transport reactions the extracellular components may experience a wider range of substrate concentrations, to which the linear approximation may not yield good fits. As shown in Figure 4.7 A, the rate-constant for lactate uptake, k_1, in astrocytes could be fitted to the function $V_{max}/(K_m+[Lac_{Ext}])$, which indicates that the uptake flux ($\Phi_1=k_1$ $[Lac_{Ext}]$) had a Michaelian kinetics with a K_m of 3.76 mM. In contrast, the rate-constants determined for the release of lactate (k_2) were linearly dependent on the concentration of the "reaction product", i.e., the extracellular concentration of lactate. This odd feature probably reflects the limitation of the assumptions used, which imposed an initial intracellular lactate concentration of 1.32 mM and did not

allow solutions with the intracellular lactate concentration above this threshold. In fact, given the nature of the facilitated lactate transport (Hertz and Dienel, 2005), it is conceivable that increasing concentrations of extracellular lactate would lead to increasing concentrations of intracellular lactate. By imposing a lack of dependence of the intracellular lactate concentration on the extracellular lactate concentration, this dependency was transferred to the rate-constant. Attempts to avoid these discrepancies were made assuming that all reactions followed Michaelis-Menten kinetics, but this led to an excessive number of degrees of freedom for the available data. Furthermore, when it was assumed that all reactions had first-order kinetics except for the uptake of lactate which was assumed to follow Michaelis-Menten kinetics, the model did not generate satisfactory fits to the data. Despite these drawbacks the conclusions rendered by the model were validated by comparison with data from other authors. The K_m of 3.76 mM obtained is in excellent agreement with the published K_m of 3.5 mM measured for MCT1 produced in *Xenopus laevis* oocytes (Carpenter and Halestrap 1994; Broer *et al.,* 1997), and is within the same range of the K_m of 7.7 mM reported for astrocytes (Broer *et al.,* 1997). Moreover, the reported K_m's for lactate uptake in neurons (0.4 mM, Nedergaard and Goldman 1993) and in *Xenopus laevis* oocytes expressing MCT2 (0.74 mM, Broer *et al.,* 1999), are lower than 1 mM, which could explain why in the range of lactate concentrations examined in neurons (5-10 mM), the rate-constant k_1 showed to be independent of the extracellular lactate concentration.

In conclusion, data presented here shows that astrocytes have a greater lactate recycling capacity than neurons, and that lactate has clearly different fates in neurons and astrocytes. These differences were primarily due to the LDH properties, since the monocarboxylate transporters performed very similar in both cell types.

Acknowledgements and Work Contributions

We are grateful to Alejandra Sierra, IIB-CSCI, Madrid, Spain for the assistance rendered in the cellular preparation, in the lactate recycling experiments, in the samples analysis, and in the ^{13}C-NMR spectra recording.

REFERENCES

Bender A. S., Young L. P. and Norenberg M. D. (1997) Effect of lactic acid on L-glutamate uptake in cultured astrocytes: mechanistic considerations. *Brain Res.* **750**, 59-66.

Bergersen L., Rafiki A. and Ottersen O. P. (2002) Immunogold cytochemistry identifies specialized membrane domains for monocarboxylate transport in the central nervous system. *Neurochem. Res.* **27**, 89-96.

Bergersen L., Waerhaug O., Helm J., Thomas M., Laake P., Davies A. J., Wilson M. C., Halestrap A. P. and Ottersen O. P. (2001) A novel postsynaptic density protein: the monocarboxylate transporter MCT2 is co-localized with delta-glutamate receptors in postsynaptic densities of parallel fiber-Purkinje cell synapses. *Exp. Brain Res.* **136**, 523-534.

Bittar P. G., Charnay Y., Pellerin L., Bouras C. and Magistretti P. J. (1996) Selective distribution of lactate dehydrogenase isoenzymes in neurons and astrocytes of human brain. *J. Cereb. Blood Flow Metab.* **16**, 1079-1089.

Bouzier A. K., Goodwin R., de Gannes F. M., Valeins H., Voisin P., Canioni P., Merle M. (1998) Compartmentation of lactate and glucose metabolism in C6 glioma cells. A ^{13}C and ^{1}H NMR study. *J. Biol. Chem.* **273**, 27162-27169.

Broer S., Broer A., Schneider H. P., Stegen C., Halestrap A. P. and Deitmer J. W. (1999) Characterization of the high-affinity monocarboxylate transporter MCT2 in *Xenopus laevis* oocytes. *Biochem. J.* **341**, 529-535.

Broer S., Rahman B., Pellegri G., Pellerin L., Martin J. L., Verleysdonk S., Hamprecht B. and Magistretti P. J. (1997) Comparison of lactate transport in astroglial cells and monocarboxylate transporter 1 (MCT 1) expressing *Xenopus laevis* oocytes. Expression of two different monocarboxylate transporters in astroglial cells and neurons. *J. Biol. Chem.* **272**, 30096-30102.

Broer S., Schneider H. P., Broer A., Rahman B., Hamprecht B. and Deitmer J. W. (1998) Characterization of the monocarboxylate transporter 1 expressed in *Xenopus laevis* oocytes by changes in cytosolic pH. *Biochem. J.* **333**, 167-174.

Carpenter L. and Halestrap A. P. (1994) The kinetics, substrate and inhibitor specificity of the lactate transporter of Ehrlich-Lettre tumour cells studied with the intracellular pH indicator BCECF. *Biochem. J.* **304**, 751-760.

Dimmer K. S., Friedrich B., Lang F., Deitmer J. W. and Broer S. (2000) The low-affinity monocarboxylate transporter MCT4 is adapted to the export of lactate in highly glycolytic cells. *Biochem. J.* **350**, 219-227.

Garcia-Martin M. L., Garcia-Espinosa M. A., Ballesteros P., Bruix M. and Cerdan S. (2002) Hydrogen turnover and subcellular compartmentation of hepatic [2-^{13}C]glutamate and [3-^{13}C]aspartate as detected by ^{13}C NMR. *J. Biol. Chem.* **277**, 7799-7807.

Gerhart D. Z., Enerson B. E., Zhdankina O. Y., Leino R. L. and Drewes L. R. (1998) Expression of the monocarboxylate transporter MCT2 by rat brain glia. *Glia* **22**, 272-281.

Hanu R., McKenna M., O'Neill A., Resneck W. G. and Bloch R. J. (2000) Monocarboxylic acid transporters, MCT1 and MCT2, in cortical astrocytes in vitro and *in vivo*. *Am. J. Physiol. Cell Physil.* **278**, C921-930.

Hertz L. and Dienel G. A. (2005) Lactate transport and transporters: general principles and functional roles in brain cells. *J. Neurosci. Res.* **79**, 11-18.

Laughton J. D., Charnay Y., Belloir B., Pellerin L., Magistretti P. J. and Bouras C. (2000) Differential messenger RNA distribution of lactate dehydrogenase LDH-1 and LDH-5 isoforms in the rat brain. *Neuroscience* **96**, 619-625.

McKenna M. C., Tildon J. T., Stevenson J. H., Huang X. and Kingwell K. G. (1995) Regulation of mitochondrial and cytosolic malic enzymes from cultured rat brain astrocytes. *Neurochem. Res.* **20**, 1491-1501.

Nedergaard M. and Goldman S. A. (1993) Carrier-mediated transport of lactic acid in cultured neurons and astrocytes. *Am. J. Physiol.* **265**, R282-289.

Pellerin L. and Magistretti P. J. (1994) Glutamate uptake into astrocytes stimulates aerobic glycolysis: a mechanism coupling neuronal activity to glucose utilization. *Proc. Natl. Acad. Sci. U.S.A.* **91**, 10625-10629.

Pellerin L. and Magistretti P. J. (2004) Neuroenergetics: calling upon astrocytes to satisfy hungry neurons. *Neuroscientist* **10**, 53-62.

Pierre K., Pellerin L., Debernardi R., Riederer B. M. and Magistretti P. J. (2000) Cell-specific localization of monocarboxylate transporters, MCT1 and MCT2, in the adult mouse brain revealed by double immunohistochemical labeling and confocal microscopy. *Neuroscience* **100**, 617-627.

Pryce J. D., Gant P. W. and Sau K. J. (1970) Normal concentrations of lactate, glucose, and protein in cerebrospinal fluid, and the diagnostic implications of abnormal concentrations. *Clin. Chem.* **16**, 562-565.

Rafiki A., Boulland J. L., Halestrap A. P., Ottersen O. P. and Bergersen L. (2003) Highly differential expression of the monocarboxylate transporters MCT2 and MCT4 in the developing rat brain. *Neuroscience* **122**, 677-688.

Rodrigues T. B., Gray H. L., Benito M., Garrido S., Sierra A., Geraldes C. F., Ballesteros P. and Cerdan S. (2005) Futile cycling of lactate through the plasma membrane of C6 glioma cells as detected by (^{13}C, ^{2}H) NMR. *J. Neurosci. Res.* **79**, 119-127.

van Winden W. A., Heijnen J. J., Verheijen P. J. and Grievink J. (2001) A priori analysis of metabolic flux identifiability from ^{13}C-labeling data. *Biotechnol. Bioeng.* **74**, 505-516.

CHAPTER 5

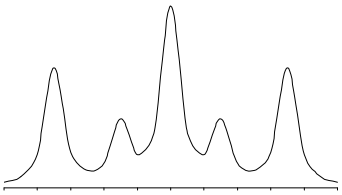

Culturing Primary Brain Astrocytes Under a Fully Controlled Environment in a Novel Bioreactor

This chapter is published in:

Santos S. S., **Fonseca L. L.**, Monteiro M. A. R., Carrondo M. J. T. & Alves P. M. (2005) J. Neurosci. Res. 79, 26-32.

Chapter | 5 | Contents

ABSTRACT

We report the first approach for growth and maintenance of primary astrocytes on a fully controlled environment. For this purpose, cells were immobilized in Cytodex microcarriers and grown in a stirred tank bioreactor. Crucial bioreaction parameters such as agitation rate, microcarrier type, and concentration, as well as cell inoculum concentration were assessed. Cytodex 3 proved the best microcarrier for astrocyte growth, with the highest cell densities obtained for 6 g/L of Cytodex 3 using an inoculum of approx. 0.15×10^6 cells/mL in vessels operated at 60 rpm, using a re-feed operational mode consisting of complete medium replacement every 5 days. Using such optimized conditions, cells were maintained in steady-state for approximately 24 days, allowing online monitoring and control of environmental variables such as temperature, pH, and O_2. To further test the advantages of this fully controlled system, astrocytes were subjected to a 5 hours hypoxic stress. The cell numbers were not affected by hypoxia but the glycolytic flux was enhanced during this period. To check whether this experimental set-up was suitable for metabolic flux analysis, the metabolism of [U-^{13}C]glucose pulse was followed by ^{13}C-NMR for a period of 24-hour. The culture system described is a novel tool to study brain cell metabolism, allowing sampling over time and the monitoring of cellular behaviour in response to stressful conditions as well as during recovery.

INTRODUCTION

Elucidation of the underlying metabolic mechanisms associated with cell degeneration in neurological disorders, such as Alzheimer's, Parkinson's, and Huntington's diseases, remains a challenge in neuroscience. Because brain networks are highly complex, simple model systems are useful to decipher basic biochemical features of individual cell types. Primary brain cell cultures are well established experimental models, in particular monolayer cell cultures (Hansson and Thorlin, 1999). Typically, cells are isolated from brains and grown as primary cultures in static conditions using tissue culture flasks (T-flasks) or culture dishes. This method, however, has restricted scalability, and working with large amounts of cells implies the manipulation of multiple culture systems, which is difficult, time consuming, and expensive. In addition, culture parameters such as pH and pO_2 are difficult to measure or control (Masters, 2000). Growing cells in stirred tank bioreactors circumvents these difficulties: being hydrodynamically well characterized, they are easy to scale-up and enable high cell densities, better homogeneity of cultures, and reproducible experimental conditions, controllable through sensors as pH and pO_2 electrodes. Ease of sampling allows cell number, viability, and intracellular and extracellular metabolites to be monitored over time.

Brain cells are anchorage-dependent and for scaling up from a static culture to a stirred tank bioreactor, it is necessary to use some kind of support. Since van Wezel (1967) first described a culture system using microcarriers as a solution for growing anchorage-dependent cells, a wide range of carriers have been developed, using different materials and surface types to culture a wide variety of cells. Microcarriers have a high surface-to-volume ratio, permitting high yields of cells in small volumes, efficient medium/cell separation, and are easily expanded and transferred, facilitating experimental manipulation. We have reported immobilization of primary brain cells in microcarriers and gel threads, under perfusion for *in vivo* NMR studies of the metabolism of neurons and astrocytes (Alves *et al.*, 1996a, 1997). However, these studies were carried out on cells cultured in microcarriers using conventional culture dishes in static conditions and not in stirred tanks.

The present work describes a novel stirred tank bioreactor system that enables growth and maintenance of primary brain cells in a fully controlled environment.

Although stirred conditions do not exist in brain, the cerebral system is vascularised and therefore, does not have a static environment. Blood flow is highly connected with metabolism of cerebral tissue (Guyton and Hall, 1996), reproduced in our system by the ability to diffuse nutrients, oxygen, and metabolites and thus simulating *in vivo* brain conditions. The concept of environmental movement was applied in earlier studies to brain slices with perfusion methods to elucidate several aspects of cerebral function; the velocity of the paddle stirrer was adjusted to ensure continuous gentle agitation of tissue preparations but damage to the slices reduced experimental lifetime to 8-10 hours (Cox *et al.*, 1983; Bachelard *et al.*, 1985, 1988).

The optimization of the culture system described here will expand the range of applications in the neuroscience field, e.g., in mimicking pathologic conditions associated with neurological diseases.

One major drawback of stirred tanks for animal cell growth is the fluid shear stress, which is most critical when microcarriers are required for cell attachment, as is the case for primary brain cells such as astrocytes. The most relevant parameters to optimize in these culture systems are related to the microcarrier characteristics (type, concentration, and inoculation procedures) and the conditions that lead to an efficient oxygen supply to the cells under the minimum shear stress (agitation and oxygenation rate) (Croughan and Wang, 1989). These variables were evaluated and optimized in this work that also describes the first attempt of culturing primary brain cell using fully environmentally controlled bioreactors.

EXPERIMENTAL PROCEDURES

Materials

Dulbecco's modified Eagle medium (DMEM), foetal bovine serum (FBS), penicillin-streptomycin, phosphate-buffered saline (PBS), and trypsin-EDTA were purchased from Invitrogen (Glasgow, UK). [U-^{13}C]Glucose was purchased from Isomed (Madrid, Spain). Culture flasks were obtained from Nunc (Roskilde, Denmark). Nonporous microcarriers, Cytodex 2 (dextran matrix with a surface layer of positive charges) and Cytodex 3 (dextran matrix with a collagen layer coupled to the surface), were purchased from GE Healthcare (Amersham Biosciences, Uppsala, Sweden). Other

chemicals used were of the purest grade available from regular commercial sources.

Cell Culture (Monolayers)

Primary cultures of astrocytes were prepared from 1-2-day-old rat brains as described previously (Richter-Landsberg and Besser, 1994). Briefly, cerebral hemispheres were carefully freed of the meninges, washed in ice-cold PBS, and mechanically disrupted. Single-cell suspensions were plated in T-flasks (3 hemispheres/175 cm^2) in DMEM supplemented with 10% FBS, penicillin-streptomycin (100 U/mL), and glucose (to obtain a final concentration of 10 mM). Cells were kept in a humidified atmosphere of 7% CO_2 in air at 37°C. After 8 days, the phase dark cells growing on the astrocytic cell layer were separated by vigorous shaking and removed as described previously (McCarthy and Vellis, 1980). The remaining astrocytes were detached by mild trypsinisation using trypsin/EDTA (0.25% wt/vol) and subcultured in T-flasks for another 3 weeks. Growth medium was changed twice a week.

Experiments in Stirred Conditions

Spinner Vessels and Bioreactor

Initial cell culture experiments were carried out in 125 mL spinner flasks (maximum culture volume) from Wheaton (Techne, USA). As Spinner flasks do not allow pH control, they have to be placed inside an incubator at 7% CO_2 in air and 37°C, with aeration taking place in the gas/liquid interface. In this work, these vessels were used to optimize critical parameters for cell culture in stirred conditions, namely: microcarrier type and concentration, agitation rate, cell inoculum concentration, and culture operational mode (batch vs. fed-batch vs. re-feed).

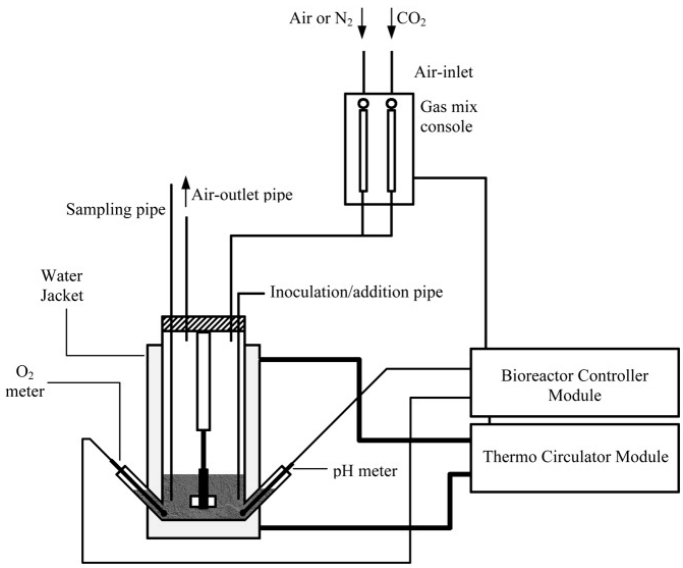

Figure 5.1 – Schematic representation of the small-scale bioreactor used. This culture system allows a fully controlled environment for cell growth and maintenance.

To ensure fully controlled cell culture environment, an improved vessel that could be adapted to a commercially available bioreactor unit (Applikon, Schiedam, Netherlands) was developed (Fig. 5.1). In this novel bioreactor vessel, the internal geometry and the stirrer are similar to the 125 mL spinners described above. A double glass wall with two lateral ports for pH and pO_2 meters (both from Mettler-Toledo, Urdorf, Switzerland) allow online measuring and control of these parameters. The pH was kept at 7.4 by injection of CO_2. The dissolved oxygen concentration was maintained at 60% via surface aeration with air. Hypoxia was induced by replacing the air with nitrogen. The pO_2 meter was calibrated beforehand at 100% by saturation of culture media with air. The temperature was maintained at 37°C by water recirculation in the vessel jacket controlled by a thermocirculator module. The bioreactor controller module was used to control pH, pO_2, and temperature. This bioreactor is easy to operate, fully sterilisable by autoclaving, and can be manipulated under sterile conditions outside the laminar flow hood. Its modularity and flexibility allows sampling, addition of nutrients or drugs, medium and gas exchanges, and medium perfusion throughout the whole cell culture time. For carbon labelling experiments astrocytes were grown in spinner flasks and when confluence was reached the entire content of the spinner flask was transferred to the bioreactor.

Cell Culture in Microcarriers

Microcarriers are used widely to grow anchorage-dependent cell lines in stirred conditions. The effect of microcarrier type and concentration in the culture of primary astrocytes was assessed using concentrations of 3 g/L (dry weight) for Cytodex 2 and 3, and 6 g/L for Cytodex 3. The microcarriers were prepared and sterilized according to the manufacturer's recommendations. Cell inocula were obtained from 3-week-old monolayer cultures of primary astrocytes. Cells were harvested by trypsinisation, pelleted by centrifugation, ressuspended in 5 mL culture medium, and immediately immobilized in the carriers. For this purpose, the cells and beads were mixed gently for approximately 3 min; afterward, 20 mL of culture medium was added. Cells were allowed to attach for 3 hours without stirring. During that period, to obtain an even more homogeneous distribution of the cells in the beads, the vessel was agitated gently for 1 min every 30 min. After this procedure, more than 90% of the cells were attached to the microcarriers. The culture volume was then adjusted to 60% of the vessel capacity by addition of culture medium, and was stirred continuously at the lowest speed that kept the beads suspended (approximately 40 rpm). After 24 hours, culture medium was added to obtain the final culture volume (125 mL) and agitation was increased to the experimental conditions, either 60 or 100 rpm. As mentioned above, the effect upon cell growth of the culture operational mode and different strategies (batch vs. fed-batch vs. re-feed) was tested. For the re-feed mode experiments, replacement of the culture medium was done easily by stopping agitation and removing/re-feeding medium immediately after the quick sedimentation of the carriers containing the cells.

Sampling

Samples containing microcarriers were taken on a daily basis. Cells growing on the microcarrier were visualized using an Olympus inverted microscope with phase contrast (Tokyo, Japan). Total cell number in Cytodex microcarriers was determined by counting cell nuclei using a Fuchs-Rosenthal haemocytometer after digestion with 0.1 M citric acid/1% Triton X-100 (wt/wt)/0.1% crystal violet (wt/vol) (Alves *et al.*, 1996b). Glucose and lactate concentrations in the culture supernatant were analyzed using a YSI 7100 Multiparameter Bioanalytical System (Dayton, OH, USA).

For NMR analysis a 30 mL sample (with microcarriers) was taken from the bioreactor after 8 hour of incubation (with labelled substrate) and the remaining volume collected 16 hours later. For both samples the microcarriers were allowed to settle for 1 or 2 min and the medium separated from the microcarriers. The medium was immediately transferred into a tube with 1 volume of ethanol at 0°C to stop all reactions and precipitate the protein and the microcarriers were washed with cold NaCl (9 g/L). The medium/ethanol mixture was centrifuged at 10000 g for 30 min at 4°C and the supernatant lyophilized to generate the extracellular sample. The cells in the microcarriers were extracted with ice-cold perchloric acid (5 M). After extraction the intracellular content was centrifuged (10000 g for 30 min at 4°C). The pellets were stored for protein analysis and the supernatants were neutralized and centrifuged and the resulting supernatant was lyophilized. For NMR spectroscopy analysis, the residues of lyophilized media and cell extracts were dissolved in D_2O.

^{13}C NMR Spectroscopy

^{13}C-NMR spectra of lyophilized culture medium samples and cellular extracts (pH 7.2) were acquired with 40 k data points using a 60° flip angle and 31 kHz spectral width. Proton decoupling was applied during the acquisition using the WALTZ sequence. The total recycle delay was 10.7 sec. For the extracellular (medium) and intracellular (cellular extracts) samples 1,024 and 4,096 transients were acquired, respectively. Spectra were recorded at a temperature of 300 K.

RESULTS

Effect of Microcarrier Type and Cell Inoculum

Cytodex 2 and Cytodex 3 were tested for their ability to support the growth of primary rat astrocytes in spinner vessels. Two cell inocula sizes were tested: 18 and 36 cells per microcarrier, corresponding to an initial cell concentration of approximately 0.15 and 0.3 $\times$ 10^6 cells/ mL, respectively, in the culture vessel. These values were chosen based on the ratio of cell per cm^2 usually recommended for the monolayer cultures in dishes and T-flasks. In these experiments, the microcarrier concentration was 3 g/L, the agitation rate was 60 rpm, and no addition or replacement was done to the culture medium, i.e., the spinners were operated in

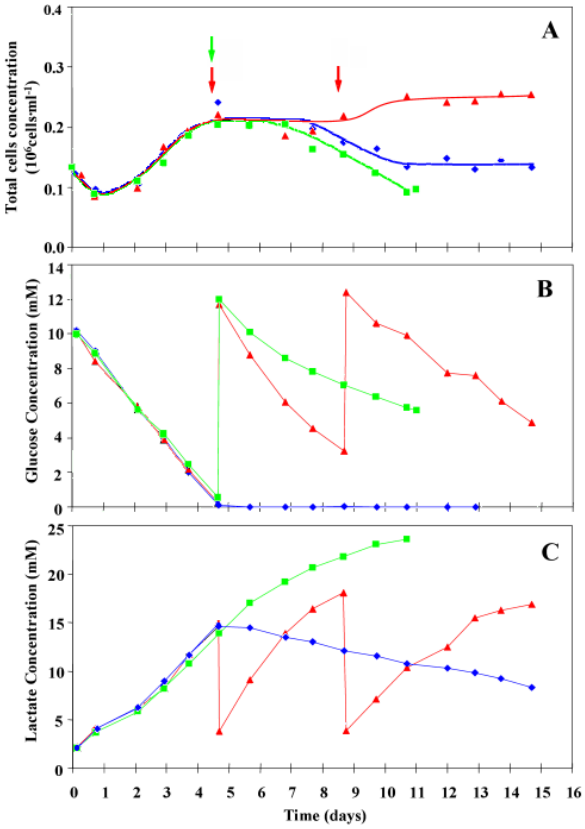

Figure 5.2 – Effect of the reactor operation mode upon cell growth (A), glucose consumption (B), and lactate production (C) through time. Batch mode (◆); fed-batch mode (■); re-feed mode (▲). The arrows indicate glucose addition (→) in the fed-batch mode or complete medium replacement (→) in the re-feed mode. The corresponding specific glucose consumption and lactate production rates are presented in Table 5.1. All experiments were carried out with Cytodex 3 microcarriers.

batch mode. Typically, after seeding (Day 0), the cells exhibited a growth curve consisting of a lag phase of 1.5–2 days followed by exponential phase leading to the maximum cell concentration at Day 4–5. Afterwards, a plateau phase was observed for 3–4 days (corresponding to cell confluence at the surface of the microcarriers), followed by a decline in the cell number (death phase) due to environmental changes such as nutrient deprivation and build-up of metabolic waste products.

The highest cell expansion ratio (maximum cell concentration/cell concentration at inoculation) of 1.82 was achieved 4 days after inoculation for Cytodex 3 microcarriers and an inoculum of 0.15×10^6 cells/mL. For both microcarrier types, the cell expansion ratio was significantly lower when the higher inoculum was used,

as expected. As the best results were obtained for Cytodex 3 and an inoculum of 0.15×10^6 cells/mL, these culture conditions were used in all following experiments.

Effect of Culture Operational Mode on Astrocyte Growth and Metabolism

It is known from the literature that the bioreactor operational mode may affect significantly the maximum cell concentration achieved in the culture as well as cell metabolism. Three different cell culture operation strategies were tested: batch (no medium change or addition); fed-batch (glucose addition at a specific time point); and re-feed (medium replenishment). The total cell concentration for each operation mode during the experimental period is presented in Figure 5.2 graph A. No significant differences were observed between the batch and the fed-batch operational modes. Adding glucose to the culture (at time 4.7 days, i.e., 113 hours) did not increase cell number and, in fact, the decrease in cell concentration was more pronounced when this strategy was used (fed batch). The best growth yield was obtained for the re-feed strategy, where a complete replacement of the culture medium was carried out twice (at time 4.7 and 8.7 days, i.e., at 113 and 209 hours, respectively, as indicated by arrows in Fig. 5.2 A). A plateau was reached after the first re-feed and the cell number increased only slightly after the second medium replacement. Afterward, no significant growth was observed and the cell number reached a new plateau that was maintained until the end of the culture (at time 15 days, i.e., 360 hours). The effect of the operational mode on cell metabolism was evaluated by measuring glucose and lactate yields (Fig. 5.2 B & C) and the respective consumption and production rates (Table 5.1). Glucose was completely depleted from the culture medium at Day 4.6 (i.e., 110 hours), coinciding with the cell growth arrest observed in Figure 5.2 A. Noteworthy, the cultures behaved similarly until this time (4.6 days, i.e., 110 hours), corresponding to the first glucose addition for cells under fed-batch and to the first re-feed for cells under this

Table 5.1 – Effect of culture operational mode on glucose uptake and lactate production rates of primary rat astrocytes growing in Cytodex 3 microcarriers in stirred conditions

	Rate (µmol/h/10^6 cells)					
	Glucose consumption			Lactate production		
Mode	Day 0-4.6	Day 4.6-8.7	Day 8.7-15	Day 0-4.6	Day 4.6-8.7	Day 8.7-15
Batch	0.61 ± 0.02	-	-	0.91 ± 0.02		
Fed-batch	0.56 ± 0.03	0.27 ± 0.03	-	0.82 ± 0.02	0.44 ± 0.05	
Re-feed	0.59 ± 0.02	0.59 ± 0.05	0.52 ± 0.04	0.96 ± 0.05	1.01 ± 0.16	0.85 ± 0.05

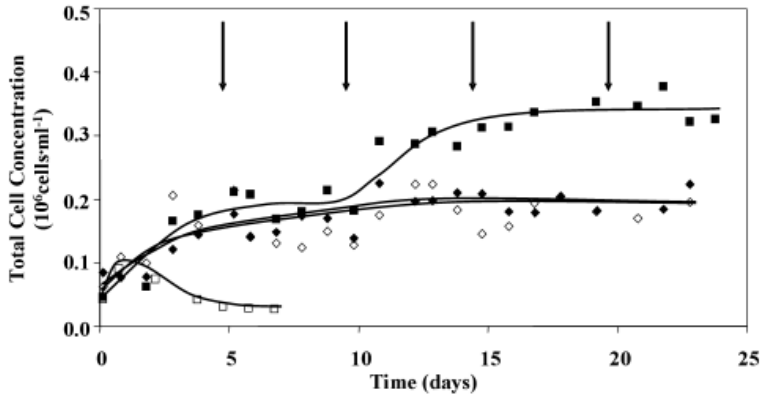

Figure 5.3 – Effect of agitation rate (60 or 100 rpm) and microcarrier concentration (3 or 6 g/L) in the growth profiles of astrocytes. Legend: ◆, 60 rpm, 3 g/L; ◇, 100 rpm, 3 g/L; ■, 60 rpm, 6 g/L; □, 100 rpm, 6 g/L. All experiments were carried out with Cytodex 3 microcarriers using a re-feed operational mode (complete medium exchanges are indicated by arrows).

operational mode. The lactate produced was derived mainly from glucose, with the ratio lactate/glucose being approximately 1.5 during the first 5 days of the culture. It is clear that glucose addition did not sufficient for astrocyte growth under fed-batch, and lactate accumulation with concomitant acidification of culture medium (pH was 6.9 when lactate concentration was above 20 mM), could lead to a more pronounced decrease in cell number. For the batch operation mode, it was possible to verify that the astrocytes used lactate for their maintenance at later stages in the culture. No significant changes in astrocyte metabolism were observed when a re-feed operational mode was used, as assessed by the lactate production and glucose consumption yields obtained for the three time periods established before and after each re-feed (Table 5.1).

Effect of Microcarrier Concentration and Agitation Rate

As mentioned above, to use stirred bioreactors for the growth of anchorage-dependent cells, several parameters have to be optimized to obtain a viable and physiologically relevant cell population. It is particularly critical to ensure that the cells have an efficient supply of oxygen under the minimum shear stress (agitation rate) and also that there is no surface limitation to their growth. To assess these issues, two groups of experiments were carried out in spinner flasks using Cytodex 3 microcarriers, an inoculum concentration of approximately 0.1×10^6 cells/mL, and a re-feeding operation mode. The microcarrier concentration in the first group was 3 g/L and in the second was 6 g/L. Two agitation rates, 60 and 100 rpm, were tested

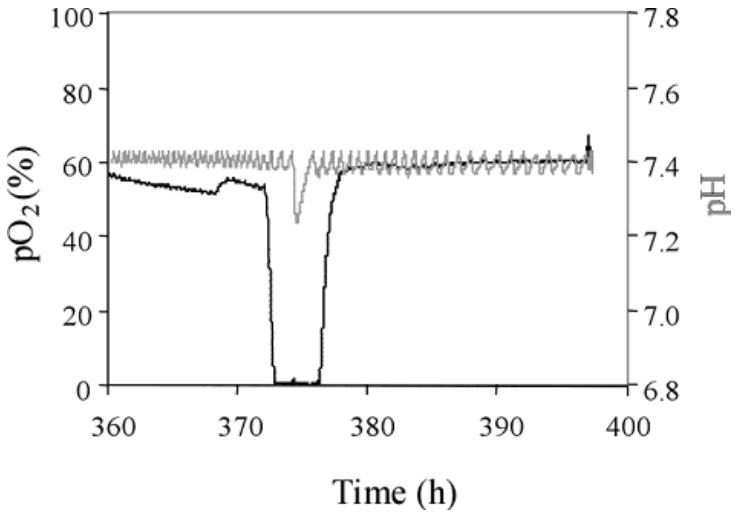

Figure 5.4 – Dissolved oxygen (pO_2, black) and pH (in grey) profiles obtained in the bioreactor used for the growth of astrocytes immobilized in Cytodex 3 microcarriers. Data was collected online using pO_2 and pH meters. To evaluate the effect of hypoxia in astrocytic metabolism, a 5-hours period without oxygen was imposed on the cells by replacing the air content inside the bioreactor by nitrogen. Manipulation and control of dissolved gases and pH in the cell culture medium is possible due to the gas mix station and the bioreactor control unit. (Time scale onset from 360 hours, corresponding to Day 15 after culture initiation).

for each group. Except for 6 g/L and 100 rpm, where no net cell growth was observed, all experimental conditions supported astrocyte growth and maintenance of a cell steady-state up to 24 days (Fig. 5.3).

Culture of Primary Astrocytes in a Bioreactor: Mimicking Hypoxic Stress

Using the cell culture parameters optimized previously for the spinner vessels, a newly designed culture vessel connected to a bioreactor control unit was tested. This experimental apparatus (Fig. 5.1) allowed a fully controlled and online monitoring of pH, pO_2, and temperature. To test further the relevance of this system for experiments in neuroscience, a pathologic episode like hypoxia was simulated. Cells were allowed to grow until they reached a steady-state (corresponding to confluence at microcarrier surface). The cell growth profile was similar to the one obtained for the correspondent spinner vessel (6 g/L Cytodex 3, 60 rpm, complete re-feed every 5 days). A hypoxic period of 5 hours was imposed on the culture. The pH and pO_2 profiles during the bioreaction run were obtained before, during, and after hypoxia (Fig. 5.4). The effect of the hypoxic insult upon cell concentration, glucose uptake, and lactate production rates was evaluated (Table 5.2). No

Table 5.2 – Temperature, pO_2, pH, and rates for glucose-specific consumption and lactate-specific production under controlled conditions (pO_2 approximately 60%), during a 5 hours hypoxic insult, and in the subsequent recovery period.

Parameter	Aerobic control conditions	5 h Hypoxic stress	Return to aerobic conditions
Temperature (°C)	36.9	37.2	37.0
pO_2 (%)	56.5	0.4	59.4
pH	7.4	7.4	7.4
Glucose consumption[a]	0.42	0.67	0.46
Lactate production[a]	0.45	0.67	0.29
Ratio lactate/glucose	0.98	1.0	0.69

[a] Rates in μmol/h/10^6 cells

significant effect on cell growth was observed within this period (data not shown). During the bioreactor steady-state (before the hypoxic insult), the glucose uptake and lactate production rates were 0.46 and 0.45 μmol/h/10^6 cells, respectively. Glucose uptake and lactate production rates increased by about 45% under hypoxic conditions but the amount of lactate produced per glucose consumed was maintained (Table 5.2). Compared to the values obtained before hypoxia, it was evident that the cell capacity to metabolize glucose was reduced only marginally by the hypoxic stress imposed, but lactate production was lowered significantly upon return to aerobic conditions.

Culture of Primary Astrocytes in a Bioreactor: Carbon Labelling Experiment

Using the optimized bioreaction parameters used previously, the performance of a primary astrocyte culture was evaluated in a carbon labelling experiment. For this, astrocytes were cultured in spinner flasks using 6 g/L of Cytodex 3 with 60 rpm. Spinners were inoculated with 0.1×10^6 cells/mL and operated under re-feed mode. After 15 days the cells were transferred to the bioreactor and left for 3 days to adapt to the new full controlled environment with an average pO_2 of 61% and pH of 7.4. As before, around 0.35×10^6 cells/mL were present in the reactor. At this point the medium was changed to DMEM containing 1 g/L of [U-^{13}C]glucose and cells were incubated for 24 hours. After, the first 8 hours of incubation a 30-mL sample was taken from the reactor and 16 hours later the rest of the reactor content was recovered (≈100 mL). The two samples were processed for ^{13}C-NMR analysis. Spectra of the intra and extracellular extracts were dominated by the [U-^{13}C]lactate multiplets; peaks due to residual glucose were observed in the spectra corresponding to the 8-h samples. Alanine and glutamine multiplets were also detected. Figure 5.5 shows the glutamine multiplets from the intracellular samples.

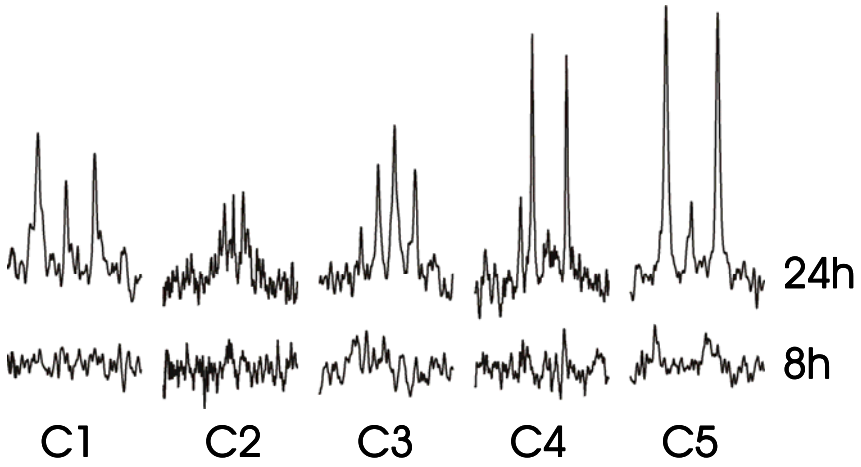

Figure 5.5 – ^{13}C-NMR multiplets of the intracellular glutamine produced from [U-^{13}C]glucose by a primary culture of astrocytes in a bioreactor with controlled pH (7.4) and pO_2 (61%).

As can be evaluated an incubation of 8 h was not enough to detect ^{13}C-resonances due to glutamine, but this was possible in the 24 hour sample. ^{13}C-labelled glutamine was also visible in the extracellular sample relative to 24 hours incubation. However, it should be noted that the cell biomass in the 24 hour sample was 3-fold greater than in the 8 hour sample. It is also noteworthy that the C2 multiplet of glutamine is smaller than the other multiplets, which could indicate a small flux through pyruvate carboxylase.

DISCUSSION

Astrocytes are strictly anchorage-dependent cells; therefore, a solid substrate is indispensable for growth and maturation. Due to their characteristics, microcarriers offer an attractive solution to grow mammalian cells in stirred tank conditions. This methodology is used currently in our laboratory for growing several cell lines (Alves *et al.*, 1996b; Merten *et al.*, 2001; Moreira *et al.*, 2003). As addressed here, the choice of the most suitable microcarrier surface to grow a certain type of cell is an important factor significantly affecting culture performance. Another critical issue in microcarrier technology is the inoculation step, because cellular proliferation occurs only after proper adhesion and a minimum amount of cells per microcarrier is necessary to avoid large lag phases (cell-cell interaction phenomena) (Hu *et al.*, 1985). Different types of microcarriers have been used to grow primary rat brain

astrocytes (Westergaard *et al*., 1991; Sonnewald *et al*., 1992; Alves *et al*., 1997). These studies were carried out in static conditions, i.e., microcarriers were either placed on top of a confluent astrocytic monolayer growing in a culture dish, or inoculated with cells and kept in T-flasks. In the present study, Cytodex 3, a nonporous microcarrier made up of a dextran matrix with a collagen layer at the surface, proved a suitable matrix for the growth of primary rat astrocytes under stirred conditions (Fig. 5.2 and 5.3). The culture operation mode strongly influenced the growth curve profiles (Fig. 5.2 A). Growth was arrested under batch conditions when glucose was completely depleted from the culture medium (4.6 days, i.e., 110 hours post-inoculation). Additionally, the previously reported astrocytic ability to switch metabolism and use substrates other than glucose (e.g., lactate) was confirmed in our culture conditions (McKenna *et al*., 1993; Tildon *et al*., 1993; Alves *et al*., 1995). Glucose addition *per se* did not improve the cell yields under fed-batch operation. In fact, lactate accumulation and concomitant medium acidification affected the capacity of cells to metabolize glucose (decrease of approximately 52%) and changed the flux through glycolysis (lactate/glucose increased by 0.17). Interestingly, the carbon flux from glucose to lactate in the bioreactor was lower than what was obtained for spinner vessels running under similar conditions (Table 5.1. and 5.2.). This suggests that due to a higher oxygen supply there is a more efficient use of glucose and, therefore, an increase in the flux through the tricarboxylic acid cycle.

Complete medium replacement (re-feed mode) permitted the supply of the primary carbon sources and the removal of waste products (possible inhibitors of cell metabolism), making it possible to maintain the cultures under steady state for up to 25 days. Astrocyte growth was limited by microcarrier surface availability when 3 g Cytodex/L was used, as indicated by the increase in the cell yield obtained for 6 g Citodex/L (60 rpm; Fig. 5.3). Lower cell concentrations were obtained for 6 g/L and 100 rpm, due to an increase in the number of collisions between supports, a concomitant increase in the shear stress, and cell death already reported for other mammalian cell systems (Cherry and Papoutsakis, 1988). Overall, our data show that the optimal conditions for growing rat astrocytes under stirred tank operation in the type of vessels used are: 6 g/L Cytodex 3 with an inoculum of $0.10\text{-}0.15\times10^{6}$ cells/mL in vessels operated at 60 rpm with a re-feeding operational mode

(complete medium replacement every 5 days). The maximum cell concentration achieved, 0.3 $\times 10^6$ cells/mL, corresponds to a cell expansion ratio approaching 3.

Brain hypoxia can occur in several pathologies, such as stroke and cardiac arrest episodes, and many studies have contributed to our knowledge about the consequences of hypoxia in brain metabolism (Cox *et al.*, 1983; Marrif and Juurlink, 1999). Nevertheless, to characterize precisely the metabolic disturbances during a complete exclusion of O_2, it is imperative to develop experimental conditions ensuring that no oxygen is available to the cells whereas all other nutrients remain present. Such complete control and monitoring of culture environmental parameters is shown here to be experimentally feasible for small-scale cultures.

As expected, during hypoxia there was an increase in the specific rates of glucose uptake and lactate production (by approximately 50%) but the lactate-to-glucose ratio was not affected significantly, possibly because glucose can also be channelled to other metabolic pathways. Indeed, previous studies have reported that under hypoxic conditions, approximately 30% of glucose consumed can be metabolized to products other than lactate (Alves *et al.*, 2000). Astrocytes can upregulate their capacity to metabolize glucose (Marrif and Juurlink, 1999) and are able to downregulate their ATP requirement (Swanson *et al.*, 1997) under hypoxic stress conditions. We have observed previously that astrocytes have the ability to maintain their energetic status during hypoxia (up to 2 hours) at the expense of increased glucose utilization under anaerobic conditions (Alves *et al.*, 2000). Other evidence of the metabolic plasticity of astrocytes is observable during the recovery period: their capacity to metabolize glucose was restored but the channelling to lactate decreased by approximately 30%. Swanson *et al.* (1995, 1997) reported that survival and function of astrocytes became compromised if acidosis also occurred during hypoxic episodes. During our hypoxia experiment under complete environment control, a small drop in pH (approximately 0.1) was detected and rapidly returned to normal by enhancement of CO_2 content in the bioreactor. Our system thus permits dissociating the effect of lactate accumulation from the pH decrease effect.

Analysis of the ^{13}C-NMR spectra revealed that 8 hour incubations and reactor samples of 30 mL (with 6 g/L of microcarriers) were too short and too small to be analyzed by this technique, given that in both intra and extracellular samples only

lactate and glucose multiplets were detected. When the incubations were extended to 24 hours, it became possible to observe glutamine both intra and extracellularly. However, the low ^{13}C enrichment of glutamine did not enable metabolic flux analysis. At least there may be two reasons for this low sensitivity: the recovery of the intracellular content from the microcarriers is low and/or the process of removing the microcarriers results in loss of the intracellular content, or the metabolism of astrocytes in the reactor is such that results in a low enrichment of glutamine. These experiments were done in DMEM supplemented with 4 mM glutamine; perhaps this glutamine concentration is too high, favouring glutamine consumption rather than glutamine release. Usually even under low rates of glutamine consumption it is possible to observe release of labelled glutamine, due to the reversibility of the reactions involved. Under the fully controlled bioreactor environment the astrocytes exhibit a slower and less wasteful metabolism (Tables 5.1 and 5.2), which suggests the need for medium manipulation with the goal to increase channelling of ^{13}C to the TCA cycle, and ultimately enable metabolic flux analysis. The changes may involve longer incubations and/or higher concentration of labelled glucose and lower concentration of glutamine in order to favour glutamine release and decrease anaplerosis of ^{12}C metabolites.

The most important conclusion from this work is that primary astrocytes can be grown in stirred tank bioreactors under a fully controlled environment. These systems are versatile, permitting experiments to run for long periods to investigate age-dependent aspects of cell metabolism. It is also possible to carry out studies using different cell types (co-cultures) in the same environment, and to manipulate the relative amounts of neurons and astrocytes, change carbon sources, mimic pathologies, and evaluate metabolism during imposed stress and during the recovery period. Ongoing efforts are directed to culture cerebellar granule cells and cortical neurons under stirred conditions.

Acknowledgements and Work Contributions

I am grateful to Miguel Monteiro, ITQB, Oeiras for the carrying out most of the experimental work and to Sónia Sá Santos, ITQB, Oeiras for writing the manuscript in the short time available in order to submit it to the Journal of Neuroscience Research.

REFERENCES

Alves P.M., Carrondo M.J.T., Santos H. (1997). Immobilization of primary brain cells in porous microcarriers for on-line NMR spectroscopy. In: Carrondo MJC , Griffiths B , Moreira JLP , editors. Animal cell technology. Dordrecht: Kluwer Academic Publishers. p 91-98.

Alves P.M., Flögel U., Brand A., Leibfritz D., Carrondo M.J.T., Santos H., Sonnewald U. (1996a). Immobilization of primary astrocytes and neurons for on-line monitoring of biochemical processes by NMR. *Dev. Neurosci.* **18,** 478-483.

Alves P.M., Fonseca L.L., Peixoto C.C., Almeida A.C., Carrondo M.J.T., Santos H. (2000). NMR studies on energy metabolism of immobilized primary neurons and astrocytes during hypoxia, ischemia and hypoglycemia. *NMR Biomed.* **13**, 438-448.

Alves P.M., Mckenna M.C., Sonnewald U. (1995). Lactate metabolism in mouse brain astrocytes studied by [^{13}C]NMR spectroscopy. *Neuroreport.* **6,** 2201-2204.

Alves P.M., Moreira J.L., Rodrigues J.M., Aunins J.G., Carrondo M.J.T. (1996b). Two-dimensional versus three-dimensional culture systems: effects on growth and productivity of BHK cells. *Biotechnol. Bioeng.* **52,** 429-432.

Bachelard H.S., Badar-Goffer R.S., Brooks K.J., Dolin S.J., Morris P.G. (1988). Measurement of free intracellular calcium in the brain by ^{19}F-nuclear magnetic resonance spectroscopy. *J. Neurochem.* **51,** 1311-1313.

Bachelard H.S., Cox D.W.G., Feeney J., Morris P.G. (1985). ^{31}P nuclear-magnetic-resonance studies on superfused cerebral tissues. *Biochem. Soc. Trans.* **13,** 835-839.

Cherry R.S., Papoutsakis E.T. (1988). Physical mechanisms of cell damage in microcarrier cell culture bioreactors. *Biotechnol. Bioeng.* **32,** 1001-1014.

Cox D.W., Morris P.G., Feeney J., Bachelard H.S. (1983). ^{31}P-n.m.r. studies on cerebral energy metabolism under conditions of hypoglycaemia and hypoxia *in vitro*. *Biochem. J.* **212,** 365-370.

Croughan M.S., Wang D.I. (1989). Growth and death in overagitated microcarrier cell cultures. *Biotechnol. Bioeng.* **33,** 731-744.

Guyton A.C., Hall J.E. (1996). Textbook of medical physiology. Philadelphia: W.B. Saunders Company. 1014 p.

Hansson E., Thorlin T. (1999). Brain primary cultures and vibrodissociated cells as tools for the study of astroglial properties and functions. *Dev. Neurosci.* **21,** 1-11.

Hu W.S., Meier J., Wang D.I.C. (1985). A mechanistic analysis of the inoculum requirement for the cultivation of mammalian cells on microcarriers. *Biotechnol. Bioeng.* **27,** 585-595.

Marrif H., Juurlink B.H.J. (1999). Astrocytes respond to hypoxia by increasing glycolitic capacity. *J. Neurosci. Res.* **57,** 255-260.

Masters J.R.W. (2000). Animal cell culture. New York: Oxford University Press. 315 p.

McCarthy H.D., Vellis J.D. (1980). Preparation of separate astroglial and oligodendroglial cultures from rat cerebral tissue. *J. Cell Biol.* **85,** 890-902.

McKenna M.C., Tildon J.T., Stevenson J.H., Boatright R., Huang S. (1993). Regulation of energy metabolism in synaptic terminals and cultured rat brain astrocytes: differences revealed using aminooxyacetate. *Dev. Neurosci.* **15,** 320-329.

Merten O.W., Cruz P.E., Rochette C., Geny-Fiamma C., Bouquet C., Goncalves D., Danos O., Carrondo M.J.T. (2001). Comparison of different bioreactor systems for the production of high titer retroviral vectors. *Biotechnol. Prog.* **17,** 326-335.

Moreira J.L., Miranda P.M., Alves P.M., Marcelino I., Carrondo M. (2003). Culture methods for mass production of ruminant endothelial cells. In: Saha BC , editor. Fermentation biotechnology. Washington: American Chemical Society. p 124-141.

Richter-Landsberg C., Besser A. (1994). Effects of organotins on rat brain astrocytes in culture. *J. Neurochem.* **63,** 2202-2209.

Sonnewald U., Petersen S.B., Krane J., Westergaard N., Schousboe A. (1992). ^{1}H NMR study of cortex neurons and cerebellar granule cells on microcarriers and their PCA extracts: lactate production under hypoxia. *Magn. Reson. Med.* **23,** 166-171.

Swanson R.A., Farrel K., Simon R.P. (1995). Acidosis causes failure of astrocyte glutamate uptake during hypoxia. *J. Cereb. Blood Flow Metab.* **15,** 417-424.

Swanson R.A., Farrel K., Stein B.A. (1997). Astrocyte energetics, function, and death under conditions of incomplete ischemia: a mechanism of glial death in the penumbra. *Glia* **142,** 142-153.

Tildon J.T., McKenna M.C., Stevenson J., Couto R. (1993). Transport of L-lactate by cultured rat brain astrocytes. *Neurochem. Res.* **18,** 177-184.

van Wezel A.L. (1967). Growth of cell-strains and primary cells on microcarriers in homogeneous culture. *Nature* **216,** 64-65.

Westergaard N., Sonnewald U., Petersen S.B., Schousboe A. (1991). Characterization of microcarrier cultures of neurons and astrocytes from cerebral cortex and cerebellum. *Neurochem. Res.* **16,** 919-923.

CHAPTER 6

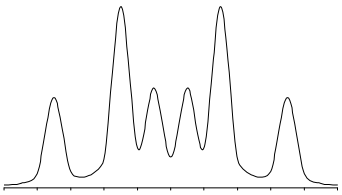

General Conclusions

Chapter | 6 | Contents

General Conclusions

The human brain is the product of around 600 million years of evolution that started with the appearance of the first animals and it is by far the most complex structure in the known universe. The vertebrates' brain is composed of several different cell types, which perform the different functions required. The two most abundant cell types are neurons, which are the brain function unit, and glial cells, which are responsible for a myriad of housekeeping, homeostatic and structural functions. Glial metabolism is so far interconnected with the neuronal metabolism, so that is difficult to state where one finishes and the other starts. Trafficking between the two compartment include metabolites of almost all metabolic pathways (glycolysis, TCA, amino acids, ketone bodies, etc) and also ions. There are several model systems to study brain metabolism and of these, primary cultures of brain cells is the most plastic technique which allows studying each cell type individually.

Effects of Ethanol on Primary Astrocytes Cultures

Ethanol effects on primary cultures of astrocytes were concentration and time dependent. Incubation of 24 hours with up to 40 mM of ethanol had no effects on either the glucose consumption or lactate production rates, lactate to glucose ratio, ATP or PCr levels, intracellular pH, protein content or protein to DNA ratio. Incubations with 80 mM ethanol for up to 24 hours altered the consumption and the production of a few amino acids, which may be related with the glutathione metabolism and reduced slightly the flux ratio between pyruvate dehydrogenase and pyruvate carboxylase. For longer periods of time ethanol lead to a time-dependent decrease of the energetic status. On another hand, 160 mM of ethanol, during 36 hour incubations, increased the glycolytic flux and decreased the flux ratio between pyruvate dehydrogenase and pyruvate carboxylase. No ethanol catabolism was ever detected.

From our studies we conclude that ethanol is not a good agent to be used as a stress inducer in a metabolic stress response study, due to physiological and experimental reasons. From the physiological point of view, the concentrations

required to observe a measurable difference in the metabolic profile of a culture of astrocytes were too high considering that, for example, under the Portuguese law a person can not drive with more than 10 mM of blood alcohol and if caught with more than 23 mM, the act is considered a crime! However, recently a new record concentration of ethanol was measured in a Portuguese motorcycle driver – 160 mM, which show that the concentrations used in this work (up to 180 mM of ethanol), although high, are still within the physiological range. Nevertheless, practical reasons also preclude the use of ethanol. Ethanol evaporates very easily from the culture medium and it was necessary to develop a system (described in the experimental procedures of chapter III) to avoid this in the culture plates. In the *in vivo* NMR experiments, the ethanol concentration had to be monitored and corrected whenever more than 10% evaporated. This was due to the fact that in this experimental setup the circulating medium is continuously gassed with O_2. Neither of these solutions would be practical in a reactor system.

The isotopomers of glucose used in this chapter were selected also for the evaluation of their potential for the determination of metabolic fluxes. This was done in order to explore other labelling strategies potentially more informative than the usual [1-^{13}C]glucose. In that regard the usage of [U-$^{13}C_6$]glucose and of [2-^{13}C]glucose yielded good results, the first being a good substrate for the study of the labelling patterns that arise from the TCA cycle, and the second, convenient for the study of the pentose phosphate pathway. It remained to be checked, however, the possibility of using a mixture of both to perform flux analysis. This would have to be simulated (*in silico*) first in order to study its applicability and information gain, taking into account also the NMR sensitivity and dynamic range due to the spectra of the resulting labelled products. These carbon labelled experiments also showed that a process was required to determine the areas of partially-overlapping peaks in ^{13}C NMR spectra. This led to the development of the program described in Appendix I.

Astrocytes Under a Steady Supply of Glutamate

Glutamate is a key metabolite in astrocytic and brain metabolism, which is taken up very rapidly by astrocytes. This kinetic is not compatible with the conditions required to perform metabolic flux analysis in bioreactor. As can be seen in chapter 5 the best enrichments were obtained after 24 hours of incubation with carbon-13 labelled glucose. However, when glutamate is supplied to a culture of astrocytes in concentrations up to 500 μM in normal culturing conditions (cell numbers/Volume of incubation medium), it is consumed within a few hours. This meant that in order to do flux analysis either the concentration of glutamate had to be higher or a larger volume of incubation medium had to be used. Nevertheless, these solutions would only extend temporally the presence of glutamate in the culture medium. Since this amino acid is continuously taken up, the concentration would not remain constant. In order to achieve this goal, a fixed concentration of glutamate through long periods, a different method was developed. By adding glutaminase to the incubation medium of a culture of astrocytes, it became possible to impose a steady supply of glutamate at the expense of glutamine. Since the astrocytes transform the transported glutamate into glutamine and release this amino acid, the glutaminase is actually closing the glutamate-glutamine cycle. Our results (chapter 3) show that astrocytes that have never been exposed to glutaminase (and glutamate) accumulate glutamate (initially) when exposed to glutamate supplies higher than 10 nmol/min/mg of protein. Above this threshold cultured astrocytes accumulate glutamate to a maximum which is proportional to the glutamate supply rate. These results show that the intensity of the applied stress may be tailored to the desired level by changing the amount of glutaminase. Also, this methodology allows targeted studies of either the adaptation to higher supplies of glutamate or of the metabolism of adapted cells. In the present study we opted for the analysis of the adaptation, as it allowed us to clarify different results obtained with either astrocytic cultures or by *in vivo* cerebral flux analysis. On the other hand, in order to use this methodology to study the effects of glutamate on the metabolic fluxes of astrocytes, the use of adapted cells would be better. Once adapted the cells are still in the presence of glutaminase, but since they are now capable of enduring

that stress, it is possible to study the metabolism under steady state conditions. Also, at this stage the concentration of glutamate besides being more or less constant, it is dependent of the quantity of glutaminase present. These are ideal conditions to be used in a flux-determination study, since in this way a metabolic steady-state is reached making it possible to perform the studies during the time required to achieve a ^{13}C-enrichment and allow obtaining good quality ^{13}C NMR spectra. Also the metabolic analysis will be simpler due to the fact that steady-state conditions apply, instead of transient conditions.

Lactate Recycling in Astrocytes and Neurons

Lactate has been in the centre of debate concerning brain energy metabolism. Some evidence support the view that astrocytes are responsible for the metabolisation of glucose to lactate, which may then be exported to the neurons where it is fully oxidised. Our data, obtained with primary cultures of astrocytes, support this hypothesis, but also show that once glucose is exhausted, astrocytes can revert to the use of lactate to meet their energetic demand. Thus, showing the astrocytic capacity to, both, produce and consume lactate. Labelling the medium with 50% $^{2}H_2O$ allowed observing the recycling of lactate between the extracellular pool and the intracellular pool of pyruvate. In order to characterize the kinetic process associated with the lactate recycling, three different models were tried, i) where all reactions were assumed to have first-order kinetics, ii) similar to the first but where the uptake of lactate was assumed to follow a Michaelian kinetics and, iil) where all reactions were modelled as having Michaelian kinetics. Of these three attempts only the first gave good fittings to the data. The second type did not generated good fits and the third had too many degrees of freedom for the experimental data available. Although simple, the first-order kinetic model allowed obtaining the first-order rate-constants for each reaction and to study the dependence of these rate-constants with the extracellular concentration of lactate. However, to do so, the intracellular concentrations of lactate and pyruvate, as well as their time-dependent variations had to be assumed as known. The concentrations were obtained from best-fits to the model and used because they were within the normal physiological range and, with a lactate to pyruvate ratio of 10:1. On the

other hand, the time-dependent variations of these concentrations were in fact unknown, but in order to get consistent results these concentrations were not allowed to increase above the initial values. Although false, this assumption affected only the rate-constant of release of lactate (k_2) and may have minor effects on the rate-constants of uptake of lactate (k_1) and of lactate oxidation (k_3). Most probably, the concentration of intracellular lactate increases very rapidly until it reaches an equilibrium concentration, which depends among other things, on the extracellular concentration of lactate and on the intra and extracellular pHs. As a consequence of the assumption made, the values of the rate-constant of release of lactate (k_2) showed to be dependent on the extracellular concentration of lactate, which most probably is an artefact generated by this assumption. In reality, the property dependent on the extracellular concentration of lactate should be the intracellular concentration. However, because this was assumed not to happen, the dependence was shifted to the rate-constant. In our opinion this assumption is the major drawback of the model used and thus of the analysis, but this only affects the absolute values, which allows the determination of the correct ratios between the rate-constants (relative values). These results also show the amount and the kind of data that can be obtained by labelling the medium water, thus revealing that this technique may have future applications in metabolic flux determinations. Furthermore, the results obtained for the ratio between the fluxes through the lactate transport and lactate oxidation as well as the ratio between pyruvate consumption and pyruvate reduction may prove useful in the full determination of the metabolic fluxes in astrocytes. Similarly, the differences in these ratios between astrocytes and neurons may improve future metabolic models of the brain. In astrocytes the transport of glutamine, in opposition to the neuronal, is bidirectional and, thus may be of interest to use this technique to study it. Also, given that these studies were performed in buffer to minimize interferences from other metabolic pathways, future work will be done in normal medium and in the presence of glucose, which has been shown to affect lactate recycling.

Culturing Primary Astrocytes in Bioreactors

Large amounts of biomass are necessary to perform metabolic flux analysis. If the cells are cultured in static conditions, like plates, each study will require several plates, because these have low amounts of cells and they do not allow sampling fractions of the cultured biomass. On the other hand, bioreactors are culturing devices that allow cells to be grown in three dimensions, which permit a large increase in cell yield. Also, because cells are no longer attached to a fixed surface it becomes possible to sample part of the biomass without having to harvest the full content of the bioreactor. Additionally, bioreactors allow cultures to be run in continuous mode, and are easily fitted with sensors that allow to monitor and control the culture environment. For these reasons a bioreactor system was developed; however, because astrocytes are anchorage-dependent cells, microcarriers had to be used in order to supply these cells with a growth surface. With the optimized culturing process described in this chapter it is now possible to grow and maintain astrocytes in a bioreactor. However, the conditions required to perform carbon labelling experiments still need to be improved, mainly, because in order to determine the fluxes associated with the TCA cycle, the α-ketoglutarate pool has to be satisfactorily followed by ^{13}C NMR. In most cells glutamate is chosen because of its large intracellular pool and fast exchange with α-ketoglutarate. However, astrocytes possess a very active glutamine synthetase which converts most of the glutamate into glutamine, thus making this amino acid the metabolite of choice. Under the conditions tried in this chapter the glutamine signal was too low, perhaps due to a low recovery (i.e. immobilized cells in microcarriers may be difficult to break), incomplete extraction or the α-ketoglutarate pool being diluted by the extracellular (unlabelled) glutamine present in the medium. As explained in the Introduction, the astrocytic glutamine transport is bidirectional, meaning that intra and extracellular glutamine are always in an equilibrium dependent on the pH and sodium transmembranar gradients. Given the high concentration of glutamine in DMEM (3-4 mM), it is possible that labelled glutamine is just being diluted. Moreover, as shown in this chapter, under the bioreactor conditions astrocytes show a lower lactate to glucose ratio, which may be evidence of a different flux distribution that

results in a lower percentage of labelling in TCA intermediates. In any case a lower glutamine concentration may favour glutamine release and, thus allow a better measurement of the labelling profile of this amino acid.

Isotopomeric Analysis by ^{13}C-NMR

^{13}C NMR is a powerful technique, which is still growing and evolving today. However spectra analysis is still a major drawback, requiring in most cases specialized training and long hours of peak identification and peak limits recognition. Programs like the one described in this chapter aim at reducing the time and work required to process NMR spectra. Apart from the possible applications mentioned throughout this chapter, this program was also useful for the analysis of *in vivo* ^{13}C NMR spectra. In opposition to ^{13}C NMR analysis of extracts, *in vivo* ^{13}C NMR experiments result in the acquisition of several hundred spectra. Also, due to the *in vivo* nature of these experiments, pH fluctuations result in small but important peak shifts. When peaks appear isolated from each other these shifts do not represent a problem if one requires to measure the areas of two semi-superimposed peaks then these shifts introduce significant errors. On another hand the usage of the program described here, not only allows to quantify these peaks with much less error but also allows this determination to take place in a fully automatic fashion, quantifying hundreds of spectra with minimum user intervention. For example, in our lab this program has been used to quantify intra and extracellular lactate in *in vivo* ^{13}C NMR spectra of lactic acid bacteria, where, due to the different intra and extracellular pHs, the C3 resonance of lactate appears split in two peaks (with half-heights of 0.014 and 0.041 ppm) separated by only 0.087 ppm.

Appendix 1

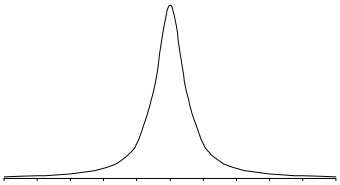

Isotopomeric Analysis by ^{13}C-NMR

Appendix | 1 | Contents

Abstract

Carbon-13 labelling experiments coupled to ^{13}C-NMR techniques are a valuable tool in metabolic flux analysis. In contrast to other techniques, ^{13}C-NMR allows the collection of quantitative as well as positional information of the ^{13}C label within molecules. These important features allow the characterization of metabolic networks that cannot be approached by any other means. This is accomplished by taking advantage of the ^{13}C homo- and heteronuclear scalar coupling. These multiple couplings result in the splitting of the original ^{13}C resonance into a large number of peaks, which makes the analysis of the ^{13}C-NMR spectra difficult and requires the use of computer assistance. ^{13}C multiplets are described as the sum of fine-structures (doublets, triplets, quartets, etc). Furthermore, each fine-structure is represented by a sum of positional constrained Pearson type VII functions. This approach provides a means to identify the fine-structures within the multiplets. The use of these simulating routines combined with a least-square fitting procedure enabled the quantification of the areas of these fine-structures in a semi-automatic fashion. This type of program may one day become fully automated, which would greatly increase the informational output of the ^{13}C-NMR techniques.

INTRODUCTION

Carbon labelling experiments have been in use since the 1940's, when the elucidation of the central metabolic pathways was achieved by using ^{14}C-radiolabeled methods. The first studies of intermediary metabolism using ^{13}C NMR were carried out three decades ago in *Saccharomyces cerevisiae* (Eakin *et al.*, 1972). Since then, ^{13}C-NMR became the technique of choice for many metabolic engineers, because carbon-labelling experiments provide the information required to quantify intracellular fluxes, which would not be available through the classical stoichiometric metabolic flux analysis (Wiechert, 2001). The three typical types of pathways which can not be resolved through the classical method (parallel pathways, cycles, and bidirectional reactions) are usually easily resolved using ^{13}C carbon labelling experiments.

^{13}C-NMR Spectroscopy

The main drawback of ^{13}C-NMR arises from the low gyromagnetic ratio of ^{13}C which renders this technique much less sensitive than ^{1}H-NMR. However, ^{13}C-NMR has several other features that make it the technique of choice for many metabolic studies. The low natural abundance of ^{13}C enables the use of site-specifically enriched exogenous compounds to monitor metabolic events. Another highly appreciated characteristic is the splitting of ^{13}C-NMR peaks into multiplets due to ^{13}C-^{13}C scalar coupling. The use of ^{13}C multiplet data to characterise metabolic processes has become known as isotopomer analysis (London, 1988). Any molecule with n carbon atoms will have 2^n isotopomers. Most of them are readily distinguishable by NMR, allowing the retrieval of unique metabolic information.

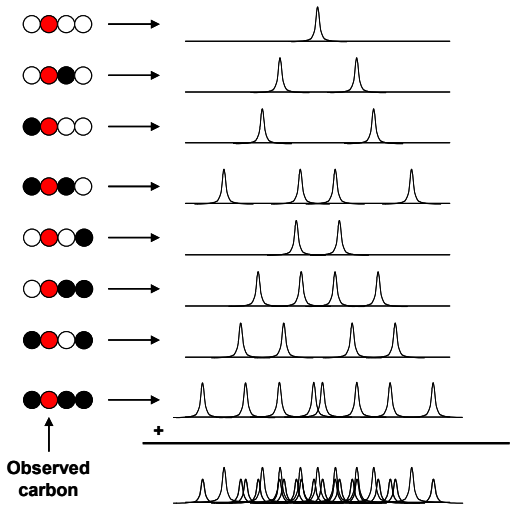

Figure 2.1 – Scheme of the multiplets arising from the ^{13}C-^{13}C scalar couplings in a 4-carbon molecule. In the bottom, shown as the sum of the 8 (2^3) fine-structures, it is represented the resulting ^{13}C-NMR multiplet due to the **observed carbon**. In the resulting multiplet, peaks arising from 1-bond couplings are represented by tall peaks, whereas peaks arising from long-range couplings are shorter. ^{13}C nuclei are represented by black circles; ^{12}C nuclei (non-enriched positions) are represented by open circles; the **observed carbon** in highlighted in red.

^{13}C-^{13}C Homonuclear Couplings

Homonuclear couplings usually arise from the use of multiple labelled or uniformly labelled substrates, but can also appear from single labelled substrates. ^{13}C homonuclear scalar couplings lead to the splitting of the original singlet into a multiplet of 2^n fine-structures with 3^n peaks (Fig 2.1), where n is the number of ^{13}C nuclei coupled to the observed nucleus. Whenever a ^{13}C is directly connected to the observed carbon (i.e. one-bond coupling) the singlet (first fine-structure in Fig 2.1) is split into a doublet (second and third fine-structures in Fig 2.1). This coupling is characterized by the coupling constant J, which value is the frequency difference between the two peaks and results from the interaction of the two nuclei involved. If another ^{13}C is present then the doublet is split into a degenerate quartet or a doublet of doublets (fourth fine-structure in Fig 2.1). Given that the coupling constant depends on the chemical properties of the carbons involved, two chemically different pairs of ^{13}C will show different coupling constants. In some cases it is also possible to detect long range coupling (two- or three-bond couplings), which will cause further splitting of the existing multiplet (fifth to eighth

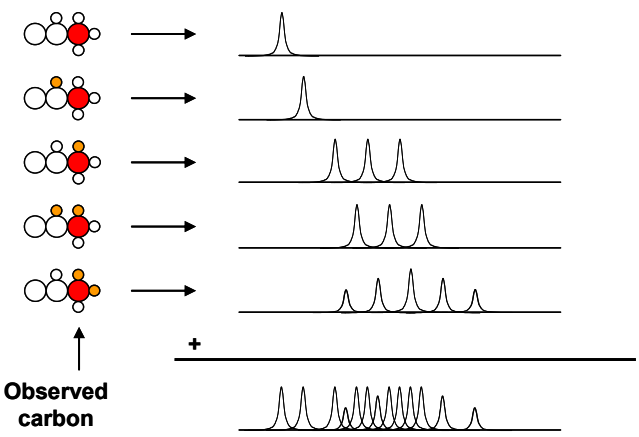

Figure 2.2 – Scheme of the multiplets arising from the ^{2}H-^{13}C scalar couplings in a lactate molecule. The labelled carbon is depicted as a large red circle and deuterium atoms as small orange circles. ^{12}C and ^{1}H are depicted as large and small open circles, respectively. Replacement of the vicinal hydrogen atom by deuterium results in an isotopic shift of the original resonance (undeuterated compound). Replacement of the geminal hydrogen atoms by deuterium results in an isotopic shift and in the splitting of the original resonance. Isotopic shifts caused by geminal deuterium atoms are larger than isotopic shifts due to vicinal deuterium atoms.

traces in Fig 2.1). These long range couplings are usually characterized by smaller coupling constants. This splitting can, very easily, produce an astonishing number of peaks which is often too complex to be deconvoluted by the naked-eye of the user (resulting multiplet in Fig 2.1).

^{13}C Heteronuclear Couplings

Heteronuclear couplings, such as those between ^{2}H and ^{13}C, can also generate large numbers of peaks due not only to the splitting but also to isotopic shift effects which are greater for ^{2}H-^{13}C than for ^{13}C-^{13}C (Fig 2.2). Given that the deuterium has a lower gyromagnetic constant than hydrogen ($\gamma_{^{1}H}/\gamma_{^{2}H} = 6.51$), the coupling constants to ^{13}C will be proportionally smaller. So, while ^{13}C-^{1}H coupling constants fall in the range 125 to 200 Hz, ^{13}C-^{2}H coupling constants vary between 19 and 30 Hz. In addition, given the different spin quantum numbers of these hydrogen isotopes ($I_{^{2}H} = 1; I_{^{1}H} = 1/2$), the splitting multiplicities are different. Increasing numbers of hydrogen nuclei, split the original resonance from a singlet to a doublet, a triplet or a quartet (in a ^{13}C NMR spectrum without proton decoupling, Table 2.1), while

deuterium nuclei split the singlet into a triplet, a quintet or a septet (in a ^{13}C NMR spectrum with proton decoupling, Table 2.1). Moreover, the usual multiplet line intensity ratios are also different: while ^{1}H originates ratios that follow the Pascal's triangle, deuterium ratios do not (Table 2.1). Deuterium substitution also results in notable isotopic shifts, which are a consequence of the higher mass of this nucleus. Heavier isotopes have lower potential energy from the ground state and smaller bond distance, which leads to a decrease of the paramagnetic shielding and consequently to an up-field shift. These shifts are usually small ($^{1}\Delta\sigma\approx$-0.3 ppm and $^{2}\Delta\sigma\approx$-0.1 ppm) but additive, with increasing number of deuterium nuclei, isotopic shifts may reach 1.5 ppm.

Multiplet Quantification

The use of multiple labelled substrates raises the problem of multiplet quantification, due to the proximity of peaks arising from ^{13}C-^{13}C couplings (Fig. 2.1). This difficulty is also pertinent in studies which use 2D NMR techniques, like [^{13}C, ^{1}H]COSY NMR, as well as in studies involving other nuclei such as ^{2}H or ^{15}N (Fig. 2.2). As with identifying, quantifying these fine-structures manually can be hard and is prone to the introduction of errors due to the subjectivity of the determination of the beginning and the end of the peaks. Moreover this task becomes virtually impossible when peaks of different fine-structures are partially overlapping. For these reasons, it was deemed useful to create a software program capable of determining the areas of fine-structures by nonlinear fitting of spectra. In the following pages it is described how to write a program for this purpose. The concepts illustrated may be applied to any programming language.

Table 2.1 –– Multiplicity and multiplet line intensity (MLI) ratios of ^{13}C signals due to coupling with n equivalent nuclei X

System	X=^{1}H		X=^{2}H	
	Multiplicity*	MLI ratio	Multiplicity*	MLI ratio
C	1	1	1	1
CX	2	1 1	3	1 1 1
CX_2	3	1 2 1	5	1 2 3 2 1
CX_3	4	1 3 3 1	7	1 3 6 7 6 3 1
CX_4	5	1 4 6 4 1	9	1 4 10 16 19 16 10 4 1

*Multiplicity is equal to $2nI_X+1$, where n is the number of coupled nuclei and I_X is the spin quantum number

THE SOFTWARE TOOLS

To quantify the fine-structures of the multiplets in ^{13}C NMR spectra several steps must be accomplished. In order to keep the routines simple these steps were divided in separate routines. Subroutine overview:

- The splicing program, **Breack13cnmr**. ^{13}C NMR spectra have a great number of peaks. Instead of trying to quantify all of them in one go, it is simpler to break up each spectrum in a collection of multiplets.
- The main program, **IntNMR**. This routine will deal with the parameters required to simulate the multiplets and perform the nonlinear regression analysis. This program will use several subroutines.
  - The subroutine **IntNMRPar**. Which calculates the first estimative of the parameters required to simulate and fit a given multiplet.
  - The multiplet simulating subroutines, **Bs**, **Bsd**, **Bsdd**, **Bsddq**. These routines simulate the multiplets and can be changed easily in order to simulate any other kind of multiplets.
  - The NMR peak simulating subfunctions, **Lorentz**, **Gauss**, **Pearson7**. In order to simulate multiplets, as a sum of peaks, the NMR peaks must also be adjusted to a function.

The Splicing Program

^{13}C NMR spectra have a relatively large chemical shift range (≈220 ppm) and peaks have a small half-height width (<0.1 ppm). In each sample, several different molecules may be present and each of these molecules will generate as many peaks as the number of carbons of which each molecule is constituted. Moreover, each peak of a given carbon may be split into a multiplet. For this reason the nonlinear fit of a complete NMR spectrum is an almost impossible task, and so, it is easier to fit individual multiplets, with the exception of some which are partially overlapped. In this case the two multiplets are fitted together. In order to accomplish this task a program must be created that breaks up the original spectrum into the different multiplets.

Given that the tools described here are intended to be used in a semi-automatic fashion, it is helpful to maintain an organization of the spectra. For this reason it's

advisable to maintain a folder for each experiment, within which subfolders should exist for each spectrum, organized in a sequential order. The files corresponding to each multiplet should be created within the subfolder of each spectrum.
The core of this program is simple, the program has to open the spectrum data file and split it into smaller segments according to the user supplied limits and save these segments with the multiplet file name. So, the input variables will be the spectrum folder, a matrix with the upper and lower chemical shift limits of each multiplet and a matrix with the file names where the data corresponding to each multiplet will be stored. For example:

```
break13cnmr('c:\13c\experiement\1',[16.4 17; 50.1 51.2;176 176.8],['alac3';'alac2';'alac1'])
```

Although this routine may be very simple it is the link between the NMR workstation and all other user implemented routines/programs, and so special attention must be paid to the way the NMR workstation supplies the spectral data. While some programs may supply a text file with the chemical shifts and the intensities of each point in the spectrum, other may not. Topspin V1.3 from Bruker Biospin supplies only the intensities of each point in text format, but supplies also the information needed for the calculation of the chemical shift vector (the first and last chemical shift and the number of points in the vector). In cases where text output is not available e.g. XWinNMR from Bruker it is possible to access the processed spectrum directly from the file where it is saved (e.g. 1r) and the vector of the chemical shifts calculated from the spectral width, the transmitter frequency offset and the size of the real spectrum (SW, O1P and SI).

The Main Program

The main program (IntNMR, Figure 2.3) deals with the parameters and the non-linear regression. In order to simplify, the functions used to fit the multiplets will be coded in separate subfunctions of the main program. This has the advantage that every time a function needs to be added (in case of a different multiplet) or changed, a new subfunction has to be created or an already exiting subfunction has to be edited, without the need to edit (or change) the main program. To reduce the

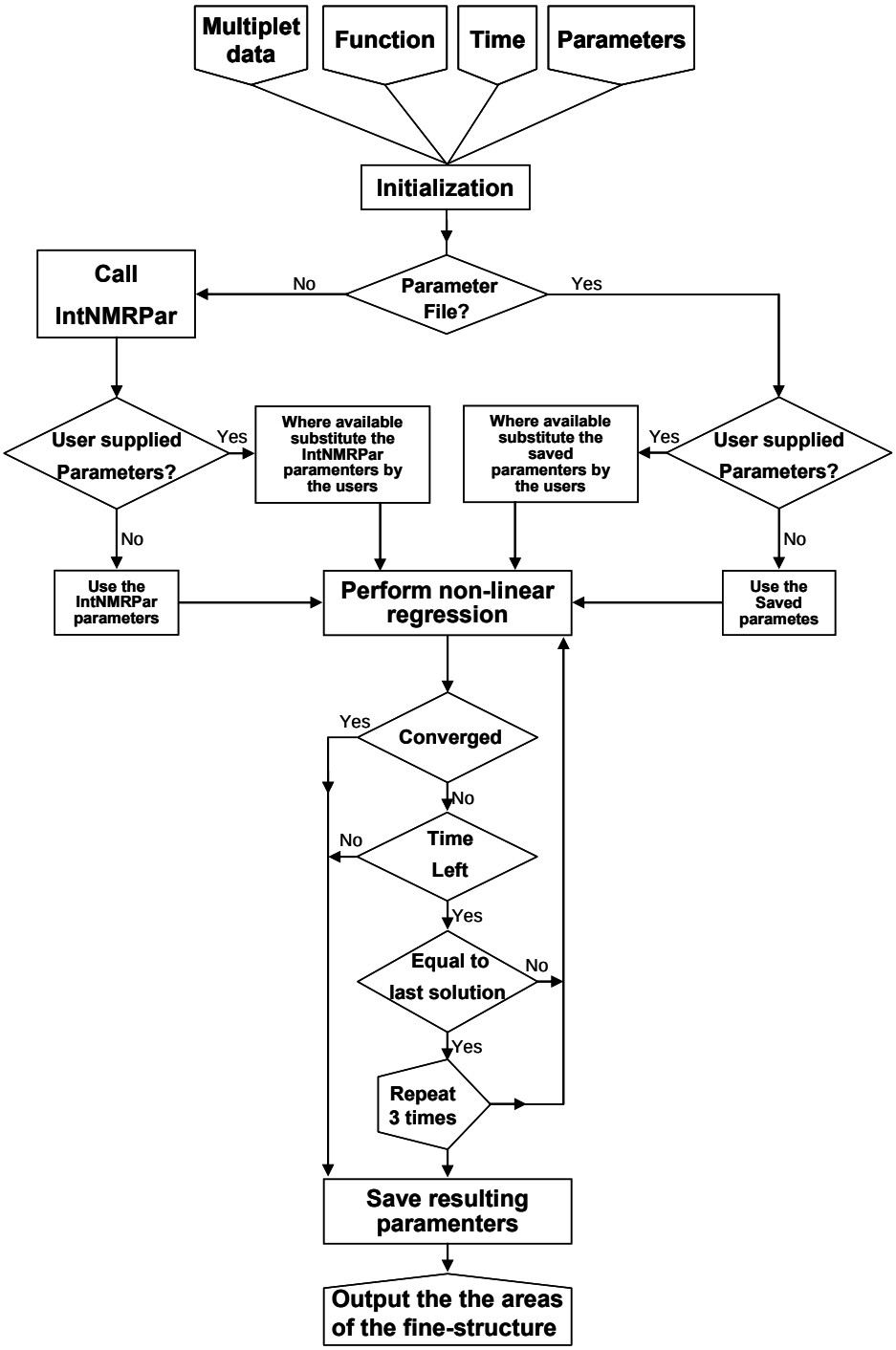

Figure 2.3 – Main program flow chart.

amount of parameters supplied by the user (keeping in mind that some regressions can have 20 or more parameters) a system was developed to automate this task as much as possible, which also allows the user to change only one parameter of the regression without having to re-supply all of them. As is depicted in Figure 2.3, after initialization the program checks if a parameter file exists. If this is the case, the program reads these parameters and merges them with the user supplied parameters. The resulting vector of parameters is a chimera of both parameter sets where the user-supplied ones have priority over the others. If a parameter file is not present the parameter vector creating subroutine (IntNMRPar) is called, and again if there are any user-supplied parameters then these take precedence over parameters supplied by the IntNMRPar subroutine. Once the parameter vector is determined the program uses a least-square method to improve the parameters supplied in order to minimize the differences between the experimental multiplet and the multiplet generated by the multiplet simulating subroutine. When a solution is found the parameters are then used to calculate the areas of the fine-structures in the simulated multiplet that best-fitted the experimental multiplet.

The IntNMRPar Subroutine

The objective of this routine is to generate the vector of parameters (base on the experimental multiplet and simulating routine) for the first time a multiplet is fitted. This routine is required to increase the level of automatization of the entire program, as this allows the user to just list what multiplets should be integrated and state what kind of multiplets they are (singlets, doublets, and so on), and the program will perform all the required calculations and present the areas as the final output. Given the level of automatization required this routine may be very simple or extremely complex. A simple way of generating an initial vector of parameters is to supply the usual parameters for a given multiplet (peaks half-width, coupling constants, isotopic shifts) and calculate the chemical shift and the height of the highest peak. However this type of solution only works if the singlet is the highest peak in the multiplet, in any other case this first guess of the parameters would be completely off. Another way of calculating an initial vector of parameters, which is a lot less error prone is for example, in the case of a multiplet constituted by a singlet and a doublet, to determined, from the experimental multiplet data, the chemical shifts and the heights of the 3 highest peaks. The middle peak may be assumed to

be due to the singlet and the other two from the doublet. The parameters may then be estimated from these values, with the exception of the widths of the peaks, which may be roughly estimated. The widths of the peaks are usually easily obtained by the least-square method so any approximated value will be a good first guess. The more successful this function is the smaller the users intervention will be and the more automated the program will be.

The Multiplet Simulating Subroutines

The multiplet simulating subroutines are the core of the program, and there may be as many as the types of multiplets encountered (e.g. 1 singlet (**BS**); 1 singlet and 1 doublet (**BSD**); 1 singlet and 2 doublets (**BSDD**); 1 singlet, 2 doublet and a doublet of doublets (**BSDDQ**); 1 singlet, 1 doublet and a doublet of doublets (**BSDQ**); 2 singlet and 1 doublet (**BSDS**); 2 singlets and 2 doublets (**BSDSD**); and so on). Usually a multiplet may be fitted to a base line plus a sum of peaks ($y=ax+b+\sum peak$). But in some exceptional cases the base line may have to be fitted to other, nonlinear, functions (as higher order polynomial functions). The multiplet simulating subroutine only has to calculate the simulated multiplet for the same chemical shifts present in the experimental multiplet data and then calculate the sum of the squared differences between the two sets (simulated and experimental). This value constitutes the standard output of these routines. Additionally these routines should also calculate the areas of each fine-structure in the multiplet, so that once the main routine as found the set of parameters which generates the smallest sum of the squared differences between the simulated and experimental multiplets, the areas may be readily available for the main program.

The NMR Peak Lineshape

Given that multiplets are simulated as sums of the fine-structures, and the fine-structures as sums of peaks, it is necessary to simulate a NMR peak. To this end several functions were evaluated (Fig 2.4). Figure 2.4 shows a ^{13}C NMR peak of dioxane and the best-fits obtained for different functions. It can be seen that the Lorentzian and the Pearson type VII functions fit best. Also, the dioxane peak in

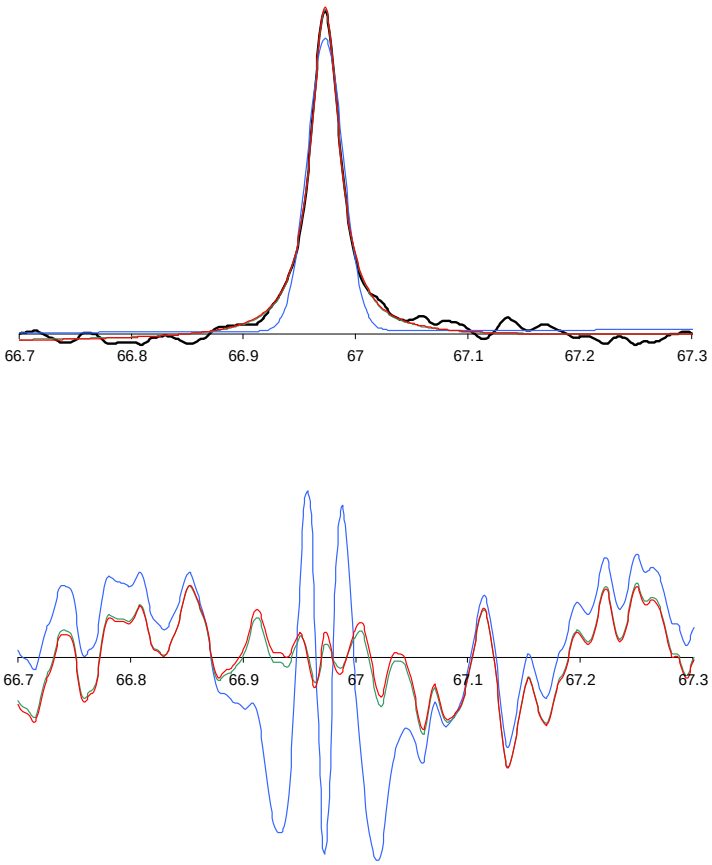

Figure 2.4 – Plot of the different functions used to fit the NMR peak. In the upper panel is shown the experimental data for a ^{13}C NMR peak of dioxane (in black) and the best-fits obtained for a Gaussian function (in blue), a Lorentzian function (in green) and a Pearson type VII function (in red). In the bottom panel are shown the differences between the experimental peak and the corresponding best-fits (amplified 7 times). It is easily seen that the Lorentzain and the Pearson type VII functions are better suited to model a NMR peak than the Gaussian function.

$$y = \frac{h}{\left(\frac{1}{p}\cdot\left(\frac{x-c}{w}\right)^2+1\right)^p} \qquad \text{(Eq. 2.1)}$$

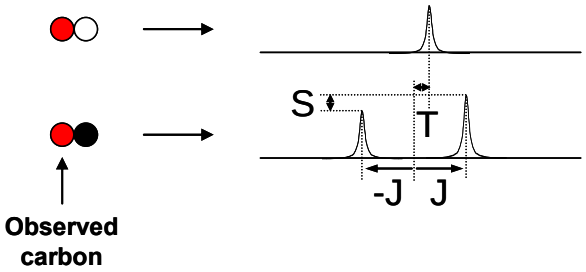

Figure 2.4 – The multiplet structure. Peaks in a fine-structure are separated from each other by the coupling constants (in a doublet each peak J Hz from the center of the fine-structure). Due to the isotopic effect the center of each fine-structure may be shifted from the center of the singlet (T). The height of the peaks might not be exactly the same due to other effects (as the strong coupling effect).

Figure 2.4 was obtained under good shimming conditions, which results in an almost pure Lorentzian peak. However, when shimming is not good, peaks tend to have a Lorentzian appearance with an increasing Gaussian component. Given that 1D NMR peaks do not have either pure Gaussian nor Lorentzian lineshapes (Marshall *et al.*, 2000), the Pearson type VII function (Eq. 2.1) was chosen to model the NMR peak lineshape, due to its ability model both functions. When p=1, equation 2.1 becomes a Lorentzian function and when p tends to infinite the Pearson type VII lineshape assumes a Gaussian shape.

Modelling ^{13}C NMR Fine-structures

^{13}C NMR fine-structures arise from ^{13}C scalar couplings and usually are composed of several peaks. These fine-structures can be modelled by a simple sum of peaks. However, this approach would mean that for a fine-structure of n peaks one would need 4n parameters i.e. one height (h), center (c), width (w) and parameter p per peak, which would lead to an excessive number of parameters. On the other hand, the peaks in an NMR fine-structure are not just scattered but are constrained and are all identical. These rules allow us to create functions that model these fine-structures using a smaller number of parameters. In Figure 2.4 are summarized the different effects which have been included in the models of the fine-structures. Each homonuclear scalar coupling splits the resonances of a fine-structure into 2 peaks which distances from the center of the resonance J Hz. The coupling constant in ^{13}C homonuclear coupling is usually between 30 and 60 Hz. Although the ^{13}C has a small isotopic effect other nuclei like ^{2}H or ^{15}N have stronger effects, and these

effects must be accounted for. The presence of another ^{13}C directly connected to the observed ^{13}C shifts the resonance of this fine-structure by around -2 Hz in respect to the resonance of the same observed ^{13}C bonded to a ^{12}C. Also, effects like the strong coupling effect may induce the appearance of unsymmetrical peaks that have to be taken into account. Usually in ^{13}C spectra peaks differ from each other only by 1 to 2%. Table 2.2 summarizes the construction of the multiplet functions.

Processing ^{13}C NMR Spectra

Spectra processing is a critical step. Special care must be taken to ensure that multiplet data is not affected by processing errors. The most important is the spectral resolution. All spectra treated using the above described program, were Fourier-transformed to, at least, 256k points, because the number of points has a strong influence on the results obtained from the spectra analysis. Figure 2.5 illustrates the effect of changing the number of points in a NMR peak. Has it can be seen peaks in spectra with small number of points appear deformed and makes it difficult to determined their center. This increases the uncertainty associated with the determination of the peak parameters and consequently it increases the uncertainly in the determination of the peak areas.

Table 2.2 – Assembly of the functions used to model ^{13}C NMR fine-structures.

Fine-structures	Function	Parameters required	Parameter (Max)*
Singlet	$Peak(c,h_S,w_S,p)$	4	4
Doublet 1	$Peak(c-J_1+T_{D1},S_{D1}\times h_{D1},w_{D1},p)+$ $Peak(c+J_1+T_{D1},(1-S_{D1})\times h_{D1},w_{D1},p)$	5	8
Doublet 2	$Peak(c-J_2+T_{D2},S_{D2}\times h_{D2},w_{D2},p)+$ $Peak(c+J_2+T_{D2},(1-S_{D2})\times h_{D2},w_{D2},p)$	5	8
Pseudo-quartet or doublet of doublets	$Peak(c-J_1-J_2+T_Q,S_{Q1}\times S_{Q2}\times h_Q,w_Q,p)+$ $Peak(c+J_1-J_2+T_Q,(1-S_{Q1})\times S_{Q2}\times h_Q,w_Q,p)+$ $Peak(c-J_1+J_2+T_Q,S_{Q1}\times(1-S_{Q2})\times h_Q,w_Q,p)+$ $Peak(c+J_1+J_2+T_Q,(1-S_1)\times(1-S_{Q2})\times h_Q,w_Q,p)$	5	16

* Max parameters represent the amount of parameter required if multiplets were modeled as a sum of unrelated peaks, which means that each peak requires 4 parameters.

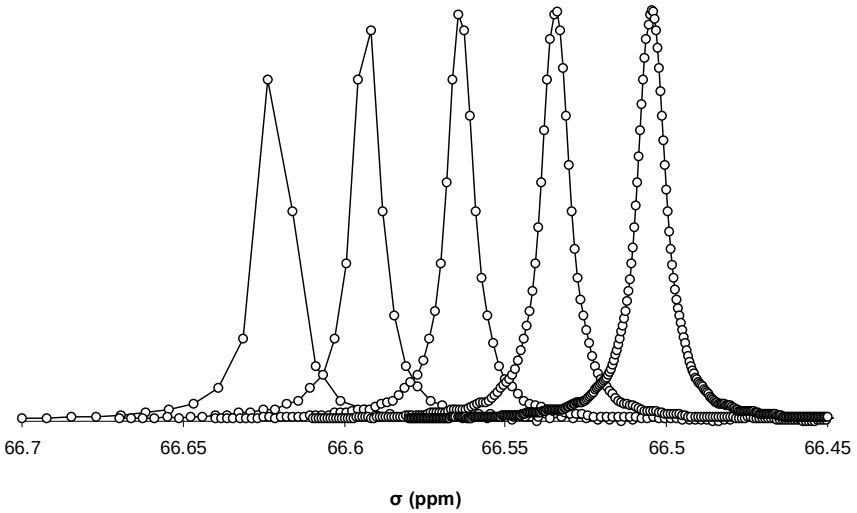

Figure 2.5 – Effect of the number of points used to Fourier-transform a NMR spectrum in the dioxane peak. From left to right the number of points (SI) used were 32k, 64k, 128k, 256k, 512k.

Practical Example of the Software Tools

To illustrate the procedure explained it is shown in Figure 2.6, a fit to a ^{13}C NMR multiplet of glutamine C4. In this multiplet three fine-structures can be recognized: a singlet, a doublet (due to the isotopomer [4,5-$^{13}C_2$]glutamine), and a quartet (due to the isotopomer [3,4,5-$^{13}C_3$]glutamine). This multiplet was fitted to a function that simulates a baseline, a singlet, two doublets with different coupling constants and one quartet. As it can be seen the difference between the simulated spectrum and the acquired was very small (Fig 2.6 A). In Figure 2.6 B, is represented the different fine-structures. Due to the mechanics of the TCA cycle, the labelling generated from [U-^{13}C]glucose, usually does not lead to the formation of the isotopomer [3,4-$^{13}C_2$]glutamine, reason because the second doublet does appear in this multiplet.

DISCUSSION

^{13}C multiplets are composed of several peaks, which are usually partially overlapped. The usage of a software tool that allows the simulation and quantification of the different fine-structures within the multiplets constitutes a real

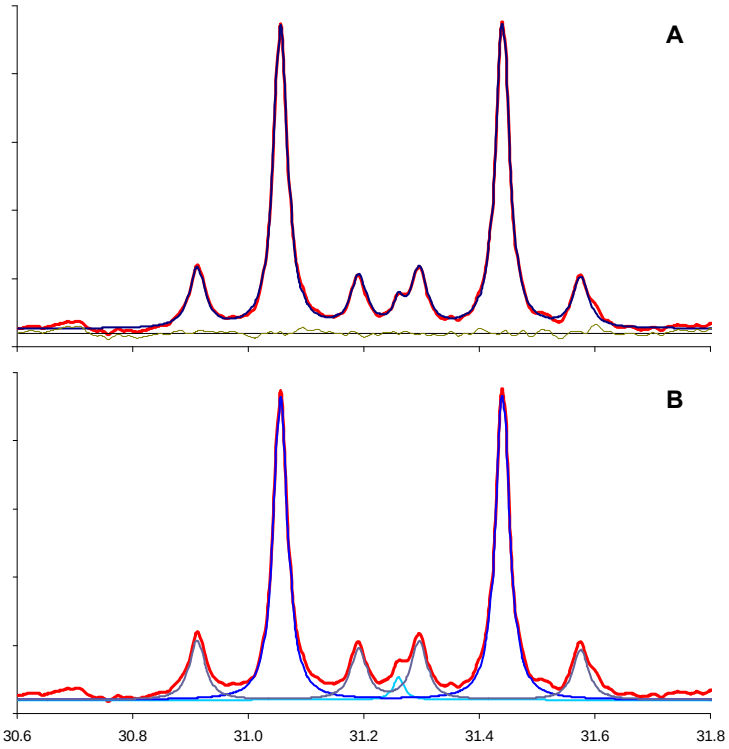

Figure 2.6 – Fitting of a ^{13}C NMR multiplet of glutamine C4 to a function that simulates a baseline, a singlet, two doublets with different coupling constants and one quartet. In **A**, is shown the acquired multiplet (in red), the fitted multiplet (in blue), and the difference between both (in green). In **B**, is shown the acquired multiplet (in red), the different fine-structures: the singlet (in light blue) the doublet (in dark blue) and the quartet (in grey). The doublet has a coupling constant of 48 Hz and is shifted upfield 1.53 Hz. The quartet results from another coupling constant of 35 Hz and is shifted upfield 2.1 Hz.

advantage in ^{13}C NMR spectra analysis. By designing this software tool to be as general as possible it becomes possible to use it in other NMR techniques, like 2D [^{13}C, ^{1}H] COSY or 1D NMR of other nuclei.

The handling of the parameters vector is troublesome and difficult task for the user given its large size. The main advantage of using a system like the one described here is that the user does not have to supply a complete vector of parameters. Also, if it is not the first time a given multiplet is being fitted the last parameters used were saved in the parameter file and no user intervention is required. Also, by having the parameters saved in files, the user can use the parameters obtained for the same multiplet in one spectrum as a first guess of the parameters in another spectrum. Usually the same multiplet in a series of spectra is very similar thus allowing the use

of the parameters of one in the next. Whenever a parameter file is not present, the IntNMRPar sub-function is called. In this function the user can store the usual first guess parameters for a given function. However, for the simpler functions (like the function used to fit a multiplet constituted by a baseline and a singlet or even by a baseline a singlet and a doublet) a small amount of code can be created that analyses the experimental multiplet and, accordingly with the function being used by the user, calculates, based on the local maxima found in the multiplet data, a very good initial guess of the parameters. In every case, the user supplied parameters, if supplied, are always used, instead of the calculated.

The lineshapes of 1D NMR peaks are not purely Gaussian or Lorentzian (Marshall *et al.*, 2000). The function that best describes a NMR resonance is the Voigtian lineshape. However, this function can not be expressed analytically, which makes it very difficult to work with, and even more difficult to integrate, which is the final objective of fitting the NMR peaks. However, there are several ways to avoid using this function and some includes using the sum or the product of a Gaussian and a Lorentzian functions (Stephenson and Binsch, 1980; Conny and Powell, 2000). Another way of approximating a Voigtian lineshape is using the Pearson type VII function (Subhash and Mohanan, 1997; van Winden *et al.*, 2001). The Pearson type VII function was chosen due to its ability to approximate both Gaussian and Lorentzian functions easily and with a small number of parameters, and in contrast with Voigtian function, it is analytically determined and is readily integrated. The use of this function together with the rationalization of the parameter usage to simulate the ^{13}C NMR fine-structures made possible the quantification of the ^{13}C NMR multiplets in a simple and fast way.

Further improvements to this program may include the addition of a graphical user interface (GUI) and the inclusion of an error estimation sub-function, which will allow estimating the errors of the determined areas, as well as, their co-variances.

REFERENCES

Conny J. M., Powell C. J. (2000) Standard test data for estimating peak parameter errors in x-ray photoelectron spectroscopy III. Errors with different curve-fitting approaches. *Surf. Interface Anal.* **29,** 856-872.

Eakin R. T., Morgan L. O., Gregg C. T., Matwiyoff N. A. (1972) Carbon-13 nuclear magnetic resonance spectroscopy of living cells and their metabolism of a specifically labeled ^{13}C substrate. *FEBS Lett.* **28,** 259-264.

London R. E. (1988) C-13 labeling in studies of metabolic-regulation. *Prog. NMR Spectroscopy* **20,** 337-383.

Marshall I., Bruce S. D., Higinbotham J., MacLullich A., Wardlaw J. M., Ferguson K. J., Seckl J. (2000) Choice of spectroscopic lineshape model affects metabolite peak areas and area ratios. *Magn. Reson. Med.* **44,** 646-649.

Stephenson D. S., Binsch G. (1980) Automated analysis of high-resolution NMR spectra I. Principles and computational strategy. *J. Magn. Reson.* **37,** 395-407.

Subhash N., Mohanan C. N. (1997) Curve-fit analysis of chlorophyll fluorescence spectra: Application to nutrient stress detection in sunflower. *Remote Sens. Environ.* **60,** 347-356.

van Winden W., Schipper D., Verheijen P., Heijnen J. (2001) Innovations in generation and analysis of 2D [^{13}C,^{1}H] COSY NMR spectra for metabolic flux analysis purposes. *Metab. Eng.* **3,** 322-343.

Wiechert W. (2001) ^{13}C metabolic flux analysis. *Metab. Eng.* **3,** 195-206.